2004-06-03

Association of Pericentrin with the γ Tubulin Ring Complex: a Dissertation

Wendy Cherie Zimmerman
University of Massachusetts Medical School

A Dissertation Presented

By

Wendy Cherie Zimmerman

Submitted to the Faculty of the University of Massachusetts Graduate School of Biomedical Sciences, Worcester

In Partial fulfillment of the requirements for the degree of

DOCTOR OF PHILOSOPHY

June 3, 2004

DEPARTMENT OF BIOCHEMISRTY AND MOLECULAR PHARMACOLOGY

PROGRAM IN MOLECULAR MEDICINE

ASSOCIATION OF PERICENTRIN WITH THE γTUBULIN RING COMPLEX

A Dissertation Presented

By

Wendy Cherie Zimmerman

Approved as to style and content by:

Kendall Knight, Chair of Committee

William Theurkauf, Member of Committee

Stephen Lambert, Member of Committee

Reid Gilmore, Member of Committee

Patricia Wadsworth, Member of Committee

Stephen Doxsey, Dissertation Mentor

Anthony Carruthers, Dean of the
Graduate School of Biomedical Sciences

Program in Molecular Medicine
June 3, 2004

COPYRIGHT INFORMATION

ACKNOWLEDGMENTS

Other authors contributed to the work presented herein. I wish to thank them all for their efforts and contributions. The first observation that pericentrin coimmunoprecipitated with γ tubulin from Xenopus extracts was made by Dr. Cynthia Sparks. I repeated and expanded upon her initial observations, to produce the biochemical analyses of Xenopus complexes presented in Chapter II. Jason Dictenberg is responsible for the high resolution imagery of the lattice and FRET analysis presented in Chapter II. Aaron Young cloned and expressed GFP-tagged pericentrin and quantified centrosome fluorescence (Chapter II, Figure 8A). Charles Vidair quantified soluble pericentrin and γ tubulin in somatic cells (Chapter II, Figure 8B). Yixian Zheng provided γ tubulin antibodies and purified γ TuRC. James Sillibourne conducted all the yeast two-hybrid work presented here. Jack Rosa microinjected the COS cells, (Chapter III, Figure 8).

I thank T. Stearns and S. Murphy for antibodies to GCP2 and 3 and for plasmids encoding GCP2, GCP3 and γ tubulin. I thank T.N. Davis for pericentrin B/ kendrin-specific antibody. I also thank C. Wiese for constitutively active RanL43E.

I thank my advisor, Stephen Doxsey for the excellent training, mentoring and patience that he has given me.

I would like to thank Andrea Pereira for her sage advise; Aruna Purohit for her assistance in many little ways throughout the years; and Keith Mikule for sharing his knowledge of siRNA.

I would like to thank the other members of the Doxsey lab: Jack Rosa, James Sillibourne, Adam Gromley, Agata Jurkzyk, Sambra Reddick, Thomas Wadzinski, Ensar Halilovic, Aaron Young, and Irina Gavenescu for their feedback and many valuable discussions. I hope that Jack will sleep better at night, without the influence of "devil frogs" and "mutant" clover. I wish them all luck in their future endeavors.

Last but foremost in my thoughts, I would like to thank my family, Steven Earl Popkes and Benjamin John Patrick Zimmerman Popkes, without their love and support this work would not have been possible.

ABSTRACT

Pericentrin is a molecular scaffold protein. It anchors protein kinases, (PKB, (Purohit, personal communication), PKC, (Chen et al., 2004), PKA Diviani et al., 2000), the γ tubulin ring complex, (γ TuRC) (Zimmerman et al., 2004), and possibly dynein (Purohit et al., 1999) to the spindle pole. The γ TuRC is a ~ 2 MDa complex which binds the minus ends of microtubules and nucleates microtubules *in vitro*, (Zheng et al., 1995). Prior to this work, nothing was known about the association of the γTuRC with pericentrin. Herein I report the biochemical identification of a large protein complex in Xenopus extracts containing pericentrin, the γ TuRC, and other as yet unidentified proteins. Immunodepletion of γ tubulin results in co-depletion of pericentrin, indicating that virtually all the pericentrin in a Xenopus extract is associated with γ tubulin. However, pericentrin is not a member of the, γ TuRC, since isolated γ TuRCs do not contain pericentrin. The association of pericentrin with the γ TuRC is readily disrupted, resulting in two separable complexes, a small pericentrin containing complex of approximately 740 KDa and the the γ TuRC, 1.9 MDa in Xenopus. Co overexpression/ coimmunoprecipitation and yeast two hybrid studies demonstrate that pericentrin binds the γTuRC through interactions with both GCP2 and GCP3. When added to Xenopus mitotic extracts, the GCP2/3 binding domain uncoupled γ TuRCs from centrosomes, inhibited microtubule aster assembly and induced rapid disassembly of pre-assembled asters. All phenotypes were significantly reduced in a pericentrin mutant with diminished GCP2/3 binding, and

were specific for mitotic centrosomal asters as I observed little effect on interphase asters or on asters assembled by the Ran-mediated centrosome-independent pathway. Overexpression of the GCP2/3 binding domain of pericentrin in somatic cells perturbed mitotic astral microtubules and spindle bipolarity. Likewise pericentrin silencing by small interfering RNAs in somatic cells disrupted γ tubulin localization and spindle organization in mitosis but had no effect on γ tubulin localization or microtubule organization in interphase cells. Pericentrin silencing or overexpression induced G2/antephase arrest followed by apoptosis in many but not all cell types. I conclude that pericentrin anchoring of γ tubulin complexes at centrosomes in mitotic cells is required for proper spindle organization and that loss of this anchoring mechanism elicits a checkpoint response that prevents mitotic entry and triggers apoptotic cell death. Additionally, I provide functional and *in vitro* evidence to suggest that the larger pericentrin isoform (pericentrin B/ Kendrin) is not functionally homologous to pericentrin/pericentrin A in regard to it's interaction with the γ TuRC.

TABLE OF CONTENTS

LIST OF FIGURES

CHAPTER I

INTRODUCTION

In this thesis I investigate the role of the centrosomal protein pericentrin in anchoring γ tubulin, shedding new light on the roles of pericentrin and γ tubulin in spindle pole/centrosome assembly and function. In general, centrosome structure and function is not well understood, however recent genetic and biochemical studies have provided new insights into the molecular basis of centrosome-mediated microtubule nucleation. In addition, molecules and mechanisms involved in microtubule severing and stabilization at the centrosome, assembly of proteins onto centrosomes and regulation of centrosome duplication and separation are being defined. Better understanding of all these processes my aid our understanding of the development of cancers, see below.

Introduction

Microtubule organizing centers (MTOCs) represent a class of organelles that are structurally diverse but share the common ability to nucleate and organize microtubules. They include the centrosome of animal cells, the spindle pole body (SPB) of yeasts and the blepharoplast of some lower plant cells, to name a few. Together with the microtubule cytoskeleton, the centrosome is involved in a number of important cellular functions including spindle function, the organization and

transport of cytoplasmic organelles, morphogenesis and determination of cell shape. Although we know that the molecular composition of animal cell centrosomes is complex, we know little about how individual components contribute to the organization and function of the organelle. The recent identification of molecular components that are conserved between MTOCs of different organisms, however, provides an opportunity to dissect the underlying functional significance of these components, rather than focus on structural differences between MTOCs. In addition, the ever increasing number of regulatory molecules that associate with centrosomes such as kinases, phosphatases and proteins of degradation pathways (see Figure 1), suggests that centrosomes will provide a fertile area for future discovery. In this chapter, I discuss recent work on MTOCs from several systems with an emphasis on the composition, assembly, organization and regulation of components involved in microtubule nucleation. For previous reviews and additional information on MTOCs in various organisms see (Balczon, 1997; Kellogg et al., 1994; Sobel, 1997; Stearns and Winey, 1997.; Vaughn and Harper, 1998)

Anatomy of microtubule nucleating structures

In this section I will discuss microtubule nucleation at three levels: the general organization of the nucleating material at the centrosome, γ tubulin complexes that appear to play a direct role in microtubule nucleation and core components of the protein complexes.

Organization of microtubule nucleating material at the centrosome

Over 100 years ago, the centrosome was described by Theodor Boveri as a "pair of centrioles surrounded by a differentiated cytoplasm" (see (Wilson, 1925)). Since that time we have learned a great deal about the structure of centrioles although, until recently, little progress has been made in understanding the structure of the 'differentiated cytoplasm' or pericentriolar material (PCM). Advances in immunofluorescence image deconvolution have been used to demonstrate that the centrosome protein pericentrin (Doxsey et al., 1994) is organized into a highly-ordered lattice structure within the PCM (Dictenberg et al., 1998). In this same study, fluorescence resonance energy transfer showed that γ tubulin, the protein thought to interact with the α/β tubulin heterodimer during microtubule nucleation (Oakley et al., 1990), colocalized with pericentrin to the lattice. Centrosome lattice structures have also been revealed using electron microscopy (EM) techniques in *Drosophila melanogaster* (Moritz et al., 1995a), the surf clam, *Spistula solidissima* (Schnackenberg et al., 1998) and the sea urchin, *Strongylocentrotus purpuratus* (Thompson-Coffe et al., 1996). Taken together, these results suggest that the pericentrin and γ tubulin lattice observed by immunofluorescence imaging may represent the general architectural framework of the PCM as observed by EM techniques.

γ tubulin rings at the centrosome

Higher magnification EM imaging of the PCM revealed ring-like structures that

contained γ tubulin and had diameters roughly similar to those of microtubules (Moritz et al., 1995a). Rings were not detectable after microtubule nucleation, suggesting that they served as templates for nucleated microtubules. This idea was supported by the observation that removal of γ tubulin and ring structures from the lattice by salt treatment abrogated microtubule nucleation, whereas re-association of γ tubulin and re-appearance of rings accompanied restoration of nucleating activity (Moritz et al., 1998; Schnackenberg et al., 1998). Further support came from the observation that the ends of centrosome-nucleated microtubules contacted elements of the pericentrin and γ tubulin lattice (Dictenberg et al., 1998). These results suggest that γ tubulin rings are organized into a centrosome lattice that may provide the structural and biochemical basis for microtubule nucleation.

Multiple γ tubulin complexes and their composition

γ tubulin ring complexes (γ TuRCs) have been purified from cytoplasmic extracts of *Xenopus laevis* eggs and shown to nucleate microtubules *in vitro*, suggesting that they may be the soluble form of centrosome-associated γ tubulin rings (Zheng et al., 1995). At present, several soluble protein complexes containing γ tubulin have been identified in a variety of organisms. Complexes of 2–3 MDa containing seven or eight protein species have been identified in *Xenopus* (Zheng et al., 1998), *Drosophila* (Moritz et al., 1998) and mammals (Akashi et al., 1997; Dictenberg et al., 1998; Murphy et al., 1998). Smaller γ tubulin complexes have also been identified in *Drosophila* (Moritz et al., 1998), *Aspergillus nidulans* (Akashi et al., 1997) and

Saccharomyces cerevisiae (see (Marschall and Stearns, 1997)). The *S. cerevisiae* complex is composed of three protein species (see below) and appears to be the only γ tubulin complex in yeast. The smaller of the two *Drosophila* complexes has been shown to nucleate microtubules, albeit at a reduced efficiency compared to the γ TuRC (Moritz et al., 1998). A 3 MDa γ tubulin complex has been identified in *Xenopus* extracts that may represent an assembly-competent form of microtubule nucleating material in animal cells (Dictenberg et al., 1998). It appears to be composed of two subcomplexes: a γ tubulin complex that is similar in molecular mass to the γ TuRC and a pericentrin complex that has not been previously described. The relationship between the various γ tubulin complexes and their respective roles in microtubule nucleation and centrosome assembly is currently unknown. For views on how γ tubulin complexes may mediate microtubule nucleation see (Erickson and Stoffler, 1996). In this study I will demonstrate that the association of pericentrin with γ tubulin in Xenopus is required for spindle pole assembly and spindle pole dependent microtubule nucleation.

Recent work has focused on determining the molecular composition of γ tubulin complexes by biochemical and genetic analyses in several systems. On the basis of genetic interactions with the *S. cerevisiae* homologue of γ tubulin, *tub4*, two additional proteins of the γ tubulin complex were identified, Spc97p and Spc98p (see (Marschall and Stearns, 1997)). The three proteins form a stable cytoplasmic complex and localize to sites of microtubule nucleation at the SPB (Knop and Schiebel, 1997).

Loss of function of any of the three proteins produces the same result, reduced microtubule nucleation and perturbation of microtubule organization (for review see (Marschall and Stearns, 1997)). Homologues of Spc97p and Spc98p have been identified in higher eukaryotes using biochemical purification methods (Martin et al., 1998) and human expressed sequence tags (ESTs) (Murphy et al., 1998; Tassin et al., 1998), and the interaction between the Spc98p homologue and γ tubulin was confirmed in these studies.

Assembly of microtubule-nucleating components

It is generally believed that cytoplasmic protein complexes containing γ tubulin represent precursors of nucleating sites at the centrosome in embryonic systems (Moritz et al., 1998; Zheng et al., 1995), mammalian cells (Dictenberg et al., 1998) and yeast (Knop and Schiebel, 1998). A better understanding of how these complexes assemble onto and disassemble from centrosomes will be important in understanding how microtubule nucleation is controlled in cells and may have important implications for human cancer (see below).

Nucleated microtubules in *S. cerevisiae* arise from two surfaces of the SPB, the electron dense plaque facing the cytoplasm and a similar plaque facing the nuclear interior (see (Sobel, 1997) for review of SPB structure). Binding of the *S. cerevisiae* γ tubulin complex to the nuclear face of the SPB appears to be mediated by the spindle pole component, Spc110p. Spc110p interacts directly with Spc97p and/or Spc98p in

the γ tubulin complex, but not with Tub4p (Knop and Schiebel, 1997; Nguyen et al., 1998). Taken together, these results indicate that Spc110p serves as the receptor for γ tubulin complexes on the nuclear face of the yeast SPB. On the cytoplasmic side, a different protein, Spc72p interacts with Spc97p and Spc98p and thus appears to be the receptor for γ tubulin complexes at this site (Knop and Schiebel, 1998). In cells carrying temperature sensitive mutations of Spc72p, cytoplasmic microtubules are absent or unattached to the SPB (Chen et al., 1998). Interestingly, a fusion protein containing the amino terminus of Spc110p and the carboxyl terminus of Spc72p will function as the cytoplasmic receptor for the γ tubulin complex, showing that this binding function is conserved between the two proteins (Knop and Schiebel, 1998) Thus, in *S cerevisiae* there are two independent, site-specific receptors for the γ tubulin complex. Two receptors may be required in organisms that undergo closed mitoses such as yeasts, since they have two nucleating surfaces in distinct, membrane bound compartments (nucleus and cytoplasm). In animal cells, one receptor may be sufficient as the centrosome is cytoplasmic throughout the cell cycle and the nuclear envelope breaks down in mitosis. Pericentrin may be functionally homologous to Spc72p and Spc100p, since it anchors the γ TuRC to the spindle pole in mitosis (Zimmerman, 2004).

Studies in a number of higher eukaryotic systems have recently demonstrated that assembly of nucleating proteins onto centrosomes is required for microtubule nucleation and appears to require factors in addition to the γ tubulin complex.

Reconstitution of microtubule nucleation on salt stripped centrosomes from *Drosophila* embryos requires γ tubulin complexes and an additional fraction of ~220 kDa (Moritz et al., 1998). One candidate for the additional activity is pericentrin, which is roughly the same molecular mass and has been implicated in the assembly of γ tubulin complexes in *Xenopus* eggs (Dictenberg et al., 1998). In mammalian cells, pericentrin and γ tubulin assemble progressively at the centrosome lattice from G1 until metaphase, and this assembly occurs concomitant with increased microtubule nucleating activity. Time-lapse imaging of green fluorescent protein (GFP) tagged pericentrin and antibody microinjection experiments have shown that pericentrin and γ tubulin assembly requires microtubules and the molecular motor dynein and is necessary for normal microtubule nucleation (Young A, Doxsey S, unpublished data). It is possible that dynein mediated transport is a common mechanism for centrosome assembly, although it may not be utilized in embryonic systems where numerous copies of centrosome proteins are stockpiled (Gard, 1990), and are able to assemble onto centrosomes in a microtubule-independent manner (Stearns and Kirschner, 1994). The recently developed assays for centrosome assembly described above should provide powerful approaches to dissect the molecular basis of centrosome assembly and function.

Mechanisms regulating microtubule nucleation

At present, little is known about how microtubule nucleating activity at the centrosome is controlled. Microtubule nucleation could be regulated by one or more

mechanisms including: assembly of nucleating proteins from cytoplasmic pools, activation and/or stabilization of preassembled nucleating proteins and re-utilization of existing nucleating sites (see Figure 1b). In addition, the total microtubule nucleating activity may be affected by the number of MTOCs in the cell.

The presence of centrosome proteins in both soluble and centrosome-associated forms (above) indicates that centrosome assembly must be a regulated process (Figure 1bi). Among the molecules that could potentially regulate centrosome assembly is the centrosome-associated Polo kinase of *Drosophila* and the human homologue Plk1 (for reviews see (Glover et al., 1996; Lane and Nigg, 1997)). Functional abrogation of these molecules by mutational analysis or antibody injection results in small centrosomes with reduced levels of centrosome components (see (Glover et al., 1996; Stearns and Kirschner, 1994)). Another protein implicated in control of centrosome assembly is the *Drosophila* protein phosphatase 4 (PP4) whose reduced expression results in decreased γ tubulin staining at centrosomes and diminished microtubule nucleation (Helps et al., 1998). These and other regulatory molecules could control assembly of centrosome proteins via signaling pathways that have yet to be identified.

The nucleation capacity of centrosomes could also be regulated by activation of preassembled nucleating sites or by the stabilization of nascent nucleated microtubules (Figure 1bii). One candidate for microtubule stabilization is Stu2p, an essential protein of the *S. cerevisiae* SPB that appears to bind laterally to

microtubules (Wang and Huffaker, 1997). Stu2p also interacts with the cytoplasmic γ tubulin receptor Spc72p (Chen et al., 1998). The ability to bind both γ tubulin receptor and microtubules suggests that Stu2p may play a role in the stabilization of the nucleating site, and could thus be involved in regulating microtubule nucleation at the SPB. Other studies have shown that the nucleation capacity of isolated centrosomes could be reduced by pretreatment with phosphatases (Centonze and Borisy, 1990) and increased by treatment with cyclin A *in vitro* (Buendia, 1992). One candidate for deactivation of nucleating sites is PP4 (above) (Helps et al., 1998). In addition to its affect on centrosome assembly, PP4 appears to reduce microtubule nucleation from centrosomes, suggesting that the phosphatase may affect centrosome-mediated microtubule nucleation at multiple levels. These results suggest that preassembled nucleating sites may be turned on and off by kinase/phosphatase cascades through modification of target proteins.

Another way to increase the nucleating capacity of centrosomes is to re-utilize existing nucleating sites (Figure 1biii). This could be accomplished by severing nucleated microtubules and reusing the severed sites for microtubule growth. Severed microtubules could be subsequently anchored at the centrosome, at other cellular sites or released into the cytoplasm (Keating et al., 1997). Microtubule severing and anchoring has been proposed to explain the increased number and dynamics of microtubules in mitotic cells (Keating et al., 1997; McNally and Thomas, 1998; Merdes and Cleveland, 1997), and to explain the genesis of apical/basal microtubule

arrays adjacent to centrosomes in specialized epithelial cells (Mogensen et al., 1997).

Centrosome duplication, separation and integrity

Centrosome duplication has been traditionally defined by the appearance and growth of nascent centrioles during the G1/S transition, culminating in the separation of the two resulting centriole pairs and associated PCM in mitosis.

The duplication of centrosomes occurs once and only once during each cell cycle and the two resulting centrosomes contribute to the organization of the poles of the mitotic spindle and thus, to the proper segregation of chromosomes in mitosis. While the process of centrosome duplication is temporally coupled to the cell cycle under normal conditions, it does not appear to be controlled by the mitosis-specific cyclin-dependent kinase (cdk)1–cyclinB complex (Hinchcliffe et al., 1998). Two recent studies indicate that centrosome duplication is regulated by the G1-specific cdk2–cyclin E complex (Hinchcliffe et al., 1999; Lacey et al., 1999). As cdk2–cyclin E has previously been shown to regulate the initiation of DNA synthesis, it may serve to couple DNA replication and centrosome duplication during cell cycle progression. Interestingly, multiple centrosomes and acentriolar MTOCs can be induced through misexpression of regulatory molecules implicated in tumorigenesis, suggesting that these molecules, like cdk2-cyclin E, may affect centrosome duplication, assembly and/or integrity (see below).

The separation of centrosomes in mitosis requires microtubule motors and astral microtubules (see (Kashina et al., 1997) for review and (Rosenblatt et al, 2004), although the biochemical events involved in this process are poorly understood. Nima related kinase (NEK2) and its substrate NEK-associated protein (C-Nap1), have recently been implicated in the biochemical modification of centrosomes during their separation at mitosis (Fry et al., 1998a; Fry et al., 1998b). C-NAP1 is concentrated at centrioles ends where they are joined together, and it becomes reduced during mitosis when centrosomes separate. Overexpression of NEK2 leads to premature centrosome splitting and apparent fragmentation of the PCM, suggesting that these proteins play a role in centriole/centrosome separation during mitosis. PCM fragmentation or ectopic assembly of PCM components is also observed in tumor cells, although the mechanism by which these centrosome defects arise is unknown (see below).

Centrosomes and cancer

At the beginning of the 20th century, Theodor Boveri speculated that centrosomes could contribute to the chromosome missegregation and aneuploidy that was commonly observed in tumor cells (Boveri, 1914). As we start the 21st century, we are getting our first glimpses of alterations in molecular determinants of centrosomes that accompany and may contribute to tumorigenesis. The centrosome components pericentrin, γ tubulin and centrin all appear to be overexpressed and ectopically assembled in many malignant tumors (Lingle et al., 1998; Pihan et al., 1998) (for reviews see (Doxsey, 1998)). Centrosomes in these tumors exhibit aberrant features

including: dramatic alterations in size and shape, absence of centrioles and excessive numbers. Regardless of their morphology, most of these structures nucleate microtubules and contribute to assembly of abnormal spindles.

The mechanism by which structural and functional centrosome defects arise in tumor cells is unknown. While recent studies suggest that overexpression of pericentrin alone can induce centrosome defects and aneuploidy (Pihan et al., 2001), other studies indicate that centrosome-associated kinases and other regulatory molecules may affect centrosomes in tumors (for reviews see (Doxsey, 1998; Pihan and Doxsey, 1999)). It is possible that aberrant centrosomes assemble dysfunctional spindles and contribute to genetic instability and tumorigenesis. Elucidation of the molecular mechanisms that control centrosome duplication, assembly and integrity in normal cells will provide insight into the role of this organelle in tumorigenesis.

Other Activities of Centrosomes

Several recent provocative observations suggest that centrosomes may be involved in much more than the nucleation and organization of microtubules. An increasing number of regulatory molecules have been localized to centrosomes (kinases, cyclins, cdks, ubiquitin enzymes), suggesting that centrosome proteins may serve as scaffolds for the organization of specific biochemical regulatory pathways (see Figure 1) (Pawson and Scott, 1997). In this regard, pericentrin shares homology with scaffold proteins involved in anchoring regulatory kinases (Dransfield et al., 1997). and is

known to anchor PKB, (Purohit, personal communication), PKC, (Chen et al., 2004), PKA Diviani et al., 2000), the γ tubulin ring complex, (γ TuRC) (Zimmerman et al., 2004), and possibly dynein (Purohit et al., 1999) to the spindle pole, (Figure 2).

Pericentrin Isoforms

During the initial isolation of pericentrin, it was noted that there appeared to be two pericentrin messages in mouse and Hela cells (Doxsey, 1994). The smaller isoform was cloned. Recent evidence suggests there may be as many as ten isoforms of pericentrin in human cells (Flory and Davis, 2003). A large isoform (pericentrin B/kendrin, (Flory and Davis, 2003)) and another centrosome protein called AKAP450/GC-NAP share homology with the calmodulin-binding domain of Spc110p (Flory et al., 2000; Gillingham and Munro, 2000; Li et al., 2001). Although these isoforms are products of the same gene, they may have distinct functions. Additional exons may confer additional binding/ interaction domains or disrupt protein-protein interactions or folding. (See Figure 3).

Prior to this work, nothing was known about the association of the γTuRC with pericentrin. Herein I report the biochemical identification of a large protein complex in Xenopus extracts containing pericentrin, the γ TuRC, and other as yet unidentified proteins. Co overexpression/ coimmunoprecipitation and yeast two hybrid studies demonstrate that pericentrin binds the γTuRC through interactions with both GCP2 and GCP3. When added to Xenopus mitotic extracts, the GCP2/3 binding domain

uncoupled γ TuRCs from centrosomes, inhibited microtubule aster assembly and induced rapid disassembly of pre-assembled asters. All phenotypes were specific for mitotic centrosomal asters as I observed little effect on interphase asters or on asters assembled by the Ran-mediated centrosome-independent pathway. Overexpression of the GCP2/3 binding domain of pericentrin in somatic cells clearly disrupted a specific subset of spindle microtubules, the astral microtubules (See Figure 4), and may disrupt the interpolar microtubules as well, resulting in mini/anastral spindles (see Chapter 3) or monopolar microtubule assemblies. Likewise pericentrin silencing by small interfering RNAs in somatic cells disrupted γ tubulin localization and spindle organization in mitosis but had no effect on γ tubulin localization or microtubule organization in interphase cells. Pericentrin silencing or overexpression induced G2/antephase arrest followed by apoptosis in many but not all cell types. I conclude that pericentrin anchoring of γ tubulin complexes at centrosomes in mitotic cells is required for proper spindle organization and that loss of this anchoring mechanism elicits a checkpoint response that prevents mitotic entry and triggers apoptotic cell death.

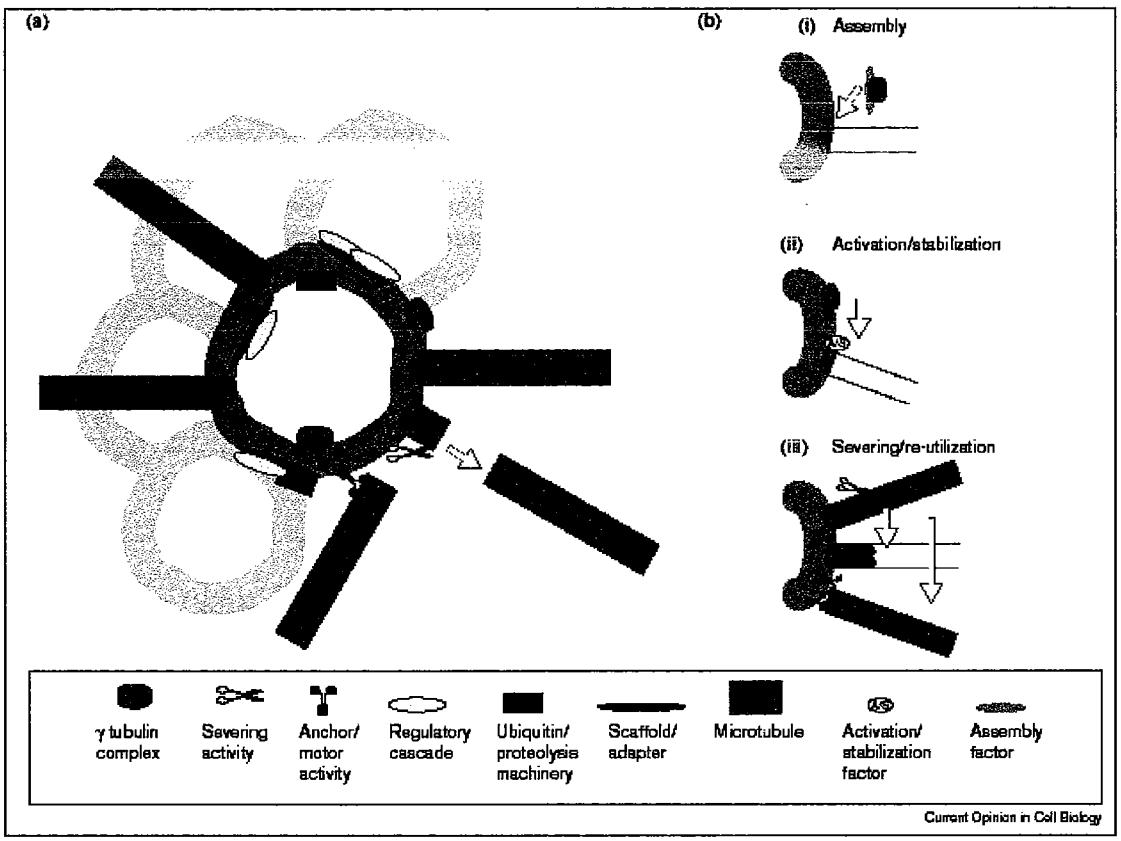
(a)
(b)
(i) Assembly
(ii) Activation/stabilization
(iii) Severing/re-utilization
γ tubulin complex
Severing activity
Anchor/ motor activity
Regulatory cascade
Ubiquitin/ proteolysis machinery
Scaffold/ adapter
Microtubule
Activation/ stabilization factor
Assembly factor
Current Opinion in Cell Biology

Figure 1

Figure 1 **(a)** Centrosome-based activities. In addition to microtubule nucleating sites, centrosomes have microtubule severing activity and perhaps microtubule anchoring sites. Kinases, phosphatases, components of the ubiquitin degradation pathway and other regulatory molecules have been localized to centrosomes. They may regulate centrosome and spindle function, and provide signals for other cellular processes. Multiple activities may be organized at discrete sites in the centrosome by scaffolding proteins. **(b)** Possible mechanisms for regulating microtubule nucleation at the centrosome. (i) Regulated assembly of microtubule nucleating proteins. (ii) Activation of preassembled nucleating sites or stabilization of nascent nucleated microtubules. (iii) Re-utilization of preassembled microtubule nucleating sites by severing and re-growth. See text for detailed descriptions.

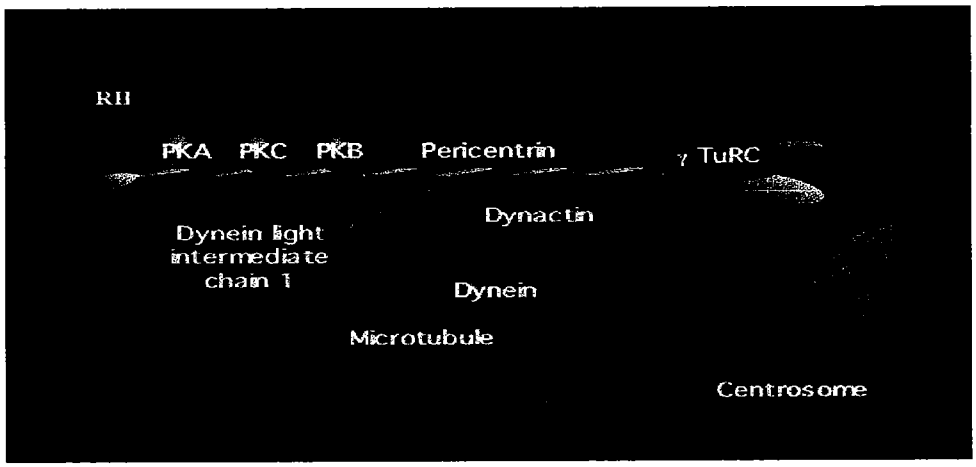
RII
PKA
PKC
PKB
Pericentrin
γ TuRC
Dynactin
Dynein light intermediate chain 1
Dynein
Microtubule
Centrosome

Figure 2

Figure 2 Pericentrin is a molecular scaffold. Pericentrin is a parallel homodimer (Zimmerman, unpublished observations) which binds (PKA) Protein Kinase A, (Diviani et al., 2000), (PKB) Protein Kinase B, (Purohit, personal communication), (PKC), Protein Kinase C, (Chen et al., 2004), (γ TuRC), the γ tubulin ring complex, (Zimmerman et al., 2004), and dynein (Purohit et al., 1999; Young et al., 2000; Tynan et al., 2000).

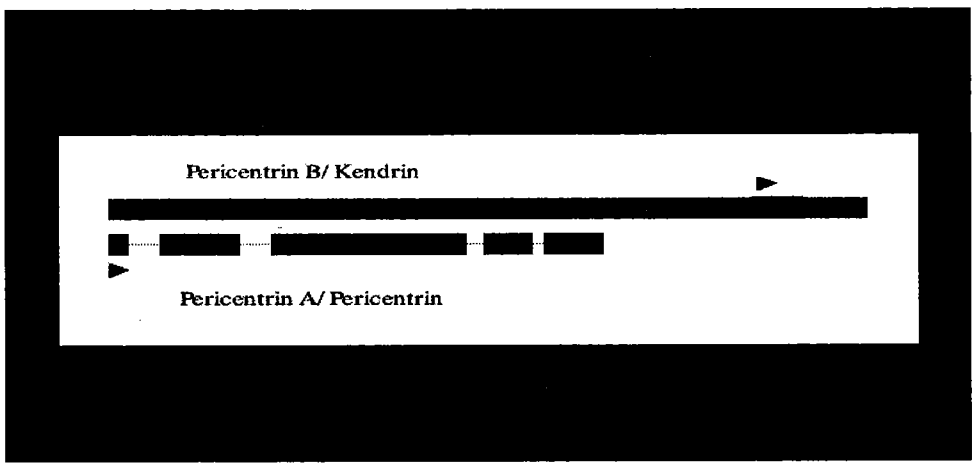

Figure 3

Figure 3 Comparison of cloned splice variants of pericentrin. Pericentrin B is also known as kendrin. Pericentrin A was first cloned and named pericentrin. Dotted lines in pericentrin indicate the location of exons present in pericentrin B but not pericentrin. The GCP2/3 binding domain (Zimmerman, 2004) is shown in lavender. The PACT domain (Pericentrin AKAP Centrosomal Targeting, (Gillingham et al., 2000)), which includes the calmodulin binding domain as well as other residues, is shown in red. Arrow heads indicate the positions of the siRNA targets used to silence pericentrin A and B in human cell lines (See Chapter 3).

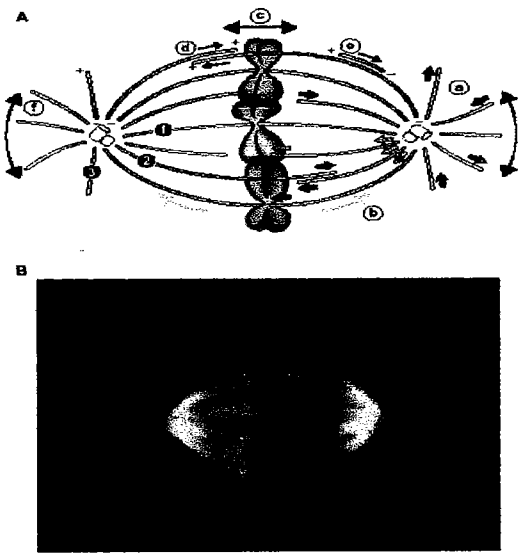

Wittman et. al. 2001. Nature Cell Biology 3:E28-E34

1 Kinetochore microtubules
2 Interpolar microtubules
3 Astral microtubules

Figure 4

Figure 4 Normal spindles contain three distinct classes of microtubules. (Whitman et. al., 2001). 1) Kinetochore microtubules, which attached to chromosomes at the kinetochore, are most often bundled, forming kinetochore fibers, and may attach to or be independent of spindle poles. 2) Interpolar microtubules which are anchored and/ or nucleated by the spindle pole and cross the central spindle. 3) Astral microtubules, which are anchored and/ or nucleated by the centrosome/spindle pole and interact with the cell cortex.

CHAPTER II

PERICENTRIN AND γ-TUBULIN FORM A PROTEIN COMPLEX AND ARE ORGANIZED INTO A NOVEL LATTICE AT THE CENTROSOME

Abstract

Pericentrin and γ-tubulin are integral centrosome proteins that play a role in microtubule nucleation and organization. In this study, we examined the relationship between these proteins in the cytoplasm and at the centrosome. In extracts prepared from *Xenopus* eggs, the proteins were part of a large complex as demonstrated by sucrose gradient sedimentation, gel filtration and coimmunoprecipitation analysis. The pericentrin–γ-tubulin complex was distinct from the previously described γ-tubulin ring complex (γ–TuRC)as purified γ-TuRC fractions did not contain detectable pericentrin. When assembled at the centrosome, the two proteins remained in close proximity as shown by fluorescence resonance energy transfer. The three dimensional organization of the centrosome-associated fraction of these proteins was determined using an improved immunofluorescence method. This analysis revealed a novel reticular lattice that was conserved from mammals to amphibians, and was organized independent of centrioles. The lattice changed dramatically during the cell cycle, enlarging from G1 until mitosis, then rapidly disassembling as cells exited mitosis. In cells colabeled to detect centrosomes and nucleated microtubules, lattice

elements appeared to contact the minus ends of nucleated microtubules. Our results indicate that pericentrin and γ-tubulin assemble into a unique centrosome lattice that represents the higher order organization of microtubule nucleating sites at the centrosome.

Introduction

A major function of centrosomes in animal cells is to nucleate microtubules. Pericentrin and γ–tubulin are centrosome proteins that are involved in microtubule nucleation and organization, although their precise roles in these processes have not been determined (Archer, 1994; Doxsey et al., 1994; Merdes and Cleveland, 1997; Oakley and Oakley, 1989; Zheng et al., 1995). They are both found at centrosomes and other microtubule organizing centers (MTOCs) in a wide range of organisms. At the centrosome, they are localized within the centrosome matrix, which is the material that surrounds the centriole pair and nucleates microtubules (Gould and Borisy, 1977). They are also present in a soluble form in the cytoplasm of somatic cells and in *Xenopus laevis* egg extracts. Since they share common cellular sites and are both required for microtubule-associated processes, it is possible that these proteins function by interacting directly or through other proteins to coordinate microtubule nucleation in the cell.

For over one hundred years, little progress has been made in understanding the structural organization of the centrosome matrix or pericentriolar material (PCM; (Kellogg et al., 1994; Wilson, 1925)). The higher resolving power of EM has been of limited use in identifying the structure of the matrix, as it appears as a complicated tangle of fibers and granular material with proteins that nonspecifically associate (Kellogg et al., 1994). Although immunogold EM techniques have provided useful information on the localization of specific molecular components at the centrosome (Doxsey et al., 1994; Moritz et al., 1995b; Stearns and Kirschner, 1994), they too are limited in their ability to reveal the overall three-dimensional (3D) organization of these molecules because of problems associated with loss of antigenicity and reagent penetration (Griffiths, 1993). Recently, ringlike structures with diameters similar to microtubules (25–28 nm) have been found in centrosomes of *Drosophila* (Moritz et al., 1995a) and *Spisula* (Vogel et al., 1997), where they appear to contact ends of nucleated microtubules. γ–Tubulin has been localized to these rings (Moritz et al., 1995a), and is also part of a soluble protein complex of similar geometry called the γ-tubulin ring complex (γ-TuRC), which is sufficient for microtubule nucleation *in vitro* (Zheng et al., 1995). Aside from the rings and the ill-defined fibrogranular material, little is known about the assembly and organization of the centrosome matrix.

Assembly of microtubule nucleating complexes onto centrosomes is considered to be a key event in regulating nucleating activity of cells (Kellogg et al., 1994). In mitosis, the higher level of centrosome matrix material and the increase in microtubule

nucleation is believed to be required for proper assembly of the mitotic spindle (Kellogg et al., 1994; Kuriyama, 1981). Assembly of microtubule asters in *Xenopus* egg extracts has been shown to require soluble pericentrin and γ–tubulin (Archer, 1994; Doxsey et al., 1994; Felix et al., 1994; Stearns and Kirschner, 1994). Although it has been hypothesized that pericentrin may provide a structural scaffold for microtubule nucleating complexes at the centrosome (Doxsey et al., 1994; Merdes and Cleveland, 1997), the precise role of the protein in centrosome organization and microtubule nucleation has not been determined. In this study, we demonstrate that pericentrin and γ–tubulin are components of a large protein complex in *Xenopus* egg extracts. When assembled at the centrosome, the proteins form a unique reticular lattice when analyzed by an improved immunofluorescence method (Carrington et al., 1995). The lattice is conserved from mammals to amphibians, it is organized independent of centrioles, and it appears to nucleate microtubules. Based on these observations, we propose that the pericentrin–γ–tubulin lattice plays a role in microtubule nucleation and organization in perhaps all animal cells.

Materials and Methods

Antibodies

A polyclonal antibody raised in rabbits against the NH2 terminus of pericentrin (glutathione-S-transferase [GST]-pericentrin 2) (Doxsey et al., 1994) was affinity purified (M8) and used, unless otherwise stated. In addition, a rat monoclonal

antibody was made against a 561–amino acid polypeptide (1293–1853) at the COOH terminus of pericentrin (A102). IgG from cell supernatants was purified by protein A binding (Harlow, 1988), concentrated and used at 2 μg/ml for immunofluorescence studies where indicated. A third pericentrin antibody was used to confirm immunoprecipitations of pericentrin from *Xenopus* extracts (RAT2, see below). This antibody was raised against gst-pericentrin 2 in a rat; it recognized pericentrin in *Xenopus* centrosomes both by immunofluorescence and by immunoblotting (data not shown). Several polyclonal (Stearns and Kirschner, 1994; Zheng et al., 1995) and monoclonal antibodies (Novakova, 1996) (T-6557; Sigma Chemical Co., St. Louis, MO) to γ–tubulin were used for immunoprecipitations, immunofluorescence, and immunoblotting as indicated. Antibodies to centrin and p50 were used as described (Echeverri et al., 1996; Salisbury, 1995). Cyclin antibodies were obtained from Santa Cruz Biotechnology (Santa Cruz, CA).

Cells and Cell Synchrony

Cell lines (CHO, COS, *Xenopus* tissue culture, and XTC) were grown as described (American Type Culture Collection, Rockville, MD) and mouse eggs were obtained as described (Doxsey, 1994 #34). Highly synchronized mitotic CHO cells were released and collected at various stages of the cell cycle (Sparks et al., 1995). Cell cycle stage was determined by time after release from metaphase, DNA morphology, microtubule pattern and centrosome number and position as described (Sparks et al.,

1995). In some cases, cells were released in the presence of cycloheximide (10 μg/ml; Sigma Chemical Co.).

Preparation of Cell Lysates and Xenopus Extracts

Xenopus extracts were prepared from eggs arrested in mitosis and interphase, centrifuged at high speed as described (Murray, 1989; Stearns and Kirschner, 1994), and used for immunoprecipitations, immunodepletions, sucrose gradients, and aster assembly reactions. Spindles and half spindles were prepared as described (Sawin, 1991; Walczak, 1996). COS cell lysates were prepared after release of cells from plates with trypsin and pelleting. Cells were washed in Hepes 100 buffer with 0.1 mM GTP and protease inhibitors (Zheng et al., 1995), and then lysed by sonication. Lysates were spun at 100,000 *g* for 30 min, and the supernatant was used for immunoprecipitations and sucrose gradients. Mitotic CHO cells were pelleted, boiled in 0.1% SDS in 50 mM Tris, pH 7.6, sonicated, and then diluted 1:20 with PBS containing 0.5% BSA. Reagents were added to lysates to achieve concentrations in radioimmunoprecipitation assay (RIPA) (Sparks et al., 1995), and immunoprecipitations were done with antibodies to pericentrin and Western blots were done with antibodies to γ–tubulin (see below).

Immunoprecipitation and Western Blotting

Antibodies to γ–tubulin, pericentrin (5 μg IgG), and preimmune IgGs (8 μg IgG) were prebound to 20 μl of packed protein A beads (GIBCO BRL, Gaithersburg, MD),

and then added immediately to freshly prepared extracts. After incubation in 100 μl of *Xenopus* extract or cell lysate for 1 h at 4 °C, beads were washed in Hepes 100 buffer with 1 mM GTP and protease inhibitors (Zheng et al., 1995) with or without 0.1% Triton X-100 or 250 mM NaCl (Sigma Chemical Co.), and proteins were run on 7% gels unless otherwise stated. Controls included extracts incubated with either preimmune sera (pericentrin), rabbit IgG, or beads alone (γ–tubulin and pericentrin). γ-Tubulin preimmune sera (Zheng et al., 1995) is no longer available. No bands were observed under any of these conditions. Proteins were electrophoretically transferred to immobilon (Millipore Corp., Bedford, MA) and immunoblotted (Harlow, 1988). When possible, blotting was performed with antibodies from another species so IgGs used for IPs were not detected by secondary antibodies. Immunoblotting of γ-tubulin was performed with one of two mouse monoclonal antibodies (Tu-31 or T-6557; Sigma Chemical Co.) or polyclonal antibody (Zheng et al., 1995); blotting of pericentrin was done with M8. For immunodepletions, 7.5 μg of γ–tubulin IgG was used per 50 μl of extract, which was 30% more than that required to remove all detectable γ–tubulin from extracts as judged by consecutive immunoprecipitations (IPs) with 5 μg of antibody and Western blot. SDS-PAGE and immunoblotting were performed essentially as described (Harlow, 1988). The bands (~100 kD) seen in pericentrin immunoprecipitations probed with pericentrin antibodies (see Fig. 3*B*) were probably nonspecifically associated as they were never seen in isolated centrosome fractions (see Fig. 3*A*), they were not consistently observed in extracts, they did not co-migrate with the γ–tubulin or pericentrin fractions in sucrose

gradients (data not shown), and they were not seen with the RAT2 antibody (data not shown).

Sucrose Gradients, Gel Filtration, and Stoichiometry

Sucrose gradient sedimentation (continuous 10–40%) was performed on crude and high speed supernatants of *Xenopus* extracts (100 μl), COS cell lysates (150 μl), or reticulocyte lysates containing in vitro–translated, [35S]methionine-labeled, full-length mouse pericentrin (20 *m*l, TNT kit; Promega Corp., Madison, WI) (Doxsey et al., 1994) essentially as described (Stearns and Kirschner, 1994). In some cases Triton X-100 (0.1%) or NaCl (250 mM) was included in the gradients and the extracts. Sucrose gradient fractions were exposed to SDS-PAGE and immunoblotted with either M8 or Tu-31. Similar results were obtained by probing with M8, stripping the same blot (Harlow, 1988) and reprobing with Tu-31.

For gel filtration experiments, crude *Xenopus* extracts (1–10 mg, see above) were prepared and kept on ice for various times (30–120 min). Extracts were diluted (1:2 to 1:4) into Hepes 100 with 10% glycerol, protease inhibitors, and GTP (final 0.1 mM) and passed through a prewetted 0.45 μm Millex-GV low protein binding filter (Millipore Corp.). Filtered extract was exposed to fast pressure liquid chromatography using a Superose-6 gel filtration column (Pharmacia Biotechnology Inc., Piscataway, NJ) equilibrated in Hepes 100 buffer with 10% glycerol at 0.3

ml/min. Fractions (0.5 ml) were collected, protein was precipitated with trichloroacetic acid, and then samples were processed for immunoblotting as above.

Standards for sucrose gradients and gel filtration analyses were run at the same time and under the same conditions as experimental samples. Standards included thyroglobulin (19.4S, 8.4 nm, Stokes radius), apoferritin (6.7 nm, Stokes radius), catalase (11.4S), alcohol dehydrogenase (3.58S) (DeHaen, 1987; Jacobson et al., 1996) and other conventional lower molecular mass standards (Sigma Chemical Co.). Values for Stokes radius were determined by gel filtration as described (Siegel and Monty, 1966), and sedimentation coefficients were estimated by sucrose density sedimentation (Martin and Ames, 1960) using published tables of sucrose density and viscosity (DeDuve et al., 1959). Our gradients deviate from linear so only approximate ranges for S values at high sucrose concentration were determined. The estimated S values and Stokes radii were used to estimate the molecular mass of the protein complexes as described (Siegel and Monty, 1966) assuming a partial specific volume of 0.74 ml/g (DeHaen, 1987).

The ratio of pericentrin to γ -tubulin in the holocomplex and the number of molecules in extracts was estimated by quantitative Western blot using bacterially expressed proteins as standards (Doxsey et al., 1994; Stearns and Kirschner, 1994) (γ-tubulin clone was a gift from B. Oakley, Ohio State University, Columbus, OH). Pericentrin was not detectable in *Xenopus* extracts without enrichment, so sucrose gradient

fractions were used for quantitation, and both proteins were quantified within the same experiment. Signals in the linear response range were quantified using a Fluor/S Multiimager (Bio-Rad Laboratories, Hercules, CA). Values represent averages from five experiments in which individual values were obtained in triplicate. From these results, we determined that pericentrin represented ~0.001% of the total protein in extracts and values obtained for *g*-tubulin were in agreement with those previously published (0.01% of total protein; (Stearns and Kirschner, 1994)). The molar ratio of pericentrin to γ–tubulin was estimated to be ~ 1:30 (n=4).

Preparation of Cells and Cell Fractions for Imaging

Unless otherwise indicated, cells were permeabilized in 0.5% Triton X-100 in 80 mM Pipes, 1 mM MgCl2, 5 mM EGTA, pH 6.8, fixed in –20°C MeOH, and then processed for immunofluorescence as described previously (Doxsey et al., 1994). Several other methods were used to confirm the lattice structure including: 1 or 2% glutaraldehyde in PBS +/- 5 mM Ca2+ followed by MeOH after fixation, 4% formaldehyde in PBS, 4% formaldehyde with 0.05% glutaraldehyde in PBS, quick freeze at liquid helium temperature (4 degrees kelvin), followed by freeze substitution in acetone alone (Nicolas, 1993), in acetone with 1.5% glutaraldehyde, and in MeOH with 1.5% glutaraldehyde. No differences were observed in lattice structure under any of these conditions or if cells were permeabilized before fixation.

Centrosome images in Fig. 8, *C–F* were obtained from an unfixed CHO cell permeabilized for 60 s and incubated for 7 min with M8 (20 μg/ml). After washing (10 changes in 1 min), cells were incubated in cy3 donkey anti–rabbit IgG (cyDAR; Jackson Immunoresearch Laboratories, Inc., West Grove, PA) at 25 μg/ml for 5 min, washed 10 times in 1 min, mounted unfixed in Vectashield (Vector Labs, Inc., Burlingame, CA), and then imaged immediately.

Mouse oocytes arrested in metaphase of meiosis II were affixed to polylysine-coated coverslips, fixed in –20°C MeOH and processed to visualize pericentrin, microtubules, and DNA as described (Doxsey et al., 1994). *Xenopus* asters and spindles were labeled with antibodies to α–tubulin, pericentrin (M8, or γ–tubulin, Tu-31), and 4,6-diamidino-2-phenylindole (DAPI) as described (Doxsey et al., 1994). Centrosomes were isolated as described (Blomberg and Doxsey, 1998), and then immunostained for pericentrin.

Expression of Green Fluorescent Protein–Pericentrin

The S65T mutant of Green Fluorescent Protein (GFP) (Heim, 1995) was cloned into Xho and EcoRI sites of the plasmid pcDNA3 (InVitrogen, San Diego, CA). EcoRI sites were engineered onto the ends of amino acids 766–1,343 of pericentrin clone *l* pc1.1 (Doxsey et al., 1994) using PCR primers p2595 (5'-GCGAATTCATGCTGAAACGCCAACATGCTGAAGAGC-3') and p4322 (5'-GCGAATTCCTCGAGGCGCTTAATTTC-3'). The fragment was cloned into the

pcDNA3 vector and the sequence was found to be identical to that in the original clone. The construct was transfected into COS cells as described (2 μg, Lipofectamine; GIBCO BRL). Centrosome localization of the chimeric protein was shown by colocalization of GFP fluorescence with endogenous pericentrin labeled by immunofluorescence with M8. Centrosomes were imaged live in a 37°C, CO_2-perfused chamber 72 h after transfection; identical results were obtained with the full-length pericentrin. Incorporation of GFP–pericentrin into the centrosome lattice confirmed the structure seen by immunofluorescence and controlled for potential artifacts introduced during specimen preparation such as fixation, permeabilization, and antibody binding. On average, the lattice elements were slightly thinner (76 +/- 9 nm) than those imaged after indirect immunofluorescence (95 +/-11 nm), suggesting that antibodies (15 nm in length) used for indirect immunofluorescence increased lattice dimensions.

Microtubule Regrowth

For imaging microtubule–lattice contacts, CHO cells were prepared essentially as described (Brown et al., 1996a). Briefly, cells were treated with nocodazole (10 μg/ml) for 1.5 h at 37°C, washed rapidly five times in PBS at 37°C and incubated for various times at 37°C in medium. Cells were fixed and stained for *a*-tubulin and pericentrin as for centrosomes (above) and those demonstrating clear microtubule nucleation at the earliest time point (usually 1–2 min) were used for analysis (below).

Microtubule nucleation times were kept to a minimum to minimize the possible release of microtubules from nucleating sites (Mogensen et al., 1997).

Image Acquisition and Deconvolution

Images were recorded on a cooled CCD camera (Photometric, Tucson, AZ) using a Nikon inverted microscope and a 100*X* PlanApo objective with a 1.4 numerical aperture (N.A.). Images were taken at 100-nm intervals through focus (in z plane) with 56 nm per pixel (x, y), and restored to subvoxels of 28 X 28 X 50 nm as described (Carrington et al., 1995). Images in Fig. 10 were taken with a 60 X PlanApo, N.A.=1.4. Fluorescent beads (189 nm) were imaged under the same optical conditions as the cell, and the microscope point spread function (PSF) was calculated on a subpixel grid. The dye density was then estimated by the non-negative function, f , that minimizes

$$\|g - PSF \times f\|^2 + \alpha \int\int\int |f|^P,$$

where g is the measured cell image. Resolution of images was improved over previous studies by using values of $P<2$. Images were reconstructed according to the algorithm with the following range of parameters: $a = 10^{-7}$–10^{-12}, P 5 1.08–2 with 1,000–1,500 iterations. The images were gradient shaded, displayed as three-dimensional projections, and in some cases pseudocolored.

Other structures imaged by this technique included a mitochondrial inner membrane protein (MCA-151A; Harlan Sprague Dawley Inc., Indianapolis, IN), a lysosomal membrane protein (provided by S. Green, University of Virginia, Charlottesville, VA), an *Escherichia coli* outer membrane protein (PLA protease; J. Goguen, University of Massachusetts Medical Center, [UMMC], Worcester, MA), and DNA of somatic cells and bacteria. DNA had the characteristic pattern described recently using a similar technique (Urata, 1995). As described in the text, centrioles imaged by this technique consistently had barrel diameters of 230 +/- 11 nm (*n* 523), similar to that seen by electron microscopy (~200 nm). Centriole length was more variable (350–500 nm) possibly because of impeded access of antibody at centriole ends enveloped by the lattice. In fact, the length of basal bodies (centrioles that lack lattice material) in tracheal epithelium (450–550 nm, *n* 5 14; data not shown), were closer to the length expected from electron microscopy (500 nm).

Quantitation of Fluorescence Signals from Centrosomes

To quantify centrosome protein levels through the cell cycle (see Fig. 12), CHO cells were fixed in –20 °C MeOH and stained for pericentrin (M8) and γ–tubulin (Tu-30) together or separately. Two-dimensional digital images were captured on a CCD camera and processed on a Silicon Graphics workstation (Mountain View, CA). A square measuring 71 *X* 71 pixels (~4 *X* 4-μm box) was centered on the centrosome and the mean intensity per pixel was determined. Background values recorded by the same method in another area of the cytoplasm and those used to correct for camera

noise were subtracted and accounted for 5% of experimental values. Similar results were obtained in five separate experiments and when secondary antibodies were switched. Values for each experiment were obtained from cells on a single coverslip. Similar results were obtained with COS cells. Each time point represents an average of 15–35 values. Similar results were obtained using an Adherent Cell Analysis System (ACAS 570; Meridian Instruments, Ann Arbor, MI). To determine the relative amount of pericentrin at the centrosome and in the cytoplasm, nonpermeabilized cells were used, and the total cellular and centrosomal levels were determined as above. Cytoplasmic fluorescence was calculated by subtracting centrosomal from total cellular fluorescence. The distribution of the pericentrin fluorescence changed in mitosis, although the total cellular fluorescence remained the same.

Coincidence of Fluorescence Signals and Fluorescence Resonance Energy Transfer

The data analysis and visualization environment (DAVE) (Lifschitz, 1994) was used to visualize images in three dimensions, to superimpose them, and to determine the extent to which they coincided. Staining coincidence was determined by imaging centrosomes within a 2-μm^3 area that included all detectable fluorescence in both wavelengths; smaller volume measurements gave similar values. To ensure proper alignment, fiducial beads were used (Carrington et al., 1995). Colocalization was expressed as the number of 28-nm voxels (volume pixels) occupied by two signals

over all voxels occupied by the pericentrin signal, (all non-zero voxels were included in the analysis). Colocalization statistics were unaffected by any visual aids used to modify images. Microtubule–lattice contacts were determined in a similar fashion by statistical analysis of coincident signals between microtubule ends and lattice elements. The percentage of microtubule ends contacting the lattice was similar when either pericentrin or γ-tubulin was used to stain the lattice.

Fluorescence resonance energy transfer (FRET) is a distance-dependent interaction between two fluorophores in their excited states where the excitation of the donor molecule (FITC) is transferred to an acceptor molecule (TRITC) without the emission of a photon. If FRET occurs, it can be monitored by the quench of the donor and the sensitized emission of the acceptor (Stryer, 1978; Wu and Brand, 1994). We created a FRET imaging system and calibrated it by adapting the methods of Ludwig et al. (1992). The two greatest obstacles to accurate, semi-quantitative FRET measurement using this system are filter bleedthrough and photobleaching. To measure sensitized emission, we created a "transfer" (FITC to TRITC) filter setup—480-nm excitation, but emission at 570 nm. Using this filter configuration, FITC excitation results in some non-FRET donor bleedthrough to the 570-nm emission (due to spectral emission overlap) as well as causing some direct (non-FRET) excitation of acceptor (due to spectral excitation overlap). These values were empirically measured with pure dye samples (conjugated to IgG) and later subtracted to correct the data (see

below). In addition, we normalized the three-dimensional data sets to the original unbleached intensities by initially imaging single planes of each channel.

CHO cells were prepared for immunofluorescence (above) using pericentrin (M8 antibody) as the donor and the second antigen (γ-tubulin, centrin, or A102 antibody) as acceptor. Using a Nikon inverted epifluorescence microscope equipped with a CCD camera we recorded single-plane images of each contributing antigen in the transfer channel, and then three-dimensional sets were captured with identical exposure times. Images were prepared for restoration (above) except that plane normalization was set to the single-plane values recorded before three-dimensional sets. After restoration and alignment, the empirically calculated spectral overlap (mean *6* 3 standard deviations) contributed by FITC and TRITC were subtracted from the transfer channel on a voxel-by-voxel basis, accounting for .99% of the total possible bleedthrough. The resulting image pairs for each set of antigens were subjected to two analyses to detect genuine FRET: (*1*) all nonzero voxels of the corrected sensitized emission (transfer channel) were displayed as a three-dimensional projection with the same scale for linear comparison of intensities and distribution, and second, the ratio of the sensitized emission to the donor emission was calculated (transfer/ FITC) within identical subregions of the corrected images. This ratio analysis relies on both donor quench and sensitized emission and is therefore very sensitive to FRET (Adams et al., 1991; Ludwig et al., 1992; Miyawaki et al., 1997). The means (n = 10–12) were determined within a 140-nm square

throughout several regions of the image chosen randomly, and the mean +/- SD were calculated for each antigen pair (n = 3).

Results

Pericentrin and γ–Tubulin Are Part of a Protein Complex in Xenopus Extracts

Xenopus eggs are an excellent source of centrosome components as each stockpiles material sufficient to assemble </=2,000 centrosomes (Gard, 1990). These components assemble into centrosomes upon fertilization and throughout the early divisions of the embryo. We characterized the state of pericentrin in *Xenopus* egg extracts by sucrose gradient sedimentation, gel filtration analysis, and immunoprecipitation experiments. We used antibodies previously generated against a mouse recombinant protein that recognized *Xenopus* centrosomes by immunofluorescence (Doxsey et al., 1994) and reacted with a single protein of ~210 kD in *Xenopus* centrosome fractions, similar in molecular mass to mouse pericentrin.

In freshly prepared extracts subjected to sucrose gradient centrifugation, pericentrin migrated in the high density fractions, suggesting that it was in the form of a large protein complex (Fig. 5 *B*). This was in contrast to the protein produced by in vitro translation of pericentrin mRNA, which sedimented much more slowly (Fig. 5 *A*). The sedimentation properties of pericentrin were roughly similar to those previously observed for γ-tubulin (Stearns and Kirschner, 1994; Zheng et al., 1995), suggesting

that the proteins may be part of the same complex. When analyzed together in the same experiment, the proteins were found to comigrate in sucrose gradients (Fig. 5, *B* and *C*). Moreover, when extracts were subjected to gel filtration analysis, both proteins co-eluted in the same fractions (Fig. 6 *A*). These results indicate that pericentrin and γ–tubulin are either part of the same complex or components of distinct complexes with similar biochemical properties.

To distinguish between these possibilities, we performed a series of immunoprecipitation experiments (Fig. 7). When γ-tubulin was immunoprecipitated from extracts, pericentrin was detected by immunoblotting (Fig. 7 *C*); conversely, when pericentrin was immunoprecipitated from extracts, γ-tubulin was detected on immunoblots (Fig. 7 *E*). Similar results were obtained when immunoprecipitations were performed with different antibodies to pericentrin and γ–tubulin and when mammalian cell extracts were used (data not shown). In contrast, neither protein was detected when preimmune IgGs or immunobeads were used (Fig. 7, *F* and *G*). When γ-tubulin was exhaustively immunodepleted from extracts, the majority (85–95%) of pericentrin was depleted as well. This was most clearly demonstrated when immunodepleted extract was analyzed on sucrose gradients (Fig. 5, *D* and *E*) and compared with starting material (Fig. 5, *B* and *C*). Taken together, the results from three independent biochemical methods demonstrate that most, if not all, of the pericentrin and γ–tubulin in *Xenopus* extracts is in the form of a large complex.

Pericentrin Is Not Part of the γ-TuRC

The association of pericentrin with a large protein complex containing γ-tubulin suggested that it may be part of the γ–TuRC. To our surprise, pericentrin was not detectable in purified γ–TuRC preparations (Zheng, 1995), even when the γ-tubulin signal was fivefold greater than that detected in immunoprecipitations (Fig. 7, *H* and *I*). A clue to this apparent discrepancy came when immunoprecipitates were washed with nonionic detergent or 250 mM salt. Under these conditions, pericentrin was no longer detected in γ–tubulin immunoprecipitations (data not shown). Furthermore, the proteins no longer comigrated on sucrose gradients in the presence of detergent, but sedimented as distinct subcomplexes in fractions of lower density (Fig. 5, *F* and *G*). γ–Tubulin shifted only slightly, whereas pericentrin shifted several fractions; the slight shift in γ–tubulin may have gone undetected in previous studies (Stearns, 1994). In gel filtration experiments, disruptive conditions (e.g., extended periods on ice) also yielded two separate subcomplexes (Fig. 6 *B*, *open arrows*). The sensitivity of the large complex to these and other treatments was decreased in the presence of glycerol and was variable between extract preparations.

Results from these biochemical analyses were used to estimate the molecular mass of the complex. From the sucrose gradients, we estimated the sedimentation coefficient of the complex to be 38–48S. From gel filtration experiments, we estimated the Stokes radius of this large complex as ~15–16.5 nm. On the basis of the sedimentation coefficient and the Stokes radius, we calculated the relative molecular

mass of the complex to be 2.5–3.5 MD as described (Siegel and Monty, 1966) using a partial specific volume of 0.74 (DeHaen, 1987). The stoichiometry of pericentrin and γ-tubulin in extracts was determined by quantitative analysis of immunoblots using recombinant proteins as standards (see Materials and Methods; (Doxsey et al., 1994; Stearns and Kirschner, 1994). By this analysis, we estimated that pericentrin and γ-tubulin represented 0.001 and 0.01% of the total protein in extracts, respectively; the estimate of γ-tubulin in extracts was in agreement with previous studies (Stearns and Kirschner, 1994). The stoichiometry of the proteins was calculated to be one pericentrin molecule for every ~30 γ-tubulin molecules. Based on the stoichiometry of pericentrin and γ–tubulin and the relative molecular mass of the complex containing both proteins, we estimate that there are two γ–tubulin subcomplexes and one pericentrin subcomplex complex in each large co-complex (see Discussion)[1].

Pericentrin Defines a Novel Lattice at the Centrosome

Identification of a soluble complex containing pericentrin and γ-tubulin suggested that these proteins may also be in close proximity at the centrosome. To address this,

[1] Following publication of these results, the molecular masses of these complexes were more accurately defined by incorporating higher S value markers in the sucrose gradients, and by running peak sucrose fractions on the gel filtration column. Based upon these revised figures, there is only one γTuRC per holocomplex. The corrected values are as follows:

Protein Complex	Sedimentation Coefficient	Stokes Radius	Calculated molecular weight
Holo Complex	41 S	16.8 nm	3.0 MDa
γTuRC	34 S	11.7 nm	1.9 MDa
Small Pericentrin Complex	14 S	11.7 nm	7.4×10^5 Da
Invitro translated pericentrin	6.0 S	16.2 nm	4.3×10^5 Da

we examined the distribution of the proteins at the centrosome using an advanced mathematical algorithm for deconvolution of immunofluorescence images that provides at least fourfold greater resolution than conventional imaging methods (theoretically ~70 nm) (Carrington et al., 1995). For this analysis, optical sections of centrosomes were taken every 100 nm through focus, captured on a cooled CCD camera, and then the resulting images were restored by deconvolution using the algorithm.

We initially examined the organization of pericentrin at the centrosome. By conventional imaging methods, the immunofluorescence signal for pericentrin appeared as a simple focus of material (Fig. 8, *B* and *C*) at the center of microtubule asters (Fig. 8 *A*). More detail was provided using previously developed deconvolution software based on exhaustive photon reassignment (Fig. 8 *D*; Scanalytics, Billerica, MA). When the image was restored using the advanced algorithm, a striking, highly organized reticular network was revealed (Fig. 8, *E* and *F*, stereo pair). This lattice-like structure was composed of a variable number of interconnected rings (273 +/- 43-nm diam) with linear projections radiating from its periphery. Elements of the lattice were ~100 nm in width (γ-TuRC diameter is 25–28 nm, for comparison) and they sometimes formed angles of 120 degrees (e.g., Fig. 8 *E*, *bottom left*). The lattice was often surrounded by smaller unconnected aggregates of pericentrin-staining material (e.g., Fig. 8, *E* and *F*), previously shown to be pericentriolar satellites (Doxsey et al., 1994). These structures were confined to the region occupied by the

centrosome (0.7–2.3-μm diam) and no other significant pericentrin-staining material was observed in the cytoplasm. Centrioles (Fig. 8, *J* and *K*) were located at the center of the pericentrin lattice (Fig. 8, *G–I*) in discrete lattice-free areas (Fig. 8 *I*) with dimensions roughly similar to those of the centriole barrels. Although not completely resolved, centrioles retained the general structure and dimensions observed by electron microscopy (~200 *X* 500 nm), demonstrating the high resolving power of the deconvolution method. Taken together, this analysis demonstrates that pericentrin forms a novel lattice structure that surrounds the centrioles of mammalian centrosomes.

To verify the unique structure defined by pericentrin staining, we analyzed centrosomes under a number of different conditions. The structural details were preserved under a wide range of fixation methods (e.g., quick freeze/ freeze substitution), in the absence of fixation (Fig. 8, *E* and *F*) and after centrosome isolation and centrifugation onto coverslips (Fig. 8, *G–K*) (Blomberg and Doxsey, 1998). An indistinguishable structure was observed when a protein chimera of pericentrin and GFP was used to label centrosomes in living cells and imaged directly without antibody incubations (Fig. 8, *L–O*) (Prasher, 1992; Young et al., 1998).

We next examined the organization of pericentrin in centrosomes of other species and in morphologically different structures that function as MTOCs. A similar network of pericentrin staining was observed in centrosomes of cultured *Xenopus* cells, at the

poles of *Xenopus* mitotic spindles assembled in vitro (Fig. 9, *A* and *B*), and in the elongated acentriolar poles of meiotic spindles in mouse oocytes (Fig. 9, *C* and *D*). The conserved organization of pericentrin in centrosomes of divergent organisms and in different types of MTOCs suggests that it may play an important role in centrosome function. Insight into the functional significance of the pericentrin lattice was initially provided when we examined the organization of γ-tubulin, the protein implicated in microtubule nucleation (Oakley and Oakley, 1989; Zheng et al., 1995).

Pericentrin and γ–Tubulin Are in Close Proximity in the Lattice

We examined the three-dimensional organization of γ–tubulin and its relationship to the pericentrin lattice using double-label immunofluorescence methods. Images restored at high resolution showed that the staining pattern of γ–tubulin was strikingly similar to pericentrin in centrosomes of somatic cells examined *in situ* (Fig. 10, *A* and *B*). Quantitative analysis of restored and aligned images using three dimensional image analysis software (Lifschitz, 1994) revealed that the distribution of the pericentrin and γ-tubulin signals was nearly identical (Fig. 10 *E*). For comparison, the degree of signal overlap (Fig. 10 *E*, bar *3*) was similar to that observed when a single pericentrin antibody was detected with two different fluorophore-conjugated secondary antibodies, or when monoclonal and polyclonal pericentrin antibodies were detected with different secondary antibodies (Fig. 10 *E*, bars *1* and *2*). In contrast, other proteins that localize to the centrosome such as dynactin (Fig. 10, *C* and *E*, bar *5*; (Echeverri et al., 1996)) and centrin (Fig. 10 *E*, bar *4*; (Salisbury, 1995)) did not

colocalize significantly with pericentrin, demonstrating the unique distribution of γ-tubulin and pericentrin at the centrosome.

The proximity of pericentrin and γ–tubulin at the centrosome was more directly measured using FRET, a method that has become a powerful approach for studying protein–protein interactions (Adams et al., 1991; Miyawaki et al., 1997). In cells colabeled for pericentrin (fluorescein) and γ–tubulin (rhodamine), fluorescein excitation (donor) resulted in strong, sensitized emission from rhodamine (acceptor), demonstrating energy transfer between the proteins (Fig. 11). Restoration of the sensitized emission signal at high resolution revealed a lattice remarkably similar to that generated by the fluorescein donor signal (Fig. 11, compare *A* with *B*). To our knowledge, the acquisition of high resolution immunofluorescence images from signals generated by energy transfer is a unique and powerful application of FRET. Little energy transfer was observed when pericentrin antibodies were used in combination with centrin antibodies as shown by the low intensity of the sensitized emission, the reduced structure generated by image restoration (Fig. 11, compare *C* with *D*) and the comparatively low FRET ratio (Fig. 11 *E*, bar *3*). The FRET ratio (sensitized emission/donor emission) is another measure of energy transfer and is highest when there is strong sensitized emission and quenching of the donor (Ludwig et al., 1992; Miyawaki et al., 1997; Wu and Brand, 1994). The FRET ratio obtained with antibodies to pericentrin and γ–tubulin (Fig. 11 *E*, bar *2*) was similar to that obtained when two pericentrin antibodies were used (Fig. 11 *E*, bar *1*), suggesting that

the proteins were in close proximity at the centrosome. Calculations based on the use of two primary –secondary antibody complexes (maximal extended length ~68 nm), and the distance at which FRET drops to <1% in this system (12 nm), suggest that the two proteins are not >80-nm apart. The proteins are likely to be much closer considering the strength of FRET and the nearly identical structure generated by the sensitized emission. The close proximity of the proteins is consistent with the idea that they remain in a complex (Figs. 5–7) after assembly at the centrosome.

Progressive Assembly and Catastrophic Disassembly of Pericentrin and γ–Tubulin during the Somatic Cell Cycle

The coexistence of pericentrin and γ–tubulin in a soluble protein complex and at the centrosome suggested a dynamic relationship between the two cellular fractions containing these proteins. As an initial test of this idea, we examined changes in the centrosome-associated fractions of the proteins in CHO cells at various cell cycle stages by quantifying immunofluorescence signals. In contrast to previous models suggesting a rapid accumulation of centrosome components shortly before metaphase (Kuriyama, 1981), we observed a progressive increase in the centrosome-associated fraction of both proteins from basal levels in G1, to maximal levels at metaphase (Fig. 12 *A*). The total centrosomal fluorescence per cell (Fig. 12 *A*, *bottom*) increased five- to sevenfold over this time period. The kinetics of protein accumulation at the centrosome was nearly identical for pericentrin and γ–tubulin demonstrating that they were incorporated coordinately.

Whereas ~16 h were required to accumulate maximal levels of pericentrin and γ-tubulin at the centrosome, it took only 15–20 min for the centrosome-associated fluorescence signals to drop to basal levels as cells exited mitosis (Fig. 12 *A*, *M Æ T*). This precipitous drop in centrosomal fluorescence of both proteins occurred with indistinguishable kinetics demonstrating, as in assembly, that they underwent coordinate disassembly from the centrosome. Both proteins redistributed quantitatively from the centrosome to the cytoplasm as shown by an increase in cytoplasmic fluorescence (pericentrin, 5.2 *X* 10^5 fluorescence units; γ–tubulin, 2.8 *X* 10^5 units) that occurred concomitant with a reciprocal decrease in centrosomal fluorescence (pericentrin, 4.9 *X* 10^5 units; γ–tubulin, 2.7 *X* 10^5 units). This protein redistribution occurred with no detectable change in the total cellular fluorescence or in the total biochemical levels of the proteins (Fig. 12 *B*, *1* and *2*). In fact, protein levels remained unchanged for several hours after mitosis and were unaffected when protein synthesis was inhibited (data not shown). In contrast, cyclin B was degraded to near completion during this time (Fig. 12 *B*, *3*). These results suggest that the bulk of pericentrin and γ–tubulin redistributes from the centrosome to the cytoplasm upon exit from mitosis and that the proteins are not significantly degraded during this time but are probably reused for subsequent rounds of centrosome assembly.

Cell Cycle Changes in the Lattice

The cell cycle changes in centrosome-associated levels of pericentrin and γ–tubulin (Fig. 12 *A*) were accompanied by dramatic changes in lattice complexity (number of rings) and overall size (Fig. 12 *C*). In G1, the lattice was smallest and least complex (Fig. 12 *C*, *left*). It enlarged progressively over a period of 16 h, reaching maximal dimensions in G2 (Fig. 12 *C*, *middle*). The lattice split in mitosis to form two metaphase structures of intermediate size and intrinsic polarity, being open at one end and rounded at the other (Fig. 12 *C*). As cells exited mitosis, the metaphase lattices rapidly disassembled (15–20 min) returning to the simple structure shown in Fig. 12 *C* (*left panel*). These data demonstrate that the dramatic cell cycle changes in the complexity of the lattice correlate closely with the levels of pericentrin and γ-tubulin at the centrosome (Fig. 12 *A*).

Relationship of the Lattice and Nucleated Microtubules

Since both pericentrin and γ–tubulin have been implicated in microtubule nucleation and organization (Doxsey et al., 1994; Zheng et al., 1995) and since γ–tubulin is found at the minus ends of microtubules in the centrosome matrix (Moritz et al., 1995a), we reasoned that the centrosome lattice containing these proteins may be involved in microtubule nucleation. To test this possibility, cells were treated with nocodazole to depolymerize microtubules, incubated briefly without the drug to capture early microtubule nucleation events, and then processed for immunofluorescence staining of microtubules and centrosome using the Carrington

algorithm (see Materials and Methods). Microtubules were resolved as single filaments or bundled and branching arrays and nucleation sites were defined as regions of contact between the minus ends of nucleated microtubules and lattice elements (Fig. 13). Centrosomes from telophase, G1, and early S phase (Fig. 13, *S*) were used for this analysis since the microtubule–lattice contacts were clearer than in more complex centrosomes (Fig. 13, *G2*). Quantitative analysis of contact sites identified by overlapping signals (Fig. 13, *inset*, *white*) showed that most microtubule ends contacted lattice elements (79 +/- 5.1%,n = 7 asters). These data suggest that the lattice composed of pericentrin and γ–tubulin may provide the structural basis for microtubule nucleation at the centrosome.

Discussion

The sites of microtubule nucleation in most animal cells are found primarily at centrosomes or other types of MTOCs. Here we show that pericentrin and γ–tubulin are part of a novel centrosome lattice that contacts the ends of nucleated microtubules and may provide the structural basis for microtubule nucleation. Pericentrin and γ–tubulin are also found together in a large protein complex and they assemble onto and disassemble from the lattice in a cell cycle–specific manner. These observations indicate that the pericentrin–γ–tubulin lattice may represent the higher order organization of microtubule nucleating sites at the centrosome and that assembly and

disassembly of the lattice may play a role in regulating microtubule nucleation in the cell.

The Pericentrin– γ–Tubulin Complex and Centrosome Assembly

We have identified a large soluble protein complex comprised of pericentrin and γ–tubulin. Since both proteins are highly conserved through evolution (Doxsey et al., 1994; Oakley and Oakley, 1989; Zheng et al., 1995), it is possible that the complex containing these proteins is conserved in all animal cells. Disruption of the complex yields two subcomplexes (Fig. 14). One subcomplex contains γ–tubulin and may be the 25S complex previously reported (Stearns and Kirschner, 1994; Zheng et al., 1995) based on its migration in sucrose gradients. The other subcomplex contains pericentrin and has not been described previously. Little is known about the origin and composition of the pericentrin subcomplex, how it interacts with the γ-tubulin complex, and the functional consequences of this interaction. Based on the estimated masses of the complexes and the calculated stoichiometry of γ-tubulin and pericentrin (30:1), we propose that the co-complex of these proteins comprises one pericentrin complex and two γ–tubulin complexes (Fig. 14). This arrangement is consistent with both models currently proposed for microtubule nucleation. If the γ-tubulin complexes were γ–TuRCs each containing 13 γ–tubulin molecules (Zheng et al., 1995) the cocomplex would contain two γ–TuRCs plus a complex with one pericentrin molecule (stoichiometry, 26:1). (More accurate modeling will require characterization of the biochemical properties of the purified γ-TuRC (Zheng et al.,

1995).) If γ-tubulin complexes were pairs of protofilaments each containing ~28 γ–tubulin molecules (Erickson and Stoffler, 1996), the co-complex would contain two protofilament complexes plus a complex with two pericentrin molecules (56:2).

Based on these and other data, we propose a model for assembly of nucleating sites at the centrosome as shown in Fig. 14. The model predicts that pericentrin and γ–tubulin assemble at the centrosome to form the unique lattice structure (Fig. 14). Support for this idea comes from the tight correlation between protein accumulation at the centrosome and lattice growth (Fig. 12) and the ability to inhibit lattice growth by immunodepletion of pericentrin and γ-tubulin (Dictenberg, J., and S. Doxsey, unpublished observations). Pericentrin may play a direct role in the assembly process since it can induce the formation of ectopic centrosomes containing both pericentrin and γ–tubulin when overexpressed in cultured cells (Purohit, A., and S. Doxsey, manuscript in preparation). On the other hand, the γ–TuRC appears to lack assembly properties since purified fractions of the γ–TuRC are unable to assemble onto salt-stripped centrosomes (Moritz et al., 1995a). It is possible that the proteins assemble together as a large complex (Fig. 14) since they accumulate at the centrosome with indistinguishable kinetics (Fig. 12 *A*) and they remain in close proximity once assembled at the centrosome (Fig. 11). In addition, both appear to assemble together as tiny particles in living cells expressing GFP-pericentrin (Young, A., and S. Doxsey, unpublished observations). It is also possible that the proteins assemble (and

disassemble) as separate subcomplexes and that assembly requires other proteins and factors.

The Pericentrin–γ–Tubulin Lattice as the Higher Order Organization of Microtubule Nucleating Sites at the Centrosome

The structure of the centrosome has remained an elusive biological problem for over a century. The use of an advanced algorithm for improved deconvolution of immunofluorescence images has provided a new view of this organelle. A major strength of this approach is the ability to uncover centrosome structure through the three-dimensional analysis of specific molecular components as shown here for pericentrin and γ–tubulin. Although the resolution is considerably less than that obtained by electron microscopy (70–100 nm), the method overcomes many of the problems associated with immunoelectron microscopic techniques such as reagent penetration and compromised antigenicity (Griffiths, 1993) and may thus provide a clearer representation of centrosome structure at these intermediate magnifications. This high resolution immunofluorescence imaging method, together with FRET analysis, will provide a powerful tool to study the organization and relationship of various molecular components at centrosomes, spindles, and other sites in the cell.

Although we have not determined the precise molecular arrangement of pericentrin and γ-tubulin within the lattice, it is possible that pericentrin forms the backbone of the structure tethering pericentrin–γ–tubulin complexes at the centrosome (Fig. 14).

Pericentrin is predicted to be a large coiled-coil protein (Doxsey et al., 1994), which could serve as a molecular building block for the lattice in much the same way as coiled-coil intermediate filament proteins serve as subunits in the assembly of intermediate filaments (Albers, 1992). Other proteins most likely contribute to lattice organization, although we have not identified any that colocalize to the structure. The structural arrangement of other essential centrosome and mitotic spindle proteins (McNally, 1996; Merdes and Cleveland, 1997; Walczak, 1996) should provide information on the overall organization of centrosomes and spindles at a level unattainable by other methods.

Our results indicate that the lattice represents the organized arrangement of microtubule nucleating sites at the centrosome (Fig. 14). This idea is analogous to one proposed previously by Mazia (1987) that depicts the centrosome as a "string of microtubule initiating units" folded into a compact structure. In our model, the microtubule initiating units are pericentrin/γ-tubulin complexes linked together to form the lattice elements or "strings." The overall configuration of the lattice may account for the distinct microtubule arrangements observed in different MTOCs, such as the sharply focused arrays formed by compact centrosomes and the elongated, less-focused arrays that emanate from mouse meiotic spindle poles (Fig. 9, *C* and *D*). Within the lattice are regions that do not appear to nucleate microtubules, although both pericentrin and γ tubulin are found there (Fig. 13, see microtubule-free regions in *yellow*). If these regions represent potential microtubule nucleation sites as we

predict, the mechanism by which they acquire the ability to nucleate microtubules will be an important future area of investigation.

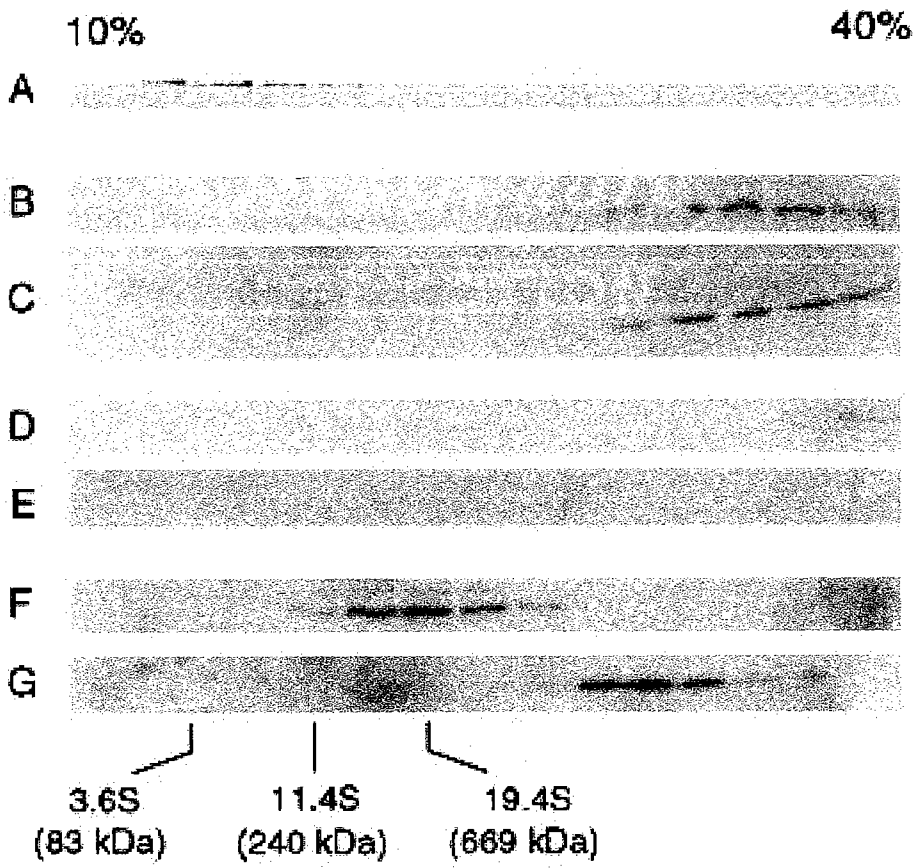

Figure 5

Figure 5. Pericentrin and γ-tubulin cosediment in sucrose gradients.

(*A*) In vitro–translated, [^{35}S]methionine-labeled mouse pericentrin was sedimented in sucrose gradients (10–40%) and exposed to SDS-PAGE as described in Materials and Methods. (*B* and *C*) *Xenopus* extracts were sedimented in sucrose gradients and immunoblotted using antibodies to pericentrin (*B*) or γ-tubulin (*C*). Parallel sample of the same extract immunodepleted of γ-tubulin (*D* and *E*) or treated with 0.1% Triton X-100 (*F* and *G*) before gradient centrifugation. Pericentrin immunoblots (*B*, *D*, and *F*); γ-tubulin immunoblots (*C*, *E*, and *G*). Molecular weight standards are for all panels.

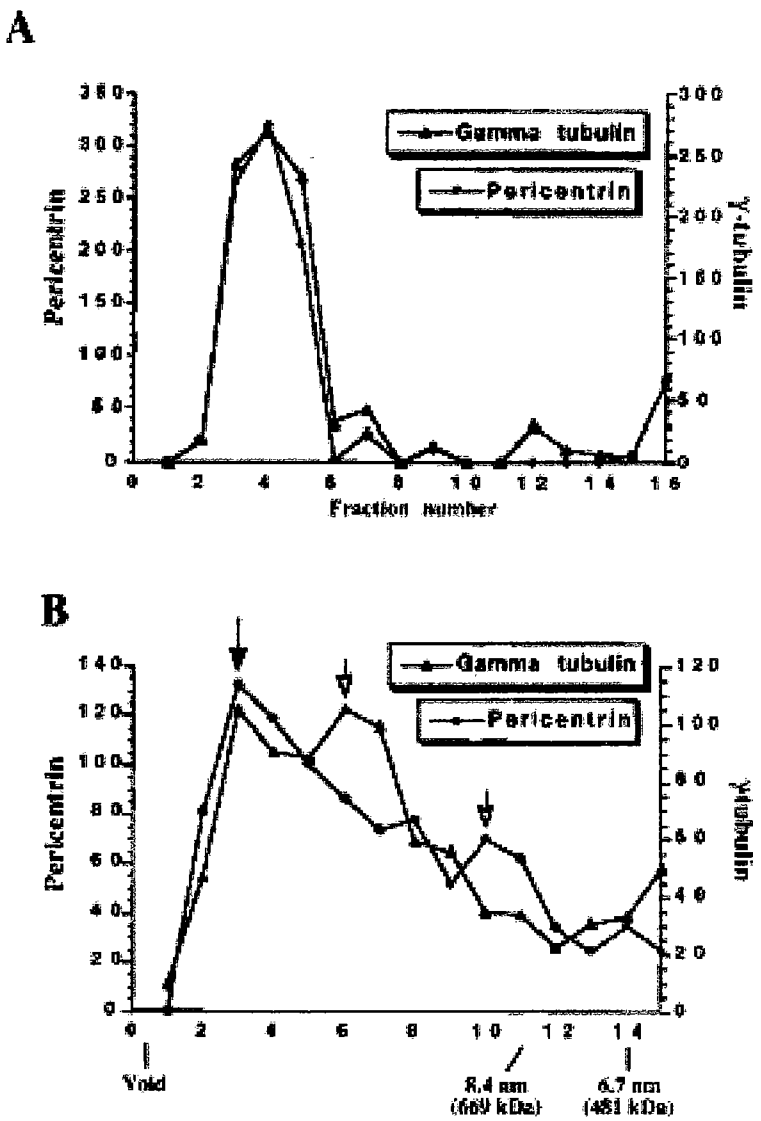
A
Gamma tubulin
Pericentrin
Pericentrin
γ-tubulin
Fraction number
B
Gamma tubulin
Pericentrin
Pericentrin
γ-tubulin
Void
8.4 nm
(669 kDa)
6.7 nm
(481 kDa)

Figure 6

Figure 6. Pericentrin and γ–tubulin cofractionate by gel filtration. *Xenopus* extracts were fractionated by gel filtration using a Superose- 6 column. Proteins were precipitated from fractions with trichloroacetic acid, immunoblotted using antibodies to pericentrin or γ–tubulin, and then resulting bands were quantified (see Materials and Methods for details). Under optimal conditions, the majority of γ-tubulin and pericentrin eluted together in fractions *3–5*, suggesting that they were part of a large complex (*A* and *B*, *closed arrow*). A variable portion of pericentrin eluted at fractions *5–7* and γ–tubulin at *9–11* (*B*, *open arrows*) when extracts were incubated for extended periods on ice (1 h). Y axes represent units of band intensity from Western blots.

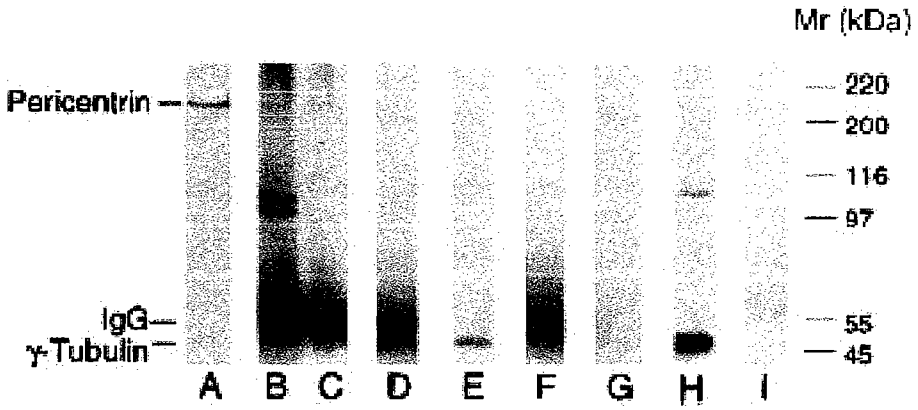
Mr (kDa)
Pericentrin
IgG
γ-Tubulin
220
200
116
97
55
45
A
B
C
D
E
F
G
H
I

Figure 7

Figure 7. Pericentrin coimmunoprecipitates with *g*-tubulin but is not part of the isolated γ–TuRC. Various cellular fractions were exposed to SDS-PAGE and immunoblotted with pericentrin or γ–tubulin antibodies. (*A*) Centrosome fractions prepared from *Xenopus* tissue culture cells as described (Blomberg and Doxsey, 1998) and probed with pericentrin antibodies. Pericentrin (*B*) or γ–tubulin (*C*) immunoprecipitated from freshly prepared *Xenopus* extracts and blotted with pericentrin antibodies. γ–Tubulin (*D*) or pericentrin (*E*) immunoprecipitated from freshly prepared *Xenopus* extracts and blotted with γ–tubulin antibodies. Precipitations performed with pericentrin preimmune sera and blotted with pericentrin antibodies (*F*) or with no antibody (immunobeads alone) and blotted with γ-tubulin antibody (*G*). Purified γ–TuRC fractions immunoblotted with antibodies to γ–tubulin (*H*) or pericentrin (*I*).

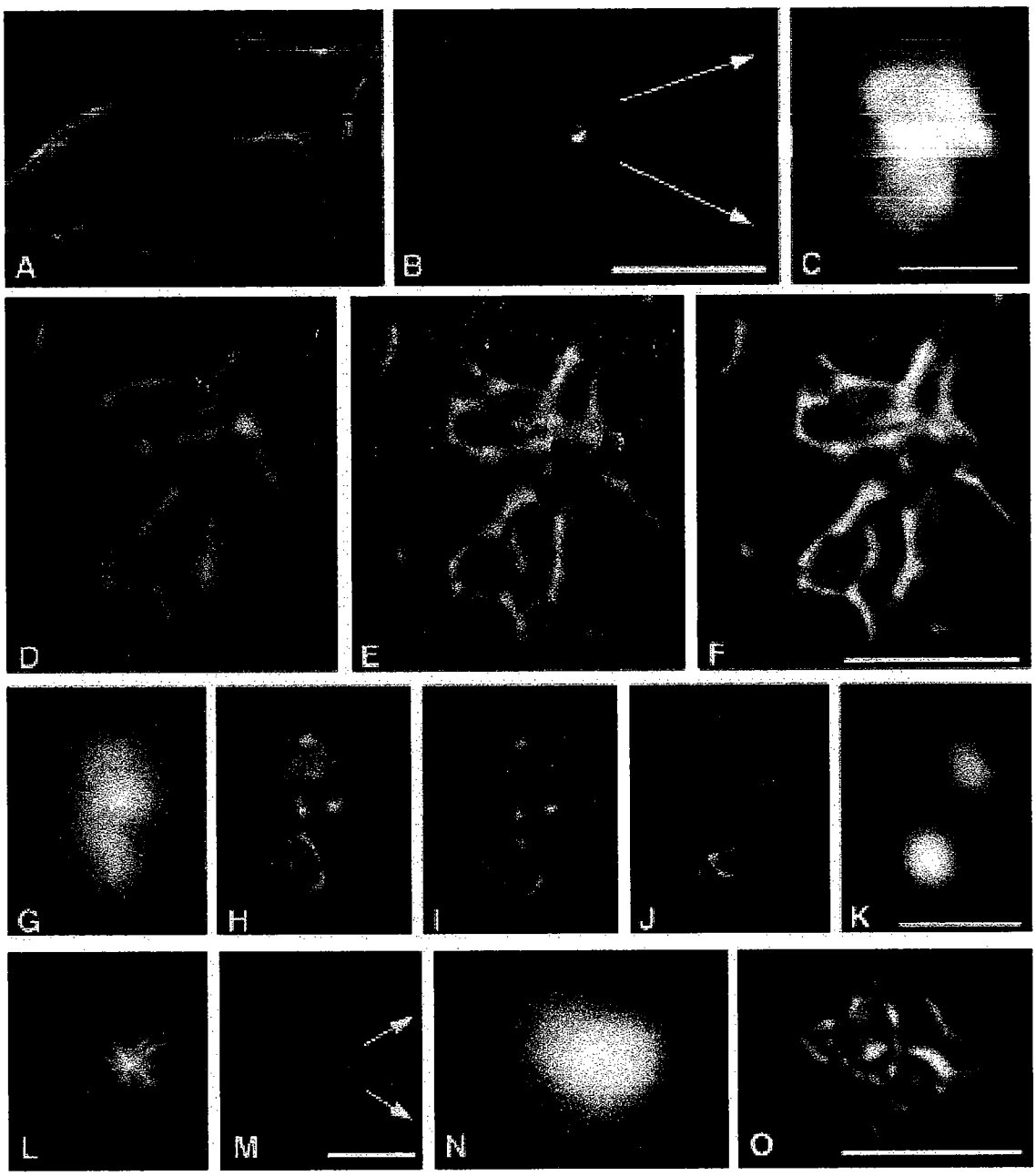

Figure 8

Figure 8. Pericentrin forms a novel lattice at the centrosome. Microtubule aster and centrosome from a CHO cell stained with antibodies to α-tubulin (*A*) and pericentrin (*B*) and imaged by conventional immunofluorescence methods. (*C*) High magnification of unfixed CHO cell centrosome imaged as in (*B*). (*D*) Image of same centrosome shown in (*C*) using commercially- available deconvolution software (Scanalytics). (*E* and *F*) High resolution stereo images of same centrosome in (*C*) restored by the algorithm of Carrington (1995) (*D*, *16* degrees; *E*, *26* degrees). (*G–K*) Centrosome isolated from a CHO cell and labeled with antibodies to pericentrin to visualize lattice (*G–I*) and α-tubulin to visualize centrioles (*J* and *K*). Before restoration, pericentrin (*G*) and α–tubulin (*K*). After restoration, pericentrin staining showing entire three-dimensional data set (*H*) or five central planes (*I*) and α–tubulin staining showing three central planes (*J*). The two areas devoid of pericentrin staining (*I*) represent positions occupied by centrioles (*J*). (*L–O*) GFP–pericentrin expressed in COS cells (*M*) localized to the center of a microtubule aster detected by α–tubulin immunofluorescence staining (*L*). GFP-pericentrin before (*N*) and after (*O*) image restoration. Bars: (*B*) 10 μm for *A* and *B*; (*C*) 1 μm; (*F*) 1 μm for *D–F*; (*K*) 1 μm for *G–K*; (*M*) 10 μm for *L* and *M*; (*O*), 1 μm for *N* and *O*.

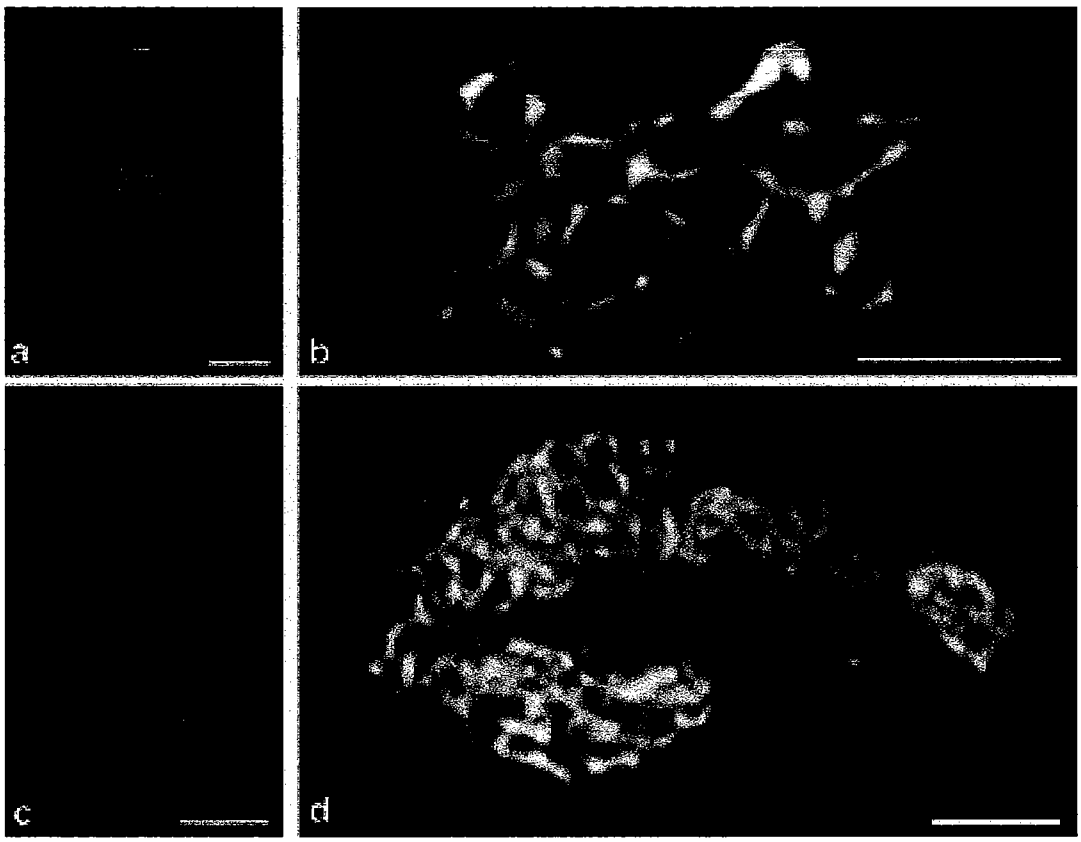

Figure 9

Figure 9. The lattice is a conserved feature of centrosomes and other MTOCs. (*A* and *B*) *Xenopus* spindle assembled in vitro. (*A*) Spindle labeled for pericentrin (*green*), α–tubulin (*red*), and DNA (*blue*), imaged by conventional methods and superimposed. (*B*) Restored image of centrosome at upper pole of spindle in *A*. (*C* and *D*) Acentriolar mouse meiotic spindle arrested in metaphase II. (*C*) Spindle labeled for α-tubulin (*green*), pericentrin (*red*), and DNA (*blue*) prepared as in *A*. (*D*) Restored image of spindle pole at top of image in (*C*). Note difference in magnification between *B* and *D*. Bars: (*A* and *C*) 5 μm; (*B* and *D*) 1 μm.

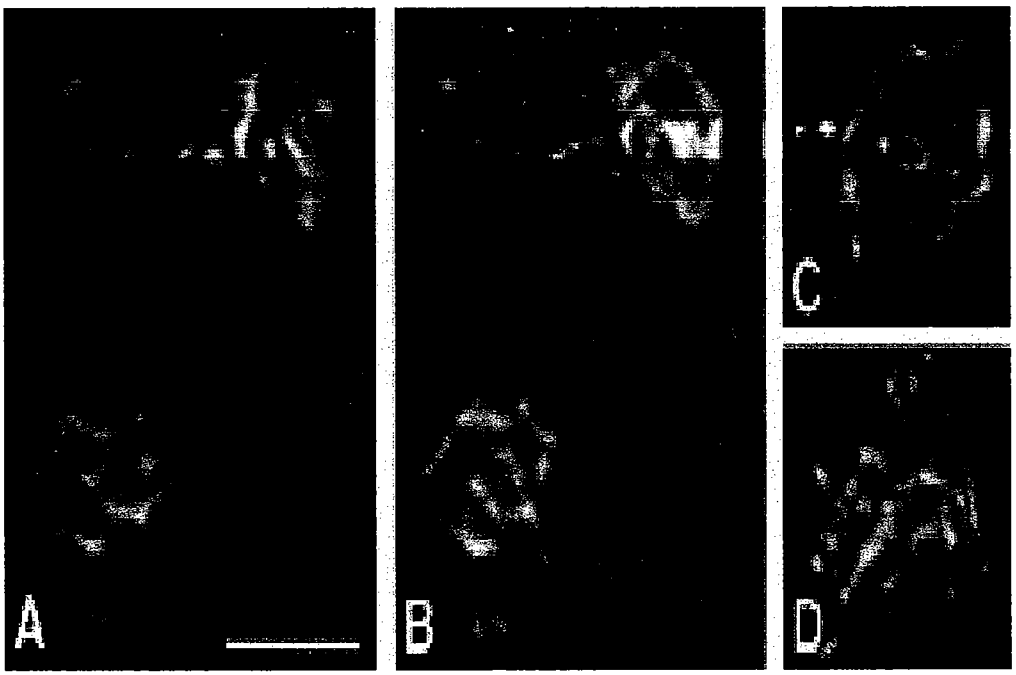

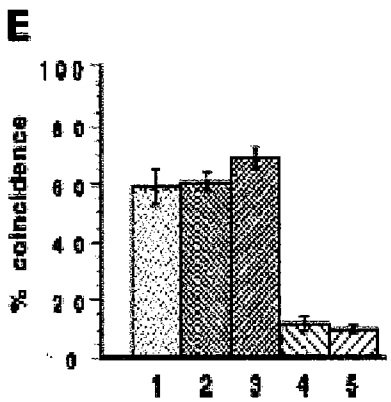

Figure 10

Figure 10. γ–Tubulin and pericentrin are part of the same lattice. (*A* and *B*) Restored images of two prophase centrosomes in CHO cells labeled by immunofluorescence for γ–tubulin (*A*) and pericentrin (*B*). (*C* and *D*) CHO cell centrosome stained for dynactin (*C*) and pericentrin (*D*). (*E*) Quantitative analysis of the coincidence of centrosome proteins in CHO cells using secondary antibodies tagged with different fluorophores (see Materials and Methods). Column *1*, rat anti-pericentrin/rabbit anti-pericentrin; column *2*, rabbit anti-pericentrin/mixed (fluorescein- and rhodamine-conjugated) anti–rabbit IgGs; column *3*, rat anti-pericentrin/ rabbit anti–γ–tubulin; column *4*, rabbit anti-pericentrin/ mouse anti-centrin; and column *5*, rat anti-pericentrin/rabbit antidynactin. Bar, 1 μm.

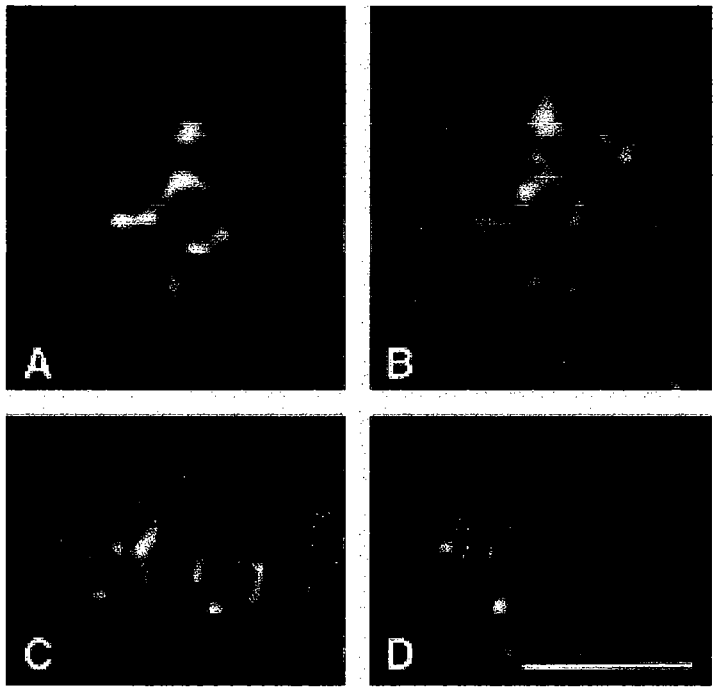

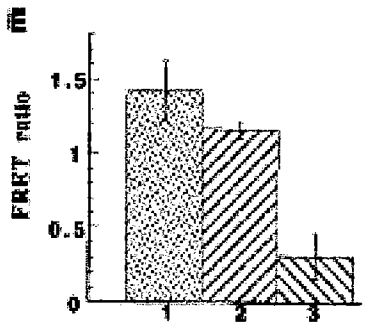

Figure 11

Figure 11. The proximity of γ–tubulin and pericentrin at the centrosome is sufficient to produce FRET. Centrosomes colabeled for pericentrin (*A*, fluorescein) and γ-tubulin (*B*, rhodamine), or for pericentrin (*C*, fluorescein) and centrin (*D*, rhodamine) were illuminated to excite fluorescein. Images were captured using fluorescein and rhodamine emission filters and restored as in Fig. 8. The image resulting from the transfer of energy to rhodamine-labeled antibody bound to γ–tubulin (*B*) is very similar to that generated by the donor signal (*A*). In contrast, images generated when antibodies bound to centrin serve as acceptor (*D*) represent a small subset of the pericentrin image (*C*). The FRET ratio (*E*) is expressed as the proportion of fluorescence generated by the acceptor over that generated by the donor (which is quenched after efficient transfer). The FRET ratio of pericentrin and γ–tubulin (*2*) is similar to that obtained with two pericentrin antibodies (*1*) and much greater than that of pericentrin and centrin (*3*). Bar, 1 μm.

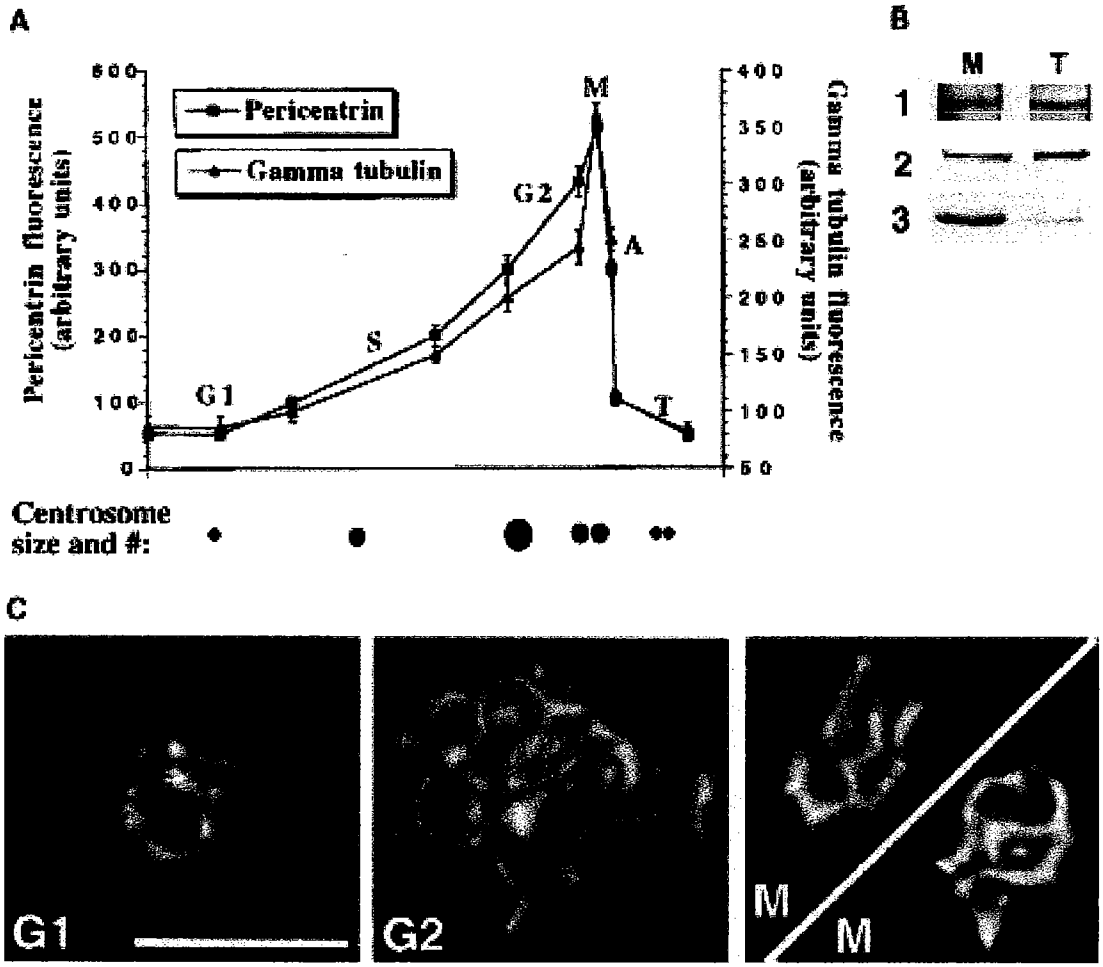
A
B
M
T
1
2
3
Pericentrin
Gamma tubulin
Pericentrin fluorescence (arbitrary units)
Gamma tubulin fluorescence (arbitrary units)
G1
S
G2
M
A
T
Centrosome size and #:
C
G1
G2
M
M

Figure 12

Figure 12. Dramatic cell cycle changes in the intracellular distribution of pericentrin and γ–tubulin and lattice structure. (*A*) Quantitative analysis of immunofluorescence signals from centrosome- associated pericentrin and γ–tubulin in CHO cells at various stages of the cell cycle (see Materials and Methods). Protein levels rise progressively from G1 until mitosis and then drop precipitously to basal levels. (*B*) Levels of pericentrin and γ–tubulin do not appear to change upon exit from mitosis. Lysates were prepared from metaphase cells (*M*) or from an equal number of metaphase cells induced to enter telophase (*T*; see Materials and Methods). Pericentrin was immunoprecipitated from lysates and immunoblotted with pericentrin antibodies as described in Fig. 3 (*panel 1*). Other lysates were used for immunoblotting with antibodies to γ-tubulin (Fig. 3 *B*, *panel 2*) or antibodies to cyclin B (Fig. 3 *B*, *panel 3*). Note that the cyclin B signal decreases from *M* to *T*, while the levels of pericentrin and γ–tubulin do not appear to change during this time. (*C*) Changes in lattice structure closely correlate with changes in the levels of centrosome-associated protein. The pericentrin lattice is simplest in G1 and enlarges to maximal size and complexity at G2, before separating to form a pair of centrosomes whose combined size at metaphase (*M*) is slightly larger than the G2 centrosome. When cells exit mitosis, the lattice rapidly returns to its simplest form (similar to that seen in G1). Similar results were observed with antibodies to γ–tubulin. Cell cycle stages: *G1*; *S*; *G2*; *M*, metaphase; *A*, anaphase; and *T*, telophase. Bar, 1 μm.

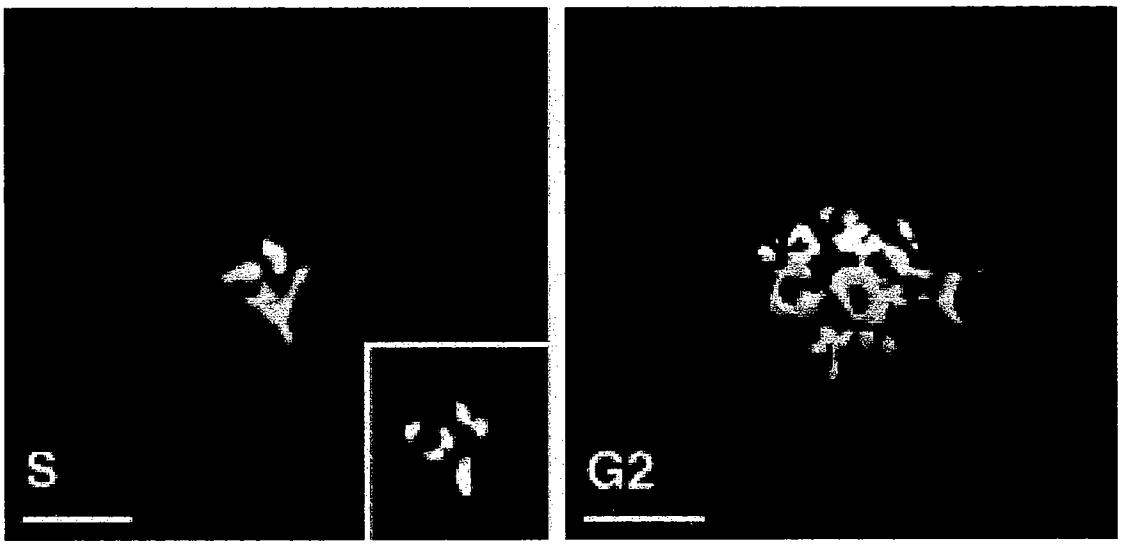

Figure 13

Figure 13. Nucleated microtubules contact the lattice. Images of nucleated microtubules (*red*) and pericentrin (*yellow*) have been merged to show that the number of nucleated microtubules converging at the centrosome (many bundled in *G2*) and the size of the pericentrin lattice increase from *S* to *G2* (also see Fig. 12, *A* and *C*). The inset in the first panel shows microtubule– lattice contacts in the simple early S phase centrosome. Inset shows the area of interaction (*white*) demonstrating near complete overlap of microtubule ends with lattice elements. See Materials and Methods. Similar results were obtained with γ-tubulin. Bars, 1 μm.

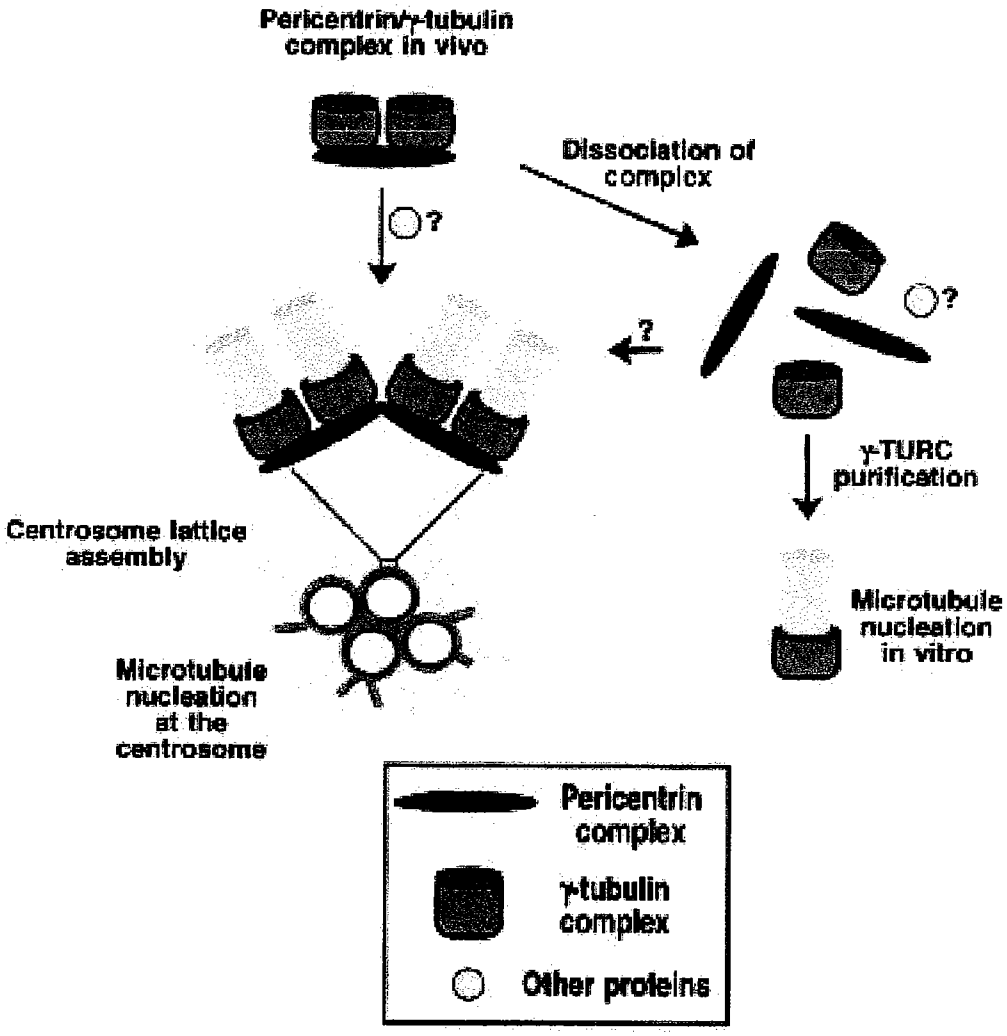
Pericentrin/γ-tubulin complex in vivo
Dissociation of complex
?
?
?
γ-TURC purification
Centrosome lattice assembly
Microtubule nucleation in vitro
Microtubule nucleation at the centrosome
Pericentrin complex
γ-tubulin complex
Other proteins

Figure 14

Figure 14. A model for centrosome assembly. The stoichiometry of pericentrin and γ–tubulin is consistent with a large complex consisting of one pericentrin complex and two γ–tubulin complexes. This model accommodates both of the current schemes proposed for microtubule nucleating complexes (Erickson and Stoffler, 1996; Zheng et al., 1995) (see Discussion). The complex appears to assemble at the centrosome to form a unique lattice (*left*). When dissociated, the complex gives rise to a pericentrin subcomplex, a γ-tubulin subcomplex and perhaps other proteins (*right*). Whereas the γ–tubulin subcomplex has not been characterized in this study, it has previously been shown that purified γ–TuRCs are capable of nucleating microtubules in vitro but are unable to assemble onto centrosomes (see Discussion). The pericentrin complex may facilitate assembly of γ–tubulin complexes into the centrosome lattice. Centrosome assembly and stabilization are likely to require other proteins.

CHAPTER III

Mitosis-specific anchoring of γ tubulin complexes by pericentrin controls spindle organization and mitotic entry.

Abstract

Microtubule nucleation is the best known function of centrosomes. Centrosomal microtubule nucleation is mediated primarily by γ tubulin ring complexes (γ TuRCs). However, little is known about the molecules that anchor these complexes to centrosomes. In this study we show that the centrosomal coiled-coil protein pericentrin anchors γ TuRCs at spindle poles through an interaction with γ tubulin complex proteins 2 and 3 (GCP2, 3). Pericentrin silencing by small interfering RNAs in somatic cells disrupted γ tubulin localization and spindle organization in mitosis but had no effect on γ tubulin localization or microtubule organization in interphase cells. Similarly, overexpression of the GCP2/3 binding domain of pericentrin disrupted the endogenous pericentrin-γ TuRC interaction and perturbed astral microtubules and spindle bipolarity. When added to Xenopus mitotic extracts, this domain uncoupled γ TuRCs from centrosomes, inhibited microtubule aster assembly and induced rapid disassembly of pre-assembled asters. All phenotypes were significantly reduced in a pericentrin mutant with diminished GCP2/3 binding, and were specific for mitotic centrosomal asters as we observed little effect on interphase

asters or on asters assembled by the Ran-mediated centrosome-independent pathway. Additionally, pericentrin silencing or overexpression induced G2/antephase arrest followed by apoptosis in many but not all cell types. We conclude that pericentrin anchoring of γ tubulin complexes at centrosomes in mitotic cells is required for proper spindle organization and that loss of this anchoring mechanism elicits a checkpoint response that prevents mitotic entry and triggers apoptotic cell death.

Introduction

The centrosome is the primary microtubule organizing center in animal cells. At the centrosome core is a pair of barrel-shaped microtubule assemblies, the centrioles (Doxsey, 2001). Centrioles are capable of self-assembly (Khodjakov et al., 2002; Marshall et al., 2001) and can serve as templates for recruitment and organization of the surrounding pericentriolar matrix (Bobinnec et al., 1998; Kirkham et al., 2003). The pericentriolar material or centrosome matrix contains a high proportion of coiled coil proteins and is the site of microtubule nucleation. Within the matrix are large protein complexes of γ tubulin and associated proteins that have a ring-like structure and mediate the nucleation of microtubules called γ tubulin ring complexes or γ TuRCs (Moritz et al., 1995a; Zheng et al., 1995). Other proteins may share the ability to nucleate microtubules because centrosomes can organize microtubules in the absence of functional γ tubulin (Hannak et al., 2002; Sampaio et al., 2001; Strome et al., 2001).

During cell cycle progression, centrosomes "mature" by recruiting additional γ TuRCs and several other proteins resulting in an increase in the nucleation capacity of the centrosome (reviewed in (Blagden and Glover, 2003)). However, we still know very little about proteins that directly anchor γ TuRCs to centrosomes in vertebrate cells. In the budding yeast, a small γ tubulin complex composed of γ tubulin (Tub4p), Spc97p and Spc98p (~700 KD) is bound to the nuclear side of the spindle pole body (the centrosome equivalent) through an interaction with Spc110p (Knop and Schiebel, 1997), and to the cytoplasmic side of the spindle pole body through Spc72p (Knop and Schiebel, 1998). Spc97p and Spc98p mediate binding of the complex to Spc110p and Spc72p (Knop and Schiebel, 1997; Knop and Schiebel, 1998; Nguyen et al., 1998). Although there is no apparent homology between their SPC97/98 interacting domains, chimeras formed by fusing the binding domain of one with the localization domain of the other can rescue knockouts of the proteins encoding the localization domains suggesting that the two binding domains are functionally homologous (Knop and Schiebel, 1998).

γ TuRCs in vertebrate cells and Drosophila contain orthologues of the three yeast proteins (γ tubulin, γ complex proteins 2 and 3, (GCP2, 3)) as well as several additional components (Martin et al., 1998; Moritz et al., 1998; Murphy et al., 2001; Murphy et al., 1998; Oegema et al., 1999; Zheng et al., 1995) (reviewed in (Job et al., 2003)). In vertebrates, the centrosome protein pericentrin (pericentrin A) forms a

large complex with γ tubulin in the cytoplasm and the two proteins are also in close proximity at the centrosome (Dictenberg et al., 1998). Recent evidence suggests there may be as many as ten isoforms of pericentrin in human cells (Flory and Davis, 2003). A large isoform (pericentrin B/kendrin, (Flory and Davis, 2003)) and another centrosome protein called AKAP450/GC-NAP share homology with the calmodulin-binding domain of Spc110p (Flory et al., 2000; Gillingham and Munro, 2000; Li et al., 2001). Other potential Spc110p orthologues have been identified in *Schizosacharomyces pombe*, *Aspergillus nudulans* and *Drosophila* based on sequence homology (Flory et al., 2002; Kawaguchi and Zheng, 2003), and in vertebrates (Xenopus, human) based on immunological cross reactivity with Spc110p-specific antibodies (Tassin et al., 1997). All proposed vertebrate orthologues of Spc110p localize to the centrosome and co-immunoprecipitate with γ TuRCs (Dictenberg et al., 1998; Takahashi et al., 2002; Tassin et al., 1997). No Spc72p orthologues have been identified in other species.

In vertebrate cells, pericentrin B and AKAP450 have recently been shown to bind GCP2 *in vitro* (Takahashi et al., 2002). Antibody inhibition and immunodepletion studies demonstrated a role for pericentrin isoforms and AKAP450 in microtubule nucleation in vertebrates and Drosophila (Doxsey et al., 1994; Kawaguchi and Zheng, 2003; Keryer et al., 2003b; Takahashi et al., 2002), perhaps by localizing the small Ran GTPase to centrosomes (AKAP450) (Keryer et al., 2003a). However, other studies show that antibody depletion of pericentrin B or reduction of pericentrin A

and B do not affect aster formation, microtubule organization or centrosome-associated γ tubulin (Dammermann and Merdes, 2002; Li et al., 2001; Takahashi et al., 2002). Moreover, loss of AKAP450 from centrosomes does not affect centrosomal γ tubulin localization even though microtubule organization is disrupted (Keryer et al., 2003b). Another potential centrosomal γ TuRC-anchoring protein has recently been identified in vertebrate cells called ninein-like protein (Nlp), which can bind γ TuRC complexes, inhibit nucleation when neutralized with antibodies and enhance nucleation when overexpressed (Casenghi et al., 2003). However, we know little about the role of these putative scaffold proteins in centrosomal anchoring of γ TuRCs during the cell cycle and the cellular consequences of specifically disrupting their interactions with γ TuRCs at centrosomes.

In this study, we show that siRNAs targeting both pericentrin isoforms (A and B) induced specific loss of γ tubulin from spindle poles in mitosis, reduction of astral microtubules and formation of monopolar spindles. This phenotype appeared to be specific for the smaller isoform of pericentrin as it was not observed when the larger pericentrin isoform was specifically reduced. A region at the C-terminus of pericentrin interacted with both GCP2 and GCP3 in vitro as shown by co-immunoprecipitation and two-hybrid analysis. Expression of the GCP2/3-binding domain of pericentrin produced a phenotype similar to that observed in cells with reduced pericentrin. It disrupted the interaction between endogenous pericentrin and γ TuRCs, and adsorbed γ TuRCs from cell extracts. It reduced astral microtubules and

centrosomal γ tubulin in mitotic cells and induced formation of small spindles and monopolar spindles. No effect on interphase microtubules was observed. When added to Xenopus extracts this domain dissociated γ tubulin from mitotic centrosomes and rapidly induced mitotic aster disassembly. The loss of γ tubulin from centrosomes in cells with reduced pericentrin levels or in cells expressing the GCP2/3 binding domain of pericentrin ultimately triggered a checkpoint inducing G2/antephase arrest and apoptosis in somatic cells. These phenotypes were not observed following specific reduction in the levels of the larger pericentrin isoform, expression of a mutant pericentrin defective in GCP2/3 binding, or expression of a homologous region of pericentrin B. We conclude that the smaller isoform of pericentrin provides a molecular scaffold for centrosomal anchoring γ TuRCs during mitosis in both embryonic and somatic cell systems.

Materials and Methods

Molecular cloning

All pericentrin constructs used in this study were cloned into pcDNA vectors (Invitrogen, Carlsbad, CA) with amino terminal hemagglutinin (HA) tags (Purohit et al., 2001; Purohit et al., 1999) except those used in two-hybrid studies (see below). Fragments of pericentrin and other genes were PCR amplified from cDNAs using primers with Not1 and Xba1 restriction sites. PCR products were digested with the appropriate enzymes, cloned into the vector and sequences were confirmed. In some

cases, EcoR1 and Xho1 restriction sites were used (peri B1826-2117, 1572-1816,1572-1816m). GCP2, GCP3 and γ tubulin containing constructs were obtained from Dr. Tim Stearns, Stanford University, Stanford, California.

SiRNA

21 nucleotide RNAs were chemically synthesized by Dharmacon Research, Inc., Lafayette, CO. and introduced to cells using oligofectamine (Invitrogen, Carlsbad, CA.) in accordance with the manufacturers instructions. The target sequences used were; AAUUGGAACAGCUGCAGCAGA, against pericentrin A and B in human (Dammermann and Merdes, 2002), AAUGAGGUUGUCCACAGGAGA against pericentrin A and B in mouse, and AAGCUCUGAUUUAUCAAAAGA against the PACT domain of pericentrin B in human. AACUGGACUUCCAGAAGAACA, which targets human lamin A and is nonspecific in mouse, was used as a control for all siRNA studies. Crude cell lysates were analysed for protein silencing. Cells were treated with 2 μM thymidine for 18 hours starting 24 hours post siRNA treatment. 6 hours after thymidine release, cells were harvested and lysed in phosphate buffered saline (PBS) supplemented with 1% Triton X100, 10 μg/ml leupeptin, 10 μg/ml pepstatin, 10 μg/ml chymotripsin,10 μg/ml PMSF, 2.0 μg/ml p amino-benzamidine, 5 mM iodoacetamide and 5 mg/ml N-ethylmaleimide. Cell lysates were clarified at top speed in a microfuge for 15 minutes at 5°C. Protein concentration for each lysate was determined using Biorad protein dye reagent, loads were adjusted, proteins were resolved by SDS PAGE and analysed by western blot.

Antibodies

Anti-myc, anti-γ tubulin, and anti-tubulin antibodies were obtained from Sigma, St. Louis, Missouri. Phosphohistone H3 rabbit polyclonal antibody was purchased from Upstate Biotechnology, Inc, (Lake placid, NY). M30 cytodeath and Anti HA rat monoclonal antibody 3F10 was obtained from Roche Diagnostics, (Indianapolis, IN.) Anti human lamin A/C antibody was purchased from Cell Signalling Technology, (Beverley, MA). Other antibodies included M8 anti-pericentrin antibody, (Dictenberg et al., 1998), human autoimmune serum 5051 that recognizes centrosome proteins, (Doxsey et al., 1994), anti pericentrin B/kendrin specific antibody (Flory et al., 2000) (obtained from Trisha Davis, Seattle Washington), anti-GCP2 antibody (Murphy et al., 1998) (obtained from Dr. Tim Stearns, Stanford, California), and anti-GCP3 antibody (a gift from Michel Bornens, Institut Curie, Paris France).

Yeast two hybrid cloning/methods

Direct yeast two-hybrid interactions were performed essentially as described previously (Gromley et al., 2003). Pericentrin, γ-tubulin, GCP2 and GCP3 coding sequences were amplified from plasmid DNA by PCR using Pfu Turbo (Stratagene), cloned into either pGBKT7 or pGADT7 (Clontech) and completely sequenced. Yeast strains AH109 and Y187 were transformed with GAL4 DNA-binding domain (GAL4-DBD) or GAL4 transactivation domain (GAL4-TAD) expression constructs, respectively, and diploid strains generated by mating. Interactions between

pericentrin and members of the γ-tubulin ring complex were tested for by streaking yeast onto synthetic defined (SD) medium lacking leucine, tryptophan, histidine and adenine.

Biochemical techniques

Immunoprecipitations from Xenopus extracts were performed as previously described (Dictenberg et al., 1998) using the antibodies to the pericentrin amino terminus (M8) (Doxsey et al., 1994) and γ tubulin (Zheng et al., 1995). For disruption of γ TuRCs from pericentrin in co-immunoprecipitations, active or heat denatured pericentrin fractions were added directly to Xenopus high speed extracts before immunoprecipitation. Protein affinity experiments to recruit γ TuRCs (Figure 15) were performed using partially purified fractions of pericentrin domains (see below). Proteins were bound to anti-HA beads, added to extracts for 60 minutes, washed in Extract Buffer (XB) (Murray, 1991), run on SDS-gels and probed with the indicated antibodies.

Proteins for recruitment of γ TuRCs (Figure 16) and for aster inhibition assays (below, Figure 18, 19) were produced in COS cells and purified as follows. Confluent COS cells were transiently transfected with 3 μg DNA per 60 mm dish using Lipofectamine Plus reagent (Gibco BRL, Gaithersburg, MD). Transfected cells were maintained for 3 days in DMEM with 5% serum, then collected with 5 mM EDTA in PBS (phosphate buffered saline). Cells were lysed in PBS supplemented

with protease inhibitor cocktail (Roche, Basel, Switzerland, #1836153), 1% Triton X-100 and 5 mg/ml N-ethylmaleimide. For recruitment of γ tubulin from extracts, HA beads were prepared by pretreating Dynabeads 450 (Dynal, Inc., Lake Success, NY, #110.05) with a saturating amount of anti-HA antibody 12CA5 (Covance, Denver, PA.). Anti-HA IgG beads were treated with COS cell lysate containing an excess of the indicated HA-tagged pericentrin polypeptides, washed 3X in PBS lysis buffer, 2X in PBS and 2X in XB, before addition of Xenopus extracts for γ TuRC recruitment experiments. For preparation of soluble HA-tagged pericentrin, 12CA5 antibody was crosslinked to protein A beads (BIORAD) using standard methods (Harlow, 1988). HA-tagged pericentrin was batch depleted from COS lysates by incubation with HA crosslinked beads at 5°C with gentle agitation for 1 hour. Treated beads (configured as a column) were washed with 10 column volumes of lysis buffer, 10 volumes of PBS with PI, and 10 volumes of 10 mM Tris pH 8.0. HA pericentrin was eluted with 2 volumes 150 mM glycine pH 2.5 into 1/4 volume 1 M TRIS pH 8.0, and dialysed against PBS overnight.

Co-immunoprecipitations

Co-immunnoprecipitation of pericentrin isoforms and γ TuRC components (Figure 17) was performed in COS cells 40-48 hours after transient co-transfection of the indicated constructs using Lipofectamine plus reagent. Cells were collected using 5 mM EDTA in PBS. Cell pellets were lysed with 1% NP-40, 1 mM DTT, 10% glycerol in buffer C (100 mM Pipes pH 6.9, 6 mM $MgCl_2$, 0.5 mM EGTA, 10 μg/ml

leupeptin, 10 μg/ml pepstatin, 10 μg/ml chymotripsin, 10 μg/ml PMSF, 2.0 μg/ml p amino-benzamidine, 5 mM iodoacetamide). Lysates were clarified 15 minutes at top speed in a microfuge at 5°C, then applied to HA Dyna beads (see above). Beads were treated for 1 hour at 5°C with end –over –end agitation, washed 2 X in lysis buffer (above) and 2X in wash buffer (buffer C with 100 mM Na acetate pH 6.9). Loads and treated beads (immunoprecipitates) were analyzed by SDS gel electrophoresis and western blot using the indicated antibodies.

Xenopus extracts

Cytostatic factor (CSF)-arrested Xenopus extracts were prepared and aster assembly assays were preformed as previously described (Murray, 1991; Stearns and Kirschner, 1994). For purpose of quantization, two hundred sperm were counted and scored for the presence of assembled microtubules. In some cases the standard fix (0.3 volume 37% formaldehyde, 0.6 volumes 80% (w/v) glycerol, 0.1 volume 10X MMR, 1 μg/ml DAPI was modified by the addition of 0.05% Oligreen (Molecular Probes, Eugene, Oregon), to facilitate visualization of sperm nuclei with a scanning confocal microscope. Centrosome assembly in the presence of nocodazole was preformed using published methods (Stearns and Kirschner, 1994). Treated nuclei were prefixed in 5% formaldehyde, spun onto coverslips through a 20% sucrose cushion using a JS13.1 rotor at 8000 rpm 15 minutes, and post fixed in methanol (-20°C) before staining for immunoflourescence. Ran-mediated asters were prepared using constitutively active RanL43E as described (Wilde and Zheng, 1999).

Centrosome-dependent and –independent Xenopus mitotic asters were fixed in formaldehyde on coverslips as described (Murray, 1991; Wilde and Zheng, 1999).

Cell lines

Cell lines (COS-7, SAOS, U2OS) were grown as described (ATTC, Rockville, MD) and prepared for transfection experiments as described (Purohit et al., 1999). Primary mouse embryonic fibroblasts (MEFs) were obtained from Dr. Geoffrey Wahl, Salk Institute for Biological Studies, La Jolla, California 92037, and used at less than 6 passages.

Transfection and Immunofluorescence

For transfection and immunofluorescence analysis logarithmically growing cells were transfected as indicated by the manufacturer with 1 μg DNA per 35 mm dish of the appropriate construct using Lipofectamine plus (Gibco BRL, Gaithersburg, MD), for COS cells; Lipofectamine for SAOS and U2OS cells. The transfection efficiency for COS cells with control constructs ranged from 35-60 percent. MEFs were transfected using Superfect (Qiagen, Valencia, CA). For immunofluorescence, cells were fixed with –20°C MeOH as previously described (Purohit et al., 1999). Data was collected as a Z series for deconvolution with 0.3 μm between planes. Images were deconvolved using Metamorph software, no neighbors algorithm. All images were rendered two dimensional by showing maximum intensity at each point.

Microinjection Experiments

For microinjection, COS cells were synchronized by thymidine block. Cells were treated 16 hours with 2 mM thymidine, and released (single block), or treated for an additional 16 hours with 2 mM thymidine following eight hours of release (double block). The mitotic index of synchronized cells was determined using replicate coverslips, fixed and stained with DAPI, then counted at the indicated times post release from thymidine block. 1000 cells were counted for each time point. Microinjection into the nucleus of released cells was performed using an Eppendorf transjector 5246, with Eppendorf femtotips, with an injection pressure of 100 hPa, injection time of 0.4 sec, and DNA at a concentration of 0.2 μg/μl in PBS.

Results

Pericentrin silencing mislocalizes γ tubulin from spindle poles and disrupts spindle bipolarity.

We previously showed that pericentrin interacts with the γ tubulin ring complex and that pericentrin antibodies disrupt spindle organization and function (Dictenberg et al., 1998; Doxsey et al., 1994). In this study, we address the molecular mechanism of the mitotic function of pericentrin. Initially, we used siRNAs designed to silence the two previously characterized isoforms of pericentrin (A and B/kendrin), although we cannot rule out silencing of other potential pericentrin isoforms under these conditions (see (Flory and Davis, 2003)). We typically observed silencing in 80-90

percent of treated cells (Figure 15A-C, G, H). Silencing of pericentrin A/B disrupted mitotic spindle organization and reduced astral microtubules, ultimately leading to the formation of monopolar spindles in most mitotic cells (Figure 15A, A', E, F). The phenotype appeared to be specific for mitotic cells as interphase microtubule organization was not detectably altered (Figure 15A, A'). γ tubulin was reduced at spindle poles in mitotic cells, although centrioles were present; centrosomes in adjacent interphase cells retained strong γ tubulin staining (Figure 15G, H). Selective silencing of the larger isoform of pericentrin (B) had no effect on interphase or mitotic microtubule organization (Figure 15C, C', C'', D), although we cannot rule out the possibility that activity of the residual protein is sufficient to support these functions. These results suggested that the phenotype observed after pericentrin A/B silencing resulted from reduction in pericentrin A, although this isoform could not be specifically targeted because it is homologous through most of its length with pericentrin B ((Flory and Davis, 2003)). Control cells with reduced lamin levels showed no detectable changes in any of the parameters described above (Figure 15B, B', E, F,) and data not shown.

Pericentrin interacts with the γ TuRC in Xenopus extracts through GCP2 and 3. We next examined the relationship of pericentrin and the γ tubulin ring complex in more detail. We found that immunoprecipitation of pericentrin from Xenopus extracts co-precipitated several components of the γ TuRC including γ tubulin, γ complex protein 2 (GCP2) and γ complex protein 3 (GCP3) (Figure 16A). Conversely,

immunoprecipitation of γ tubulin co-precipitated pericentrin in addition to GCP2 and GCP3. Additional evidence for the pericentrin-γ TuRC interaction was obtained by showing that an HA-tagged C-terminal region of pericentrin affixed to beads could be used to specifically pull out endogenous γ tubulin and associated proteins from Xenopus extracts (1340-1920, Figure 16B and data not shown). Moreover, the C-terminal region of pericentrin was able to disrupt the endogenous pericentrin-γ TuRC interaction when added to extracts as shown by the loss of γ tubulin from pericentrin immunoprecipitates (Figure 16C). These results demonstrate that pericentrin interacts with the γ TuRC and that the interaction is mediated by a domain at the C-terminal region of the protein.

To determine the molecular basis of the interaction of pericentrin with the γ TuRC, we tested whether pericentrin could bind individual proteins of the complex in vitro. We found that HA-tagged full-length pericentrin and the C-terminal third of pericentrin co-immunoprecipitated myc-tagged GCP3 when the proteins were co-overexpressed in COS-7 cells (Figure 17A and B). In parallel assays, the pericentrin C-terminus co-immunoprecipitated myc-tagged GCP2 (Figure 17A and C) but not myc-tagged γ tubulin (Figure 17D). GCP2/3 binding was specific for the C-terminus of pericentrin as several domains comprising the amino terminal two thirds of the molecule showed no interaction (Figure 17B and C). Direct two-hybrid analysis confirmed the interaction of the pericentrin C-terminus with both GCP2 and GCP3 (Figure 17E) and failed to detect an interaction with γ tubulin or amino terminal

domains of pericentrin (data not shown). In addition, domains of the larger isoform (pericentrin B) that included the GCP2/3 interacting region of pericentrin as well as an additional exon not present in pericentrin (66% identical; 78% similarity), did not interact with GCP2 (or GCP3) by immunoprecipitation (Figure 17G) or two-hybrid analysis (Figure 17F, see accession numbers gi458668, and gi31296687 for more details on sequence differences). Results from these two independent assays demonstrate that pericentrin interacts specifically with at least two members of the γ TuRC, GCP2 and GCP3. The C-terminus of pericentrin appeared to bind GCP2 and GCP3 more efficiently than the full length molecule. Similar binding patterns have been observed for other pericentrin- interacting proteins such as the dynein light intermediate chain and they could result from increased accessibility to epitopes that are masked in the full length protein (Tynan et al., 2000).

The C-terminus of pericentrin disassembles mitotic asters and centrosomal γ tubulin in Xenopus extracts.

Microtubule aster formation on nascent centrosomes of sperm nuclei in Xenopus extracts is dependent on the recruitment of soluble γ TuRCs to these sites (Felix et al., 1994; Stearns and Kirschner, 1994). Previous studies implicated pericentrin in this process (Dictenberg et al., 1998; Doxsey et al., 1994). To address this issue directly, we examined the effect of the GCP2/3 interacting domain of pericentrin on microtubule aster assembly in mitotic Xenopus extracts. Addition of this domain to extracts prior to the aster assembly reaction significantly reduced aster formation

(Figure 18A and B). Even after extended periods of time (30 minutes) few asters were detected and they had few microtubules and were highly disorganized, a phenotype almost never observed in controls. Aster activity was quantified by counting at least 200 sperm per treatment. Sperm nuclei which organized microtubules were scored as positive. This likely underestimated inhibitory activity, since at higher concentrations few microtubules were associated with sperm scored as positive. Half maximal aster inhibitory activity was seen at a protein concentration approximately 4:1 with endogenous pericentrin (Figure 18C). No change in aster assembly was observed in the presence of the pericentrin N-terminus, heat-denatured C-terminus, BSA or buffer alone (Figure 18D, 1-6). The activity appeared to be specific for mitotic extracts as there was no detectable effect on aster assembly in interphase extracts (Figure 18D, 7-9).

The mechanism of aster inhibition was examined in more detail by monitoring recruitment of γ tubulin onto nascent centrosomes in Xenopus mitotic extracts as previously described (Doxsey et al., 1994; Felix et al., 1994; Stearns and Kirschner, 1994). The pericentrin C-terminal domain and sub-domains of this protein specifically inhibited recruitment of γ tubulin onto centrosomes to the same extent and at the same concentration that prevented microtubule aster assembly and disrupted the interaction between pericentrin and the γ TuRC (Figure 18, E-G). These results suggested that the pericentrin C-terminus inhibited microtubule aster

formation in mitotic extracts by preventing recruitment of γ tubulin to pericentrin sites on the nascent centrosome.

To more directly test whether pericentrin anchored γ TuRCs to nascent centrosomes, we examined the effect of the pericentrin C-terminal polypeptide on asters pre-assembled in extracts. Within 60 seconds after addition of the protein, the focus of microtubules in pre-assembled asters was disrupted and free microtubules were observed in the region surrounding the aster (Figure 18, H-K). By two minutes after addition of the protein most microtubules appeared to have lost their attachment to the centrosome; the remaining microtubules were of normal length and often formed bundles. By 3-5 minutes no microtubules were detected at most centrosomes. In contrast, pre-assembled asters exposed to heat-inactivated pericentrin C-terminus (Figure 18L), other pericentrin domains, the pericentrin B homology domain or buffer alone showed no detectable loss of centrosomal microtubules, no change in microtubule organization and few to no free microtubules in the vicinity of the aster. Pericentrin C-terminal peptide was just as effective at disrupting pre-existing asters as it was at inhibiting their assembly, through a range of test concentrations. Pericentrin C terminal peptide caused loss of γ tubulin from preassembled centrosomes within the same time frame that it caused loss of microtubules from asters (90 percent reduction in 5 minutes). These results indicate that the pericentrin C-terminus disrupts the interaction of γ TuRCs with centrosomes releasing the complexes and attached microtubules.

Microtubule asters can form in Xenopus extracts by a centrosome-independent pathway that requires the Ran GTPase (reviewed in (Dasso, 2002)). Ran-mediated aster assembly can be inhibited by a dominant negative form of Ran and enhanced by a dominant active form of the protein. Under conditions that resulted in rapid disassembly of mitotic asters, the pericentrin C-terminus did not significantly affect Ran-mediated aster assembly even after extended periods of incubation (Figure 18M and N). Thus, while formation of Ran asters requires γ tubulin (Wilde and Zheng, 1999) it appears to be less dependent on pericentrin than does centrosome-mediated aster assembly.

Mapping the GCP2/3 binding domain and aster disrupting activity of pericentrin.

We further defined the pericentrin-GCP2/3 interaction site and made point mutants that inhibited the pericentrin-GCP2/3 interaction. The GCP2/3 binding domain spanned approximately 200 amino acids and contained multiple regions that interact with GCP2 and /or GCP3 (Figure 19A, B). The interaction with both GCP2 and GCP3 is likely direct because the binding regions are separable (Figure 19A,B). The minimal domain required for aster inhibitory activity was 144 amino acids. This fragment was unstable, so the more stable Pc1618-1810 construct was used for most analyses. Based upon directed two-hybrid and co-immunoprecipitation analyses, we cloned a sub domain of the C-terminus that was required for strong GCP2/3 binding

in both assays (Figure 19A "consensus"). We identified a point mutation in this domain with significantly reduced binding to GCP2 invitro, and lacked aster activity in Xenopus extracts. We do not understand the exact nature of this mutant since the mutations are 3 and 5 amino acids outside the minimal 144 amino acid domain for activity. The un mutated region containing these sites shows GCP2 interaction by yeast two hybrid but not by co-ip. The mutant has reduced GCP2 and GCP3 interaction by yeast two hybrid, but retains the ability to co-ip GCP3, suggesting that it is not fully denatured. A full understanding of this mutation site and the full wild type binding domain will require X ray crystallographic analysis. GCP2 and GCP3 bind cooperatively to pericentrin with in the consensus region since myc-tagged GCP2 showed cooperative binding to HA-tagged pericentrin in the presence of GCP3 (Figure 19C). In functional assays, pericentrin domains that bound GCP2/3 showed aster inhibitory activity in Xenopus extracts (Figure 19A). Those that did not interact with GCP2/3 lacked aster inhibitory activity including the pericentrin mutant, a domain of pericentrin B containing all pericentrin sequences required for activity (Figure 19A), and several pericentrin domains outside the GCP2/3 interacting domain (Figure 19A, consensus). The strong correlation between regions of pericentrin that interacted with GCP2/3 and those that showed mitotic aster and γ TuRC disrupting activity, indicated that pericentrin was required for anchoring γ TuRCs to centrosomes in Xenopus mitotic extracts.

To further address differences in GCP2/3 binding between pericentrin (A) and pericentrin B, we excised most of an extra exon (and some additional sequences) that is present in the homologous region of pericentrin B. Truncated pericentrin B proteins lacking the amino acids encoded by these sequences had weak GCP2 binding activity (Fig 19A,D), suggesting that pericentrin B binding to the γ TuRC in this region may be blocked by incorporation of an extra exon.

GCP2/3 interacting domains of pericentrin disrupt mitotic asters and spindles in vertebrate cells.

We next tested whether the GCP2/3-interacting domains of pericentrin affected microtubule organization in vertebrate cells. We found that these domains had no detectable effect on the organization or nucleation of microtubules or the organization of centrosomes in interphase SAOS cells (Figure 20A). However, the same domains disrupted microtubule structures in mitotic cells (Figure 20B-K). The most common phenotype was monopolar spindles, which represented ~15% of all mitotic cells at early times post-transfection (20-22 hours) and increased to ~90% at later times (44 hours post-transfection, Figure 20H, H', M). Most monopolar spindles had two duplicated and separated centrosomes. We also observed spindles with reduced numbers of centrosome-associated astral microtubules (Figure 20C', G, J, K'), bipolar spindles with shortened pole-to-pole axes (minispindles, Figure 20C' and G) and half spindles with single focused poles (Figure 20I-II"). In many spindles, we observed a decrease in the centrosome level of γ tubulin (Figure 20E and I) and other centrosome

proteins (Figure 20C), although the proteins were never reduced to undetectable levels. Pericentrin domains that bound both GCP2 and GCP3 induced the same defects and those that did not interact had little or no effect (Figure 20K-K''). Moreover, we were unable to detect aster inhibitory activity in Xenopus extracts (Figure 18D, 19A), disruption of spindle organization (Figure 20 M-M') or apoptosis (below) associated with the homologous region of pericentrin B, suggesting that these two molecules may not be functionally analogous. Taken together, these results suggest that uncoupling of the pericentrin A-γ tubulin interaction in mitotic cells caused a reduction in the centrosome-associated γ TuRCs and disrupted astral microtubules and spindle organization, ultimately producing monopolar spindles.

Overexpression of the GCP2/3 binding domain of pericentrin and reduction in pericentrin levels both induce G2/antephase delay and apoptosis.

During the course of these studies, we observed a marked reduction in cell density in cultures transfected with the GCP2/3 binding domain (Figure 21A and A'). Typically, half the cells detached from their substrate by 44 hours, while there was little change in cell density prior to protein expression (20 hours, Figure 21, A'). To investigate this further, we examined cells for apoptosis and found that a significant fraction of the cells stained with an apoptosis-specific marker that detects a caspase 3 product of cytokeratin 18 produced early in apoptosis (M30, Figure 21A"); control cells showed low levels of M30 staining.

Apoptosis required that cells be actively cycling, as we did not detect apoptosis when cells were plated at high density to induce G_1/G_0 arrest during the period of protein expression. In cycling cells of several different origins, we observed a low mitotic index (Figure 21C) suggesting that cells were delayed at some point in the cell cycle. We found that cells accumulated in a premitotic stage based on their ability to stain for a form of histone H3 that is phosphorylated by aurora B in early mitotic cells (Hans and Dimitrov, 2001; Swedlow and Hirano, 2003); control cell staining was significantly lower (Figure 21D, F). The cell cycle period between late G2 and mitosis (before chromosome condensation occurs) is termed antephase (Pines and Rieder, 2001). Antephase arrest was linked to apoptosis because most early mitotic cells (phospho-H3-positive) were also early apoptotic (M30-positive, Figure 21H). Moreover, most centrosomes in apoptotic cells appeared duplicated and separated (two γ tubulin spots, Figure 7I), consistent with cells in late G2 or early prophase.

To confirm the link between cell cycle arrest and cell death, we microinjected cDNA into nuclei of COS cells arrested in S phase by thymidine block. Approximately eight hours after release from the block, cells entered mitosis. At this time, a significant proportion of cells expressing the GCP2/3 binding domain of pericentrin detached from the substrate, while control cells remained attached and often increased in number (Figure 22A, B). Cell loss was cell cycle specific because pre-mitotic cycling cells or cells kept under S phase arrest remained viable and adherent (Figure 8C). These results suggested that uncoupling the pericentrin-γ TuRC interaction and

disruption of astral microtubules induced apoptosis at the G2/M transition. (Figure 22C, 22D).

We reasoned that if apoptosis resulted from a cellular defect common to both overexpression and reduction of pericentrin, we should observe cell cycle arrest and apoptosis following pericentrin silencing. Significant cell death was in several cell types knocked down for pericentrin A and B at 48-72 hours post treatment (data not shown). Pericentrin A/B silencing also induced a significant increase in antephase, and a decrease in mitotic index 48-72 hours after protein silencing (Figure 21C, D). These provide further support for the idea that antephase arrest and apoptosis may be caused by disruption of the pericentrin/γ tubulin interaction.

Discussion

Our previous results demonstrated that pericentrin and γ tubulin interacted in Xenopus extracts and that the proteins were in close proximity at centrosomes in vertebrate cells, suggesting that they interacted at this site as well (Dictenberg et al., 1998). The additional data provided in this study shows that pericentrin interacts with the γ TuRC via domains that bind GCP2 and GCP3 and that this interaction is important for microtubule organization in mitotic cells. The results of this study are consistent with our previous work showing that pericentrin overexpression induces severe spindle defects (Purohit et al., 1999). We propose a model in which

pericentrin acts as a scaffold for anchoring γ TuRCs at mitotic centrosomes/spindle poles. This interaction appears to be required not only for astral microtubule organization but also for maintaining spindle bipolarity and for mitotic entry. The monopolar spindles and 'minispindles' induced by disruption of the pericentrin-GCP2/3 interaction, indicate that pericentrin anchoring of γ TuRCs may also play a role in organizing microtubules of the central spindle.

Centrosomal anchoring of γ TuRCs by pericentrin is required for mitotic microtubule aster organization in Xenopus extracts and somatic cells.

Our results indicate that pericentrin anchoring of γ TuRCs at centrosomes is required for mitotic aster organization. If anchoring is disrupted, γ tubulin is dramatically depleted at mitotic centrosomes in Xenopus extracts and reduced at spindle poles in somatic cells. The more dramatic loss of centrosomal γ tubulin from Xenopus asters suggests that pericentrin plays a more dominant role in the organization of γ TuRCs at centrosomes in this system and perhaps in embryonic systems in general. We have not investigated the fate of γ TuRCs once dissociated from centrosomes although one possibility is that they remain attached to the minus ends of microtubules where they could cap microtubule growth (Wiese and Zheng, 2000). In somatic cells, a fraction of γ tubulin remains at centrosomes/spindle poles under conditions that disrupt the GCP2/3-pericentrin interaction. This fraction could be anchored by other proteins that have been shown to bind γ TuRC components such as AKAP450, pericentrin B

(Takahashi et al., 2002) Nlp (Casenghi et al., 2003) and centrosomin (Terada et al., 2003).

In this study, we map the GCP2/3 binding site of pericentrin to the C-terminus of the protein, a region that shows no apparent homology to AKAP450, Spc110, Spc72 or CP309 (Kawaguchi and Zheng, 2003; Takahashi et al., 2002), although it is conserved between mouse, human and rat (66-75% identical, 78-84% similarity). While the amino terminus of pericentrin B binds GCP2 (Takahashi et al., 2002) (W. Zimmerman and S. Doxsey, unpublished observations), a similar region in the smaller pericentrin isoform does not, perhaps because it lacks exons found in pericentrin B. More information on the GCP2/3 interacting domain will require mapping these sites in all the GCP2 binding proteins.

The phenotype observed with the GCP2/3-pericentrin disrupting polypeptides and after pericentrin silencing is similar in many respects to that seen following functional abrogation of γ tubulin and other proteins of the γ TuRC. Under these conditions, centrosomes in C. elegans and Drosophila embryos were compromised in their ability to form mitotic asters (Hannak et al., 2002; Strome et al., 2001), separate from one another (Barbosa et al., 2003; Sampaio et al., 2001) and organize meiotic and mitotic spindles (Barbosa et al., 2003; Barbosa et al., 2000; Sunkel et al., 1995). It is of interest that mitotic asters in some of these systems formed in the absence of γ tubulin or other γ tubulin ring complex proteins (Barbosa et al., 2003; Hannak et al.,

2002; Strome et al., 2001). This is in contrast to our results in Xenopus extracts where microtubule asters did not form in the presence of the pericentrin interacting domain of GCP2/3 even after extended periods of time (30 minutes). Moreover, preformed mitotic asters were rapidly disassembled following addition of this polypeptide. Future studies will be required to determine whether pericentrin and γ tubulin are more critical for mitotic aster formation in Xenopus extracts than in the other systems, or if uncoupling γ tubulin from pericentrin prevents both γ tubulin-mediated microtubule nucleation and nucleation by a proposed γ tubulin-independent pathway (Hannak et al., 2002).

Pericentrin is not essential for assembly and anchoring of γ TuRCs at interphase centrosomes.

The GCP2/3-interacting pericentrin domains described in this study had no detectable effect on assembly of asters in interphase extracts prepared from Xenopus or in interphase somatic cells. Moreover, silencing of both isoforms also had no apparent effect on localization of γ tubulin at the centrosome or microtubule organization in interphase cells. This suggests that the protein does not play a major role in γ tubulin assembly or anchoring at interphase centrosomes but rather that the aster-organizing function of pericentrin is mitosis-specific. Since both proteins are normally present at the centrosome throughout the cell cycle, we cannot conclude that they do not interact during interphase, only that this specific interaction is not necessary for γ tubulin localization. It has been shown that γ tubulin and associated proteins are crucial for

microtubule nucleation from interphase centrosomes (Hannak et al., 2002; Joshi , 1992). It is thus likely that proteins other than pericentrin provide microtubule-anchoring sites at centrosomes in interphase cells.

Other proteins involved in centrosomal γ TuRC anchoring and microtubule organization.

Several other proteins play a role in centrosome organization and microtubule nucleation. However, their ability to directly anchor components of the γ TuRC and thus serve as molecular scaffolds for tethering these complexes to centrosomes has not been demonstrated. These include the centrosome proteins Asp (do Carmo Avides and Glover, 1999), NuMA (Merdes et al., 1996), TPX-2 (Garrett et al., 2002; Wittmann et al., 2000), SPD-5 (Hamill et al., 2002), PCM-1 (Dammermann and Merdes, 2002), Sas-4 (Kirkham et al., 2003) centrosomin (Megraw et al., 1999; Terada et al., 2003) and several regulatory molecules including Aurora A (Giet et al., 2002; Hannak et al., 2001), Polo (Barbosa et al., 2000; Lane and Nigg, 1996), PP1 (Katayama et al., 2001) and PP4 (Sumiyoshi et al., 2002)).

Some of these proteins play a critical role in a centrosome-independent spindle assembly pathway mediated by the Ran GTPase (see (Dasso, 2002)) including NuMA (Nachury et al., 2001; Wiese et al., 2001) and TPX-2 (Gruss et al., 2001). This is in contrast with pericentrin, which appears to be critical for assembly of mitotic asters but not Ran-mediated asters. In this regard, the proposed function of

pericentrin in aster formation also differs from that of epsilon tubulin, which seems to be required for centrosome-independent but not centrosome-dependent microtubule aster formation (Chang et al., 2003). From this discussion, it seems that different molecules are required to organize asters in centrosome-dependent and independent pathways as well as at different stages of the cell cycle.

Regulation of the pericentrin-GCP2/3 interaction.

Pericentrin, γ tubulin, and γ tubulin-associated proteins are localized to centrosomes throughout the cell cycle (Dictenberg et al., 1998; Stearns, 1991; Zheng, 1991). However, the pericentrin-GCP2/3 interaction appears to be involved in γ TuRC anchoring only during mitosis. This suggests that the interaction of pericentrin and γ TuRCs is regulated. The mechanism and regulation of cell cycle specific binding between these centrosome components is unknown. One model is that γ TuRCs are anchored to different centrosome scaffold proteins at different cell cycle stages and that these interactions are regulated in a cell cycle-dependent manner. For example, the γ TuRC-binding activity of pericentrin could be regulated by phosphorylation by mitotic kinases. γ TuRC-binding could also be regulated at least in part, through differential patterns of protein expression. Consistent with this idea is the observation that pericentrin, (which is expressed primarily in mitosis and in tissues that are highly proliferative ((Doxsey et al., 1994), Figure 20N)), has a mitotic phenotype. Future experiments will be required to determine the contribution of these and other

centrosome proteins in the anchoring of γ TuRCs to centrosomes at different cell cycle stages.

G2/antephase delay and apoptosis

G2 accumulation of cells expressing the GCP2/3 binding domain of pericentrin or following silencing of pericentrin A/B suggests that disruption of the pericentrin γTuRC interaction in vivo elicits a checkpoint response at this time in the cell cycle. Recent studies have implicated γ tubulin as well as the Spc110p homologue Pcp1p in regulation of the metaphase to anaphase transition (Prigozhina et al., 2004; Rajagopalan et al., 2004), but this is the first study suggesting a role for these or related molecules in regulation of mitotic entry. We do not yet know what this checkpoint may be monitoring. We favor a model in which the checkpoint senses spindle pole assembly/ centrosome maturation since disruption of the γ tubulin-pericentrin interaction disrupts spindle pole assembly and possibly centrosome maturation, which increases in size four fold between G2 and early prophase (Piehl et al., 2004), concurrent with the onset of γ tubulin mislocalization and antephase arrest that we observe.

Our results showing that pericentrin A/B silencing has no significant affect on interphase microtubule arrays confirms previous work (Dammermann and Merdes, 2002). In this earlier study the authors did not address mitotic defects most likely because a G2 checkpoint is activated, apoptosis follows and mitotic cells are rarely

observed, a phenomenon which we have encountered in two of the cell lines used by these authors; U2OS and Hela (Figure 21C and data not shown). In this study, we overcame this problem by using a cell line (SaOS), that that apparently lacks this checkpoint and fails to undergo apoptosis.

Apoptosis is commonly observed following checkpoint activation if a cellular imbalance cannot be repaired. We have not determined which molecular pathway is involved in the G2/antephase arrest identified in this study. DNA damage induces two molecularly distinct pathways involved in G2 arrest, one ATM dependent, the other ATM-independent (Xu et al., 2002). Cellular insults other than DNA damage can also induce late G2 arrest including: microtubule disruption, hypothermia, fluoride treatment, and viral protein expression (Elder et al., 2002; Mikhailov and Rieder, 2002; Pines and Rieder, 2001; Tyler et al., 2001).

Antephase delay and subsequent apoptosis can also be activated through pathways that include p53 and Rb. Our data demonstrate that p53 is not involved because primary MEFs lacking p53 retain the checkpoint response. SAOS cells, which do not arrest and apoptose have been reported to lack Rb (Scolnick and Halazonetis, 2000). We are currently testing the role of Rb in the checkpoint response. We are also investigating other mechanisms for inducing apoptosis. For example, apoptosis can be triggered by mislocalization of anti-apoptotic signals from centrosomes (Li et al., 1998). γ tubulin has recently been shown to associate with DAP-like kinase (Dlk),

which is implicated in apoptosis (Preuss et al., 2003). However, the role of γ tubulin mislocalization from centrosomes and induction of apoptosis through Dlk has not been explored. Mislocalization of survivin and other anti-apoptotic proteins from centrosomes can induce apoptosis (Piekorz et al., 2002; Reed and Reed, 1999; Sandal et al., 2003). Additional studies will be required to identify the proteins and pathways involved in the apoptotic response observed following disruption of the pericentrin-GCP2/3 interaction.

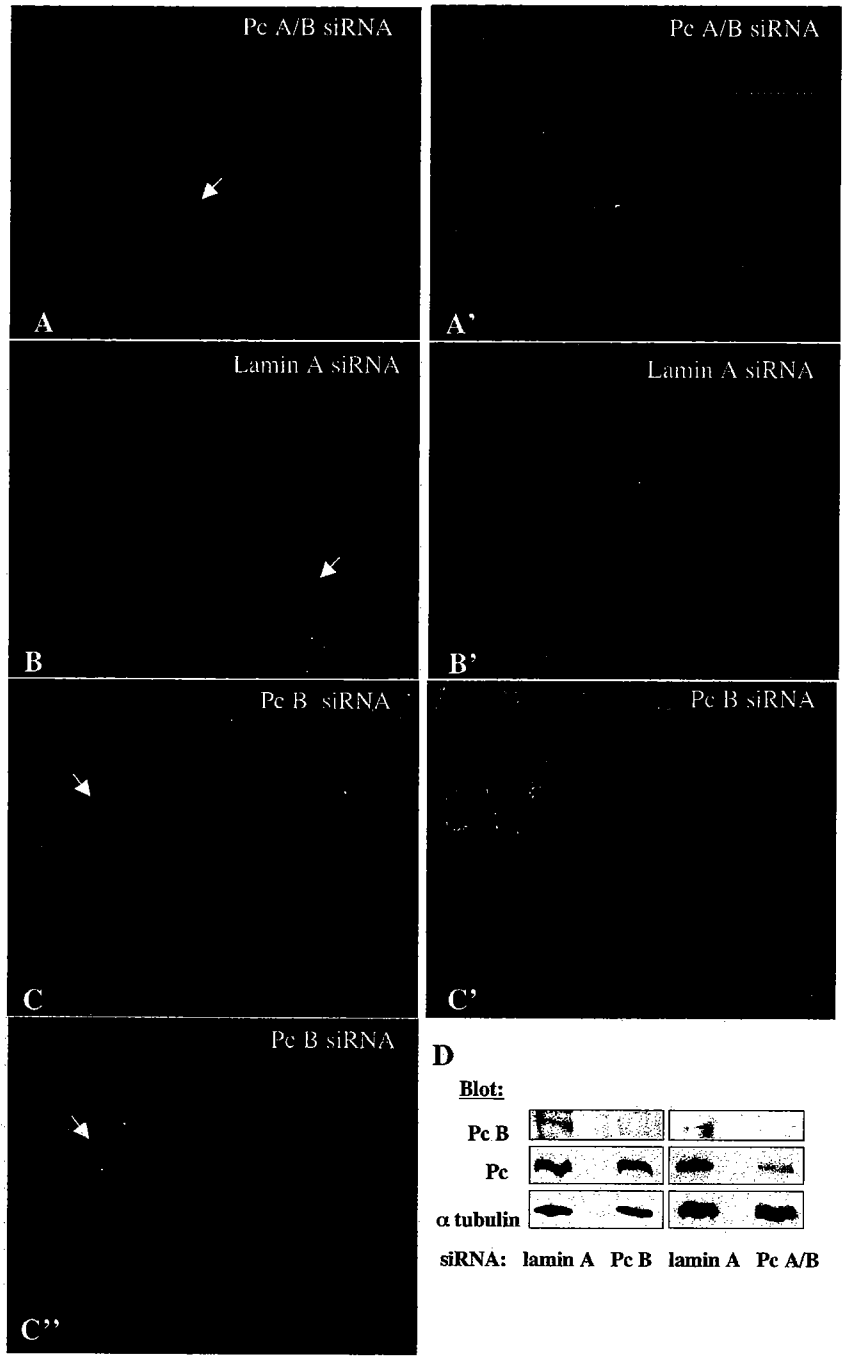
Pc A/B siRNA
A
Pc A/B siRNA
A'
Lamin A siRNA
B
Lamin A siRNA
B'
Pc B siRNA
C
Pc B siRNA
C'
Pc B siRNA
C''
D
Blot:
Pc B
Pc
α tubulin
siRNA: lamin A Pc B lamin A Pc A/B

Figure 15

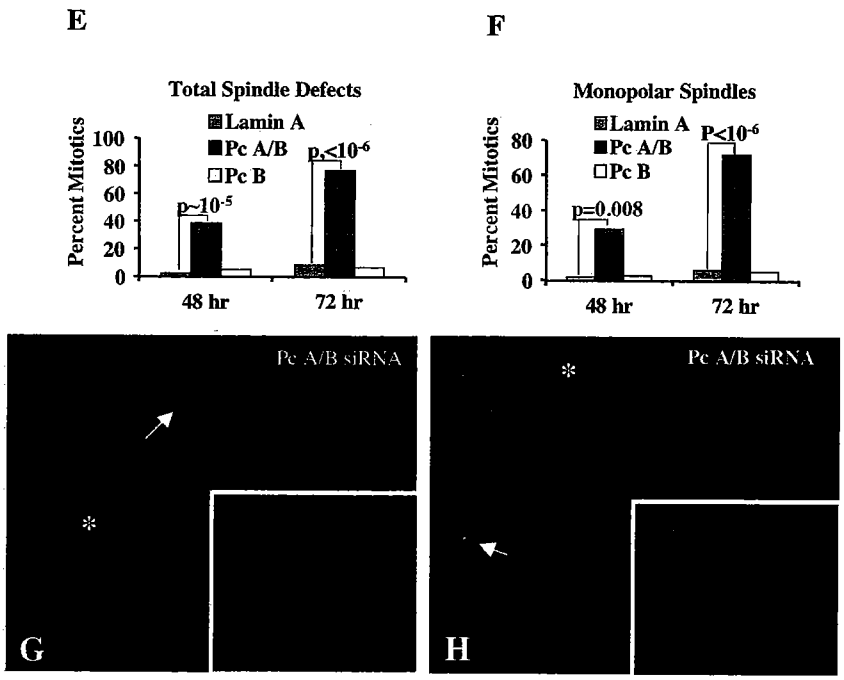

Figure 15 (continued)

Figure 15. Silencing of pericentrin A and B causes mitotic defects. (A) SAOS cells with reduced pericentrin following siRNA treatment stained with a pericentrin antibody (M8, green) which recognizes both isoforms of pericentrin (Pc A/B) and DNA (DAPI, blue). (A') Same field as in A co-stained for microtubules (α tubulin, red). (B) Cells with reduced lamin A stained for lamin A (green) and DNA. (B') Same field as in B stained for centrosomes with 5051 autoimmune sera (green) and microtubules (red). (C, C') Cells with reduced pericentrin B (targeting the C-terminal PACT domain) stained with pericentrin B-specific antibody, Pc B, (C, green), together with microtubule label (C') or pericentrin antibody that recognizes both isoforms (C"). (A, B, C, C'') represent maximum projection of z series without deconvolution. (A'B'C') represent maximum projection of deconvolved z series. Note the improvement in the resolution of the DNA. Arrows indicate cells expressing near normal levels of the targeted protein. (D) Western Blots of crude cell lysates demonstrating reduction of pericentrin B (Pc B) but not pericentrin A (Pc) using Pc B specific siRNA, or reduction of both isoforms relative to lamin A siRNA control, by siRNA targeting Pc A and Pc B (Pc A/B). Pericentrin isoforms probed with Pc A/B anti-pericentrin antibody (M8). α tubulin loading control probed with DM1α anti-alpha tubulin antibody. (E) Graph showing percent of mitotic SAOS cells with spindle defects (monopolar, multipolar and reduced astral microtubules) at 48 and 72 hours following siRNA treatment. 100-150 mitotic cells scored per bar. (F) Graph indicating percent of mitotic cells with monopolar spindles at 48 and 72 hours. (G) Cells with reduced pericentrin A/B (Pc A/B, red) retain the centriole marker GT335

(green) in interphase and mitosis. (H) γ tubulin in cells with reduced pericentrin A/B appears largely unchanged at centrosomes in interphase but is reduced at spindle poles. Pc A/B (red), γ tubulin (GTU88, green), DAPI (blue). G-H are maximum projection of z series with no neighbor deconvolution. Arrows indicate cells with near normal staining levels of pericentrin or lamin A. Asterisks indicate mitotic cells. Mitotic cells are show at higher magnification in insets.

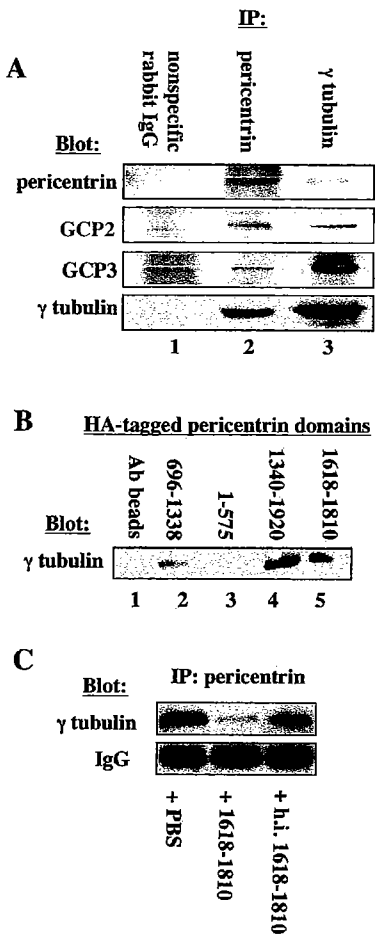
A
IP:
nonspecific rabbit IgG
pericentrin
γ tubulin
Blot:
pericentrin
GCP2
GCP3
γ tubulin
1
2
3
B
HA-tagged pericentrin domains
Ab beads
696-1338
1-575
1340-1920
1618-1810
Blot:
γ tubulin
1
2
3
4
5
C
Blot:
IP: pericentrin
γ tubulin
IgG
+ PBS
+ 1618-1810
+ h.i. 1618-1810

Figure 16

Figure 16. Pericentrin interacts with the γ TuRC in Xenopus extracts. (A) Immunoprecipitation of endogenous pericentrin pulls down γ TuRC proteins (γ tubulin, GCP2, GCP3) from Xenopus extracts (lane 2) and immunoprecipitation of γ tubulin pulls down pericentrin (lane 3) while nonspecific rabbit IgG precipitates none of these proteins (lane 1). (B) HA-tagged C-terminal domains of pericentrin bound to anti-HA beads pull down endogenous γ tubulin from Xenopus extracts (lanes 4, 5), while beads alone and HA-tagged central and amino-terminal domains do not pull down significant γ tubulin (lanes 1-3). (C) A C-terminal domain of pericentrin (1618-1810) disrupts the interaction between endogenous pericentrin and the γ TuRC in extracts as shown by immunoprecipitation with anti-pericentrin antibodies, while heat-inactivated protein (h.i. 1618-1810) and PBS have no effect. Numbers in B and C represent amino acid numbers of pericentrin.

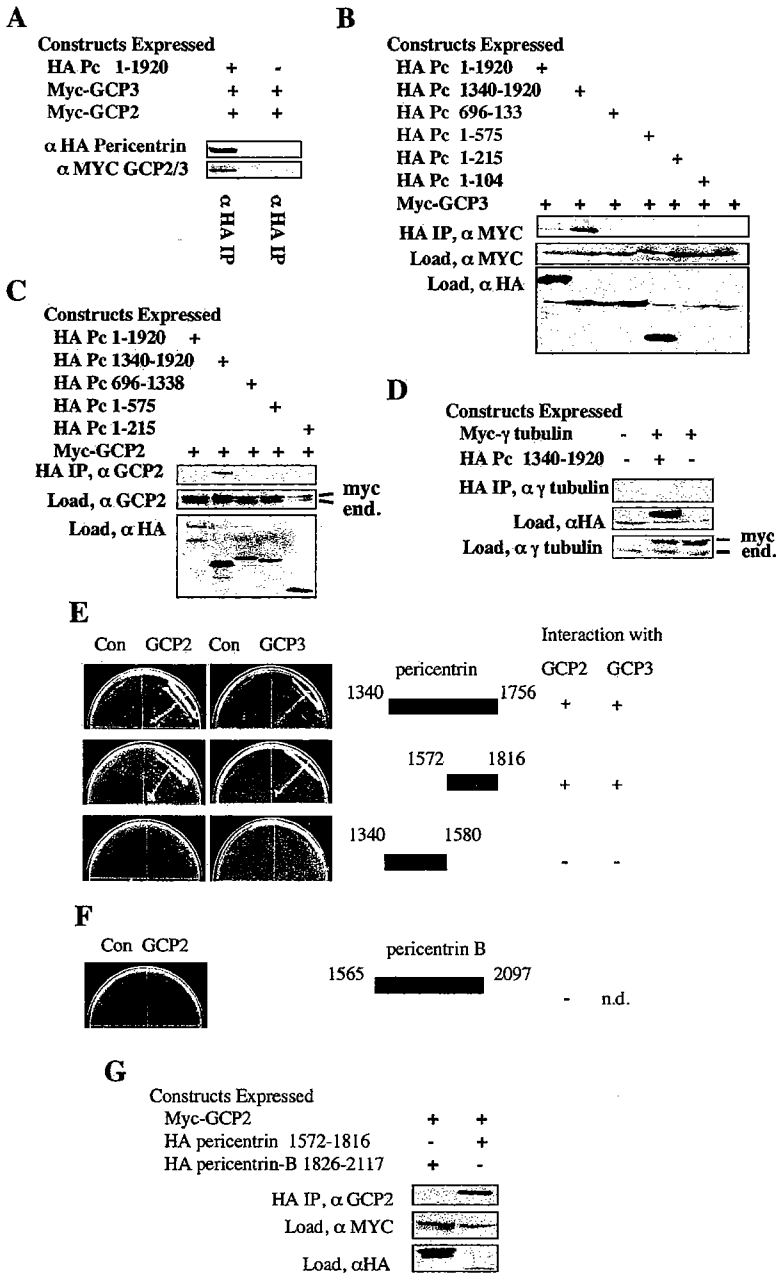
A
Constructs Expressed
HA Pc 1-1920 + -
Myc-GCP3 + +
Myc-GCP2 + +
α HA Pericentrin
α MYC GCP2/3
α HA IP
α HA IP
B
Constructs Expressed
HA Pc 1-1920 +
HA Pc 1340-1920 +
HA Pc 696-133 +
HA Pc 1-575 +
HA Pc 1-215 +
HA Pc 1-104 +
Myc-GCP3 + + + + + + +
HA IP, α MYC
Load, α MYC
Load, α HA
C
Constructs Expressed
HA Pc 1-1920 +
HA Pc 1340-1920 +
HA Pc 696-1338 +
HA Pc 1-575 +
HA Pc 1-215 +
Myc-GCP2 + + + + +
HA IP, α GCP2
Load, α GCP2
Load, α HA
myc end.
D
Constructs Expressed
Myc-γ tubulin - + +
HA Pc 1340-1920 - + -
HA IP, α γ tubulin
Load, αHA
Load, α γ tubulin
myc end.
E
Con GCP2 Con GCP3
Interaction with
pericentrin GCP2 GCP3
1340 1756 + +
1572 1816 + +
1340 1580 - -
F
Con GCP2
pericentrin B
1565 2097 - n.d.
G
Constructs Expressed
Myc-GCP2 + +
HA pericentrin 1572-1816 - +
HA pericentrin-B 1826-2117 + -
HA IP, α GCP2
Load, α MYC
Load, αHA

Figure 17

Figure 17. C-terminal domains of pericentrin interact with γ TuRC proteins GCP3 and GPC2 in vitro. (A) When co-expressed in vertebrate cells myc-tagged GCP2 and/or myc-tagged GCP3 co-immunoprecipitate with HA-tagged pericentrin (similar mobility of GCP2 and GCP3 prevents their individual identification in this experiment). (B-D) A C-terminal domain of pericentrin (amino acids 1340-1920) interacts with GCP3 (B) and GCP2 (C) but not γ tubulin (D) when co-expressed in vertebrate cells. Immunoprecipitation and immunoblotting performed as indicated. End.; endogenous protein. (E) Two-hybrid analysis confirms the interaction of the pericentrin C-terminus with GCP2 and GCP3 but not with γ tubulin (data not shown). (F, G) Segments of pericentrin-B corresponding to the C terminal region of pericentrin do not interact with GCP2 in two-hybrid (F) or co-immunoprecipitation experiments (G).

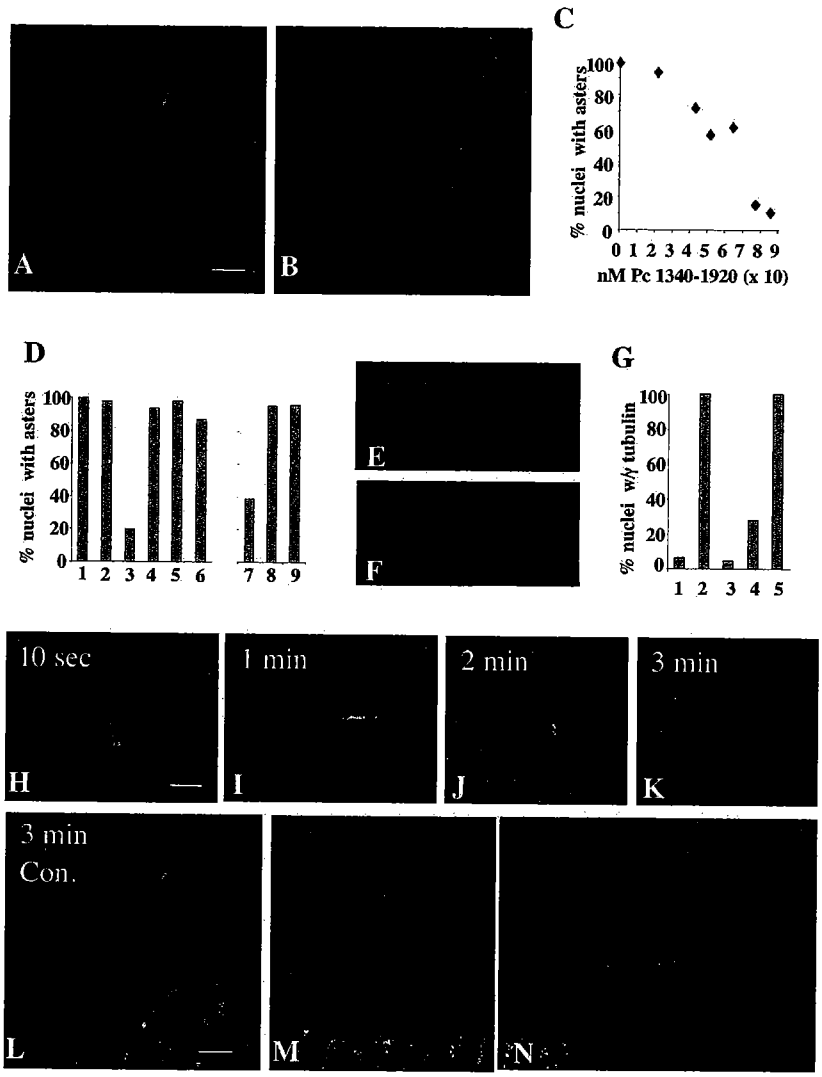
A
B
C
% nuclei with asters
100
80
60
40
20
0
0 1 2 3 4 5 6 7 8 9
nM Pc 1340-1920 (x 10)
D
% nuclei with asters
100
80
60
40
20
0
1 2 3 4 5 6
7 8 9
E
F
G
% nuclei w/γ tubulin
100
80
60
40
20
0
1 2 3 4 5
10 sec
H
1 min
I
2 min
J
3 min
K
3 min
Con.
L
M
N

Figure 18

Figure 18. C-terminal fragments of pericentrin disrupt aster formation and stability and γ tubulin assembly onto centrosomes in Xenopus mitotic extracts. (A, B) Mitotic asters assembled in the presence of equal amounts of pericentrin 1340-1920 (B) or heat inactivated (h.i.) 1340-1920 (A). (C) Mitotic aster assembly in the presence of increasing concentrations of pericentrin (Pc) 1340-1920. (D) Quantification of aster assembly in mitotic extracts in the presence of pericentrin domains. Amount of protein added per 10 μl of extract is indicated. (1. PBS, 2. 33 ng 1-535, 3. 12 ng 1340-1920 ($p < 0.0001$), 4. 12 ng h.i. 1340-1920, 5. 10 ng peri B1826-2117, 6. 10,000 ng BSA). Quantification of aster assembly in interphase extracts (D7-9) using a pericentrin domain (1618-1810) that inhibits aster assembly in mitotic extracts (7. $p < 0.0001$) and is inactivated by heat (8), but has no activity in interphase extracts in the same experiment (9). (E, F) γ tubulin assembly onto nascent centrosomes in the presence of h.i. 1340-1920 (E) or 1340-1920 (F, $p<0.0001$). (G) Quantification of γ tubulin assembly onto centrosomes in the absence of mitotic extract (1), in extracts with 1-595 (2), 1340-1920 (3, $p<0.0001$), 1618-1810 (4, $p<0.0001$), or heat inactivated 1618-1810 (5). For C, D, G, 200 sperm nuclei were counted/bar or point. (H-K) Rapid disassembly of pre-assembled mitotic asters over time following addition of 1340-1920. (L) h.i. Pc 1340-1920 has no effect on pre-assembled asters. (M, N) Ran-mediated aster assembly in extracts in the presence of h.i 1618-1810 (M) or 1618-1810 (N). A-D, H-N, microtubules or γ tubulin, red, nuclei, green. Bar in A, 10 μm for A and B, in L, 10 μm for H-N.

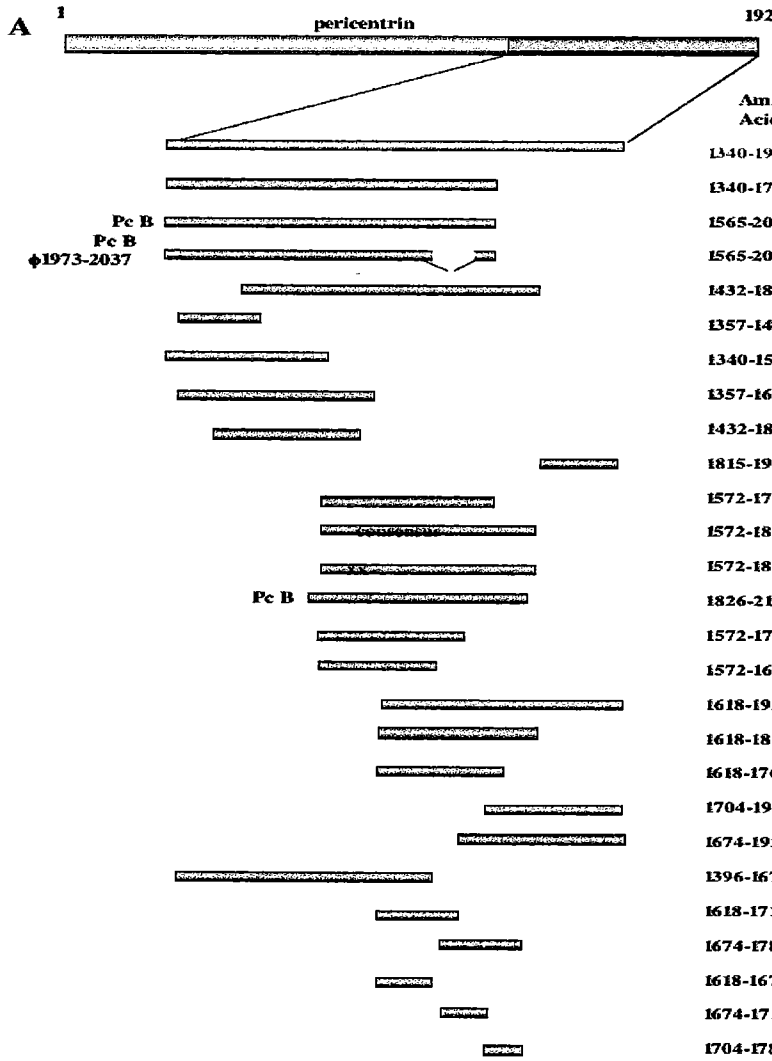

Amino Acids	Co-IP 2	Co-IP 3	2-Hyb 2	2-Hyb 3	Aster
1340-1920	+	+	ND	ND	+
1340-1756	ND	ND	+	+	ND
1565-2097	ND	ND	-	-	ND
1565-2097	ND	ND	+/-	+/-	ND
1432-1816	ND	+	ND	ND	+
1357-1478	ND	-	ND	ND	ND
1340-1580	ND	ND	-	-	ND
1357-1614	-	-	ND	ND	-
1432-1817	ND	+	ND	ND	+
1815-1920	-	-	ND	ND	ND
1572-1756	ND	ND	+	+	ND
1572-1816	ND	+	+	+	+
1572-1816	ND	+	+/-	+/-	-
1826-2117	-	-	ND	ND	-
1572-1715	ND	ND	+	ND	ND
1572-1680	ND	ND	+	ND	ND
1618-1920	ND	+	ND	ND	+
1618-1810	+	+	ND	ND	+
1618-1760	+	+	ND	ND	+
1704-1920	ND	ND	ND	ND	-
1674-1920	ND	ND	ND	ND	-
1396-1674	ND	ND	ND	ND	-
1618-1715	+	+	ND	ND	ND
1674-1784	+	+	ND	ND	ND
1618-1674	+	-	ND	ND	ND
1674-1715	-	-	ND	ND	ND
1704-1784	-	+	ND	ND	ND

Figure 19

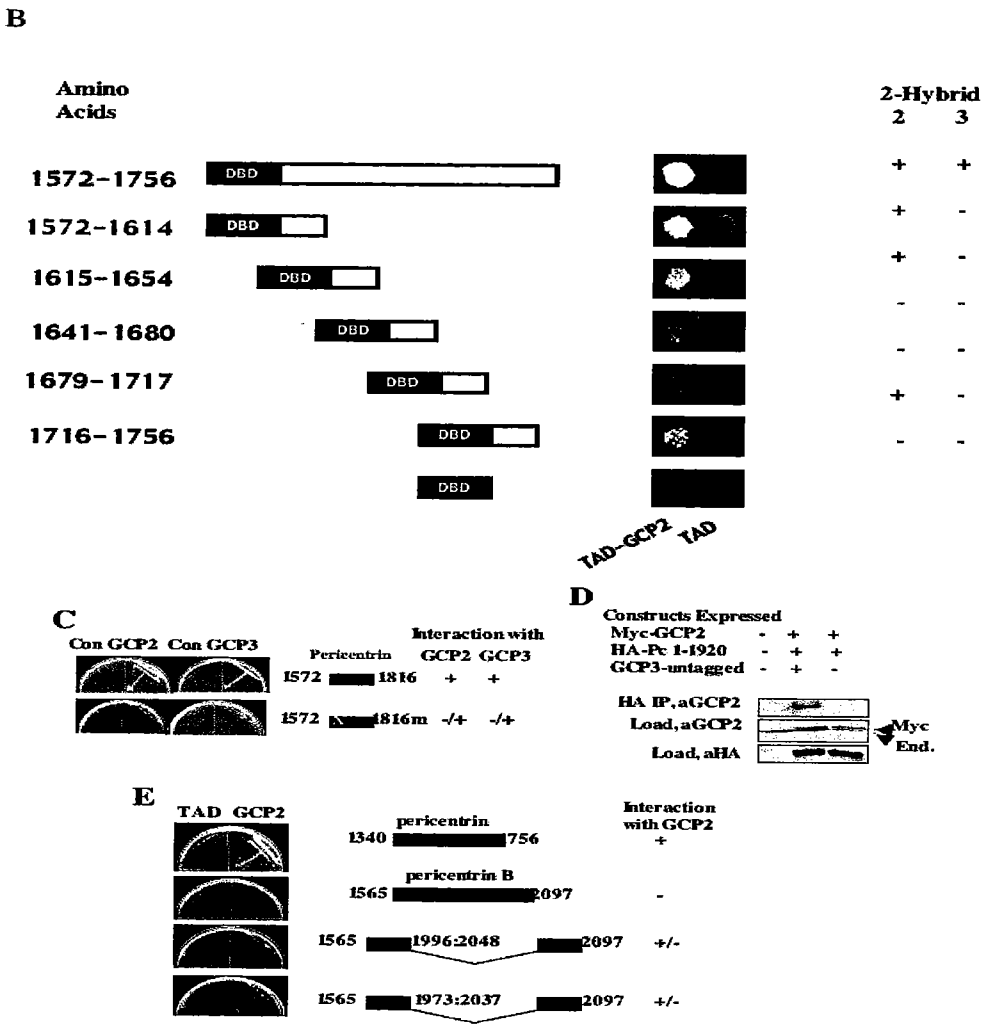

Figure 19 - continued

Figure 19. Summary of GCP2/3 binding and aster inhibitory activity of pericentrin domains. Pericentrin fragments were subcloned into an HA tagged expression vector for analysis by coimmunoprecipitation and aster inhibition in Xenopus or into yeast two hybrid vectors for analysis of protein interactions by yeast two hybrid. (A) Binding and aster activity of various pericentrin constructs. Co-IP, co-immunoprecipitation, 2-hyb, yeast two-hybrid, aster, aster inhibitory activity, consensus, smallest domain identified in both co-IP and 2-hyb that has high affinity binding activity to both GCP2 and GCP3, XX, E to A mutations in 1613 and 1615, Pc B ϕ 1973-2037 lacks an exon encoding the indicated amino acids. Although variable, interactions of all affinities were scored as "+" unless they were at the limit of detection (then scored as "+/-"). ND denote data not acquired for these parameters. Proteins were considered positive in the aster inhibition assay if they showed at least 31% reduction in aster assembly relative to control activity. For clarity, the pericentrin B constructs are arbitrarily sized and aligned with homologous regions of pericentrin. (B) Yeast two hybrid data showing interaction of smallest yeast two hybrid clones with GCP2 and GCP3. (C) Yeast two-hybrid data showing significantly reduced binding of mutant pericentrin domain for GCP2 and GCP3. Con, control. (D) Co-overexpression, co-immunoprecipitation data showing enhanced binding of GCP2 to pericentrin 1-1920 in the presence of GCP3 (see figure legend 16 for details). (E) Yeast two-hybrid data showing binding of GCP2 by a pericentrin A fragment and lack of GCP2 binding by the homologous pericentrin B fragment as well as mutants lacking a pericentrin B specific exon (see Materials and Methods for details).

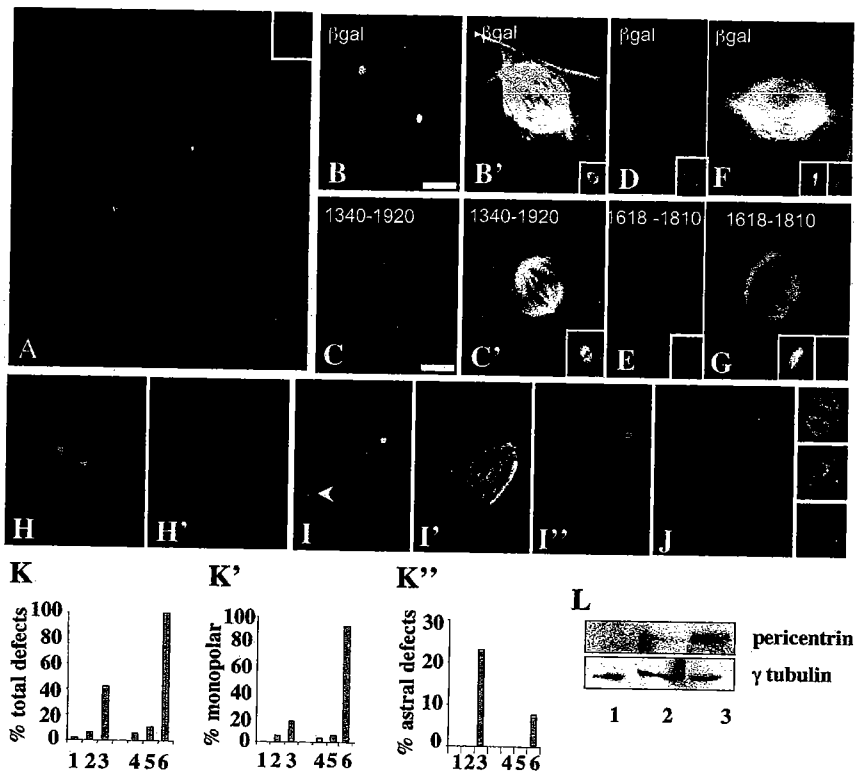
βgal
B
B'
D
F
1340-1920
C
C'
1618 -1810
E
1618-1810
G
A
H
H'
I
I'
I''
J
K
% total defects
100
80
60
40
20
0
1 2 3 4 5 6
K'
% monopolar
K''
% astral defects
30
20
10
1 2 3 4 5 6
L
pericentrin
γ tubulin
1 2 3

Figure 20

Figure 20. GCP2/3 binding domain of pericentrin affects astral microtubules and spindle organization in vertebrate cells. (A) Interphase cell expressing pericentrin 1680-1810 (inset top right) shows no difference in microtubule organization compared to surrounding control cells (red, microtubules; blue, DNA stained with DAPI; yellow, 5051 centrosome staining). (B, B') Control mitotic cell expressing β galactosidase. (C, C') Cell expressing pericentrin 1340-1920 and spindles with reduced astrals and pole-to-pole distance (C', compare with B, B'). Insets at bottom right of B', C' show protein-expression. (D) β galactosidase-expressing control cell. (E) Cell expressing pericentrin 1680-1810 shows reduced γ tubulin at spindle poles (compare with D). D, E, γ tubulin (red), DNA (blue), insets show 5051 staining. (F) β galactosidase-expressing cell. (G) Cell expressing 1680-1810 (inset bottom right) shows reduced astral microtubules and decreased pole-to-pole distance compared with F. DNA, insets, left. Overexpressed protein, insets, right. (H) Monopolar spindle in cell expressing 1680-1810 showing centrosomes (yellow, 5051) and microtubules (H) or DNA (H'). (I) Spindle from cell expressing 1680-1810 with one tiny spindle pole (arrowhead, 5051) and unfocused microtubules at this pole (I', merge, I''). (J) Telophase cell expressing 1680-1810 undergoing tripolar division. One nascent daughter cell lacks a centrosome (bottom). Images at right show protein expression (top), microtubules (middle) and centrosomes (bottom). (A-J), immunofluorescence images of SAOS cells. All images except H and H' are shown with deconvolution. Paired images were stained in parallel and collected on the same day, without modification to the laser or acquisition settings between images. (K-K'') Graphs

showing percent of transfected mitotic SAOS cells with total mitotic defects (K), monopolar spindles (K') and reduced or absent astral microtubules (K''). 1-3, 20 hours post transfection, 4-6, 40 hours post transfection. 1, nontransfected mitotics n=368. 2, βgal, n=82. 3, Pc1618-1810, n=31. 4, Pc B 1826-2117, n=95. 5, βgal, n=39. 6, Pc 1618-1810, n=14. P values comparing βgal and 1618-1810 expressing cells were calculated using the student t test for both time points. Graph K, $p<0.0001$ at 22 hours, $p<0.0001$ at 44 hours. Graph K', $p=0.049$ at 22 hours, $p< 0.0001$ at 44 hours. (L) Soluble pericentrin is more abundant in mitotic cells. Western Blot of HeLa whole cell lysates from asynchronous cells (lane 1), from cells treated 4 hours with nocodazole (lane 2), and from mitotic cells after shake-off (lane 3). Total protein loads were normalized for each lane using the Biorad protein assay.

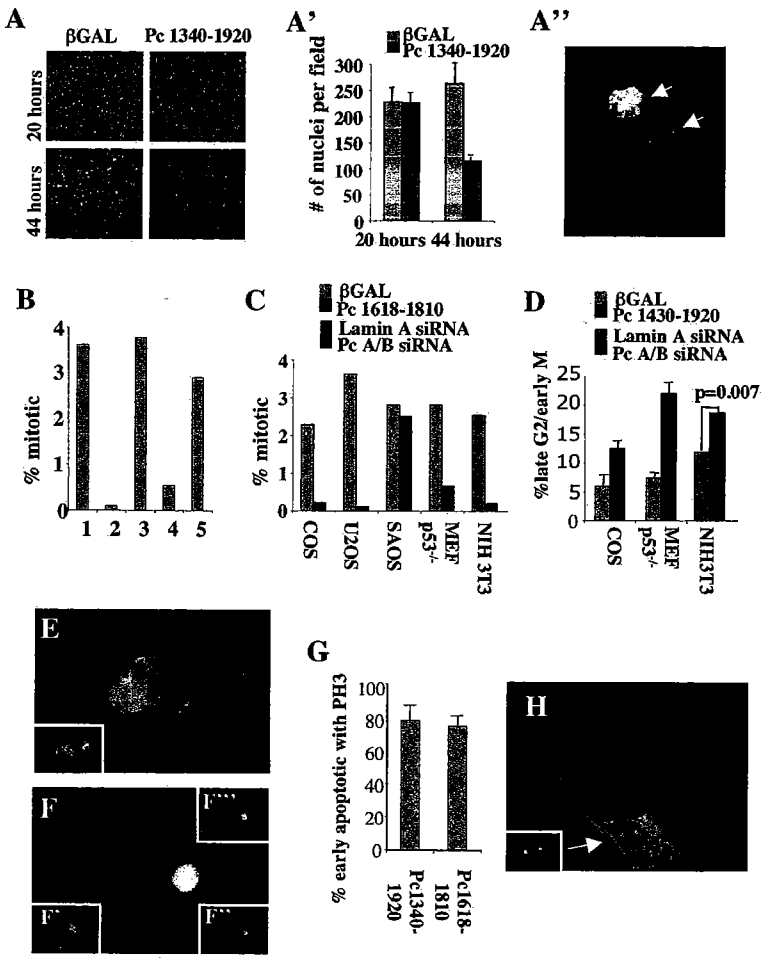
A
βGAL
Pc 1340-1920
20 hours
44 hours
A'
βGAL
Pc 1340-1920
# of nuclei per field
300
250
200
150
100
50
0
20 hours 44 hours
A''
B
% mitotic
4
3
2
1
0
1 2 3 4 5
C
βGAL
Pc 1618-1810
Lamin A siRNA
Pc A/B siRNA
% mitotic
4
3
2
1
0
COS
U2OS
SAOS
p53-/-
MEF
NIH 3T3
D
βGAL
Pc 1430-1920
Lamin A siRNA
Pc A/B siRNA
%late G2/early M
25
20
15
10
5
0
p=0.007
COS
p53-/-
MEF
NIH3T3
E
F
F'''
F'
F''
G
% early apoptotic with PH3
100
80
60
40
20
0
Pc1340-1920
Pc1618-1810
H

Figure 21

Figure 21. Overexpression of GCP2/3 binding domain or silencing of Pc A/B induces cell cycle arrest and apoptosis at the G2/M phase of the cell cycle. (A) Cells expressing the GCP2/3 binding domain are lost through apoptosis. Low magnification image of COS cells stained with DAPI showing cell loss when 1340-1920 is expressed for 44 hours compared with non-expressing cells (20 hours) or β galactosidase (βgal) expressing cells. (A') Quantification of cells in A, (mean and standard deviation, 10 fields). (A'') Image of COS cells from A stained for DNA (blue), 1340-1920 (red) and M30 cytodeath (green). Arrows, cells with both 1340-1920 and M30. (B) Mitotic index of U2OS cells expressing: 1, βgal; 2, Pc1618-1810 $p<0.001$; 3. Pc B1826-2117 $p=0.437$; 4, Pc1572-1816 $p=0.011$; 5, Pc 1572-1816m $p=0.226$ ($n=1000$ cells /bar at 40-44 hours post transfection. P values were calculated using the t test relative to βgal controls). (C) Mitotic index in indicated cell types overexpressiong the indicated constructs or treated with siRNA. P values calculated as above; COS $p<0.001$; U2OS $p<0.001$; SAOS $p=0.479$; Mefp53-/- $p=0.001$, NIH3T3 (siRNA) $p=0.0004$ (D) Cells expressing GCP2/3 binding domain constructs or treated with Pc A/B siRNA have a greater proportion of late G2 cells. Shown are mean and standard deviation of 3 experiments or p value based upon scoring from 1000 treated cells. Cells immunostained for overexpressed protein (green), phosphorylate histone H3 (PH3, red) and DAPI (blue). (E) Antephase cell overexpressing 1340-1920 (stains for phosphorylated histone H3 and does not show condensed chromatin). Inset, DAPI. (F) Apoptotic antephase cells expressing 1340-1920. M30 (red), phosphorylated histone H3 (green, and inset bottom right), DNA

(blue, inset above), overexpressed protein (inset bottom left). (G) Graph showing that most early apoptotic cells expressing GCP2/3 binding domains stain for phosphorylated histone H3. Shown are mean, standard deviation, n =3 experiments. (H) Early apoptotic cell expressing 1340-1920 stained for centrosomes (5051, green), DNA (blue), HA pericentrin (red), M30, yellow. Inset 5051. Imaged as in Figure 19.

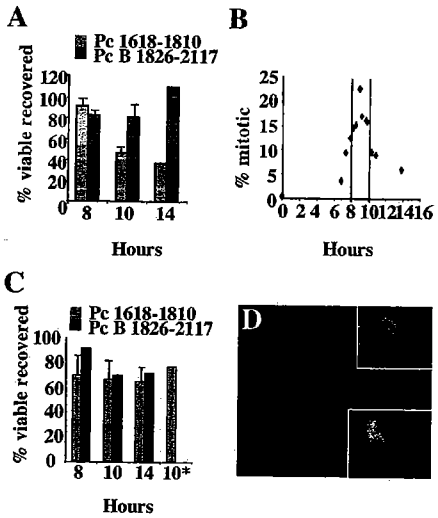
A
Pc 1618-1810
Pc B 1826-2117
% viable recovered
120
100
80
60
40
20
0
8
10
14
Hours
B
% mitotic
25
20
15
10
5
0
0 2 4 6 8 10 12 14 16
Hours
C
Pc 1618-1810
Pc B 1826-2117
% viable recovered
100
80
60
40
20
0
8
10
14
10*
Hours
D

Figure 22

Figure 22. COS cells expressing Pc1618-1810 undergo apoptosis during the G2/M transition. (A) Cells expressing 1618-1810 undergo apoptosis at mitosis. Microinjected cells released from a double thymidine block were stained for DNA (DAPI) and overexpressed protein (250 cells/bar). 1618-1810-expressing cells were apoptotic or detached 8-10 hours after injection, while control cells (Pc B1826-2117) increased in number. At 14 hours p value comparing the two treatments $p<0.0001$ (B) Mitotic index of COS cells following release from double thymidine block as in A (peak, 9 hours). (C) 1618-1810-expressing cells arrested in S phase do not undergo apoptosis. Microinjected cells retained in thymidine for the times indicated. No loss of cells was observed 8-14 hours later. 10*, microinjected cells arrested in S phase for 6 hours, and then released from the block for 4 hours (10 hours total $p=0.25$). (D) Immunofluorescence image of an apoptotic cell expressing 1618-1810 at 10 hours post injection as in A. D (overlay), DNA (blue and upper inset), M30 (red), overexpressed protein (lower inset).

FUTURE DIRECTIONS

While complete in itself, this work leaves several unanswered questions. Among them: How is the pericentrin γTuRC association regulated? What is the mitotic entry checkpoint monitoring? And what regulatory molecules are involved with this checkpoint?

I believe that the association of pericentrin and γ TuRC in somatic cells must be regulated because overexpression of full length or dominant negative pericentrin does not mislocalize γ tubulin from interphase centrosomes, suggesting that it is not competitive in interphase. The interaction could be regulated by mitosis-specific phosphorylation of pericentrin or a component of the γTuRC. In budding yeast Spc110p, Spc98p (GCP3), and Tub4p (γ tubulin) all undergo mitosis-specific phosphorylation, (Vogel, 2001; Friedmann et al., 1996; Friedmann et al., 2001; Pereira et al., 1998). Phosphorylation of Tub4p has been shown to influence microtubule organization in mitosis (Vogel et al., 2001). We know that pericentrin is phosphorylated at multiple sites in interphase and is more highly phosphorylated in mitosis (Zimmerman, Stukenberg, Doxsey, unpublished observations). Likewise, γ tubulin is phosphorylated in mitosis (T. Stearns, personal communication). Whether or not any of these known phosphorylation events affect the pericentrin/ γ tubulin interaction is currently unknown. How the association of γ tubulin and pericentrin is regulated should be fruitful grounds for further study.

This study did not determine what the mitotic entry checkpoint may be monitoring or what regulatory pathways may be involved. I favor a model in which the checkpoint senses spindle pole assembly/ centrosome maturation since disruption of the γ tubulin-pericentrin interaction disrupts spindle pole assembly and possibly centrosome maturation, which increases in size four fold between G2 and early prophase (Dictenberg et al, 1998; Piehl et al., 2004). This occurs with the onset of γ tubulin mislocalization and antephase arrest that I observe. I do not know why SaOS cells do not display the checkpoint response. They are known to be deficient in both p53 and Rb. I have demonstrated that p53 is not involved in the arrest that I observe. Further work must be done to determine if RB or some other currently undefined deficiency in SaOS cells is responsible for their insensitivity to the checkpoint.

Why are most of the disrupted mitotic spindles monopolar? In this study we were unable to distinguish between the possibility that poles failed to separate properly initially, or that poles separated but the bipolar spindle, lacking astral microtubules and containing reduced numbers of microtubules in the central spindle, was unstable and subsequently collapsed (see Figure 23). Real time studies using GFP labeled tubulin could address this question.

This study produced new reagents that should prove useful in addressing other questions. For instance, the pericentrin B specific siRNA should help address

questions about the role of pericentrin B in other cellular processes. Likewise the dominant negative constructs could be used to address questions about the role of astral microtubules in localizing other spindle components, in spindle positioning and in microtubule dynamics.

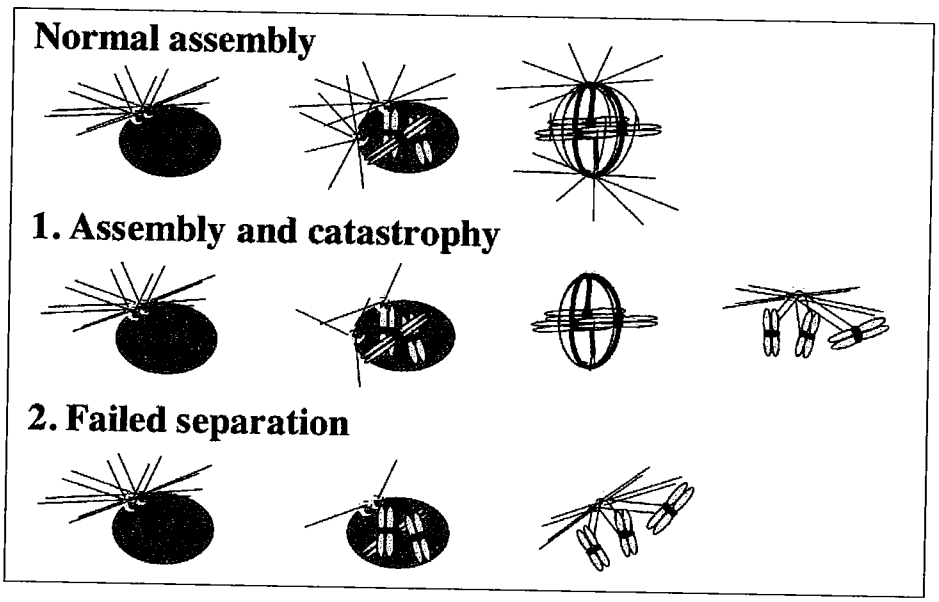
Normal assembly
1. Assembly and catastrophy
2. Failed separation

Figure 23

Figure 23. Models for monopolar spindle formation. In normal cells centrosomes separate in early prophase, before nuclear membrane breakdown, and bipolar spindles are formed. In cells with disrupted pericentrin/γ TuRC interactions centrosomes may separate to form bipolar "mini" spindles lacking astral microtubules which may be unstable and collapse to form monopolar spindles (1), or nascent spindle poles lacking γ tubulin anchored astral microtubules may fail to separate at the onset of mitosis (2) yielding monopolar spindles.

BIBLIOGRAPHY

Adams, S.R., A.T. Harootunian, Y.J. Buechler, S.S. Taylor, and R.Y. Tsien. 1991. Flourescence ratio imaging of cyclic AMP in single cells. *Nature*. 349:694-697.

Akashi, T., Y. Yoon, and B.R. Oakley. 1997. Characterization of g tubulin complexes in Aspergillus nidulans and detection of putative g tubulin interacting proteins. *Cell Motil. Cytoskeleton.* 37:149-158.

Albers, K., and Fuchs, E. 1992. The molecular biology of intermediate filaments. *Int. Rev. Cytol.* 134:243-279.

Archer, J., and Solomon, F. 1994. Deconstructing the microtubule-organizing center. *Cell.* 76: 589-592.

Balczon, R. 1997. The centrosome in animal cells and it's functional homologues in plant and yeast cells. *Int. Rev. Cytol.* 169:25-82.

Balczon, R., L. Bao, K. Brown, R.P. Zikowski, and B.R. Brinkley. 1995. Dissociation of centrosome replication events from cycles of DNA synthesis and Mitotic division in hydroxyurea-arrested Chinese hamster ovary cells. *J. Cell Biol.* 42:60-72.

Balczon, R., L. Bao, and W.E. Zimmer. 1994. PCM-1, A 228-kD centrosome autoantigen with a distinct cell cycle distribution. *J Cell Biol.* 124:783-793.

Balczon, R., C.E. Varden, and T.A. Schroer. 1999. Role for microtubules in centrosome doubling in Chinese hamster ovary cells. *Cell Motility and the Cytoskeleton.* 42:60-72.

Barbosa, V., M. Gatt, E. Rebollo, C. Gonzalez, and D.M. Glover. 2003. Drosophila dd4 mutants reveal that gammaTuRC is required to maintain juxtaposed half spindles in spermatocytes. *J Cell Sci.* 116:929-941.

Barbosa, V., R.R. Yamamoto, D.S. Henderson, and D.M. Glover. 2000. Mutation of a Drosophila gamma tubulin ring complex subunit encoded by discs degenerate-4 differentially disrupts centrosomal protein localization. *Genes Dev.* 14:3126-3139.

Bassell, G.J., Y. Oleynikov, and R.H. Singer. 1999. The travels of mRNAs through all cells large and small. *FASEB.* 13:447-454.

Blagden, S.P., and D.M. Glover. 2003. Polar expeditions--provisioning the centrosome for mitosis. *Nat Cell Biol.* 5:505-511.

Blangy, A., L. Arnaud, and E.A. Nigg. 1997. Phosphorylation by p34cdc2 Protein kinase regulates binding of the kinesin-related motor HsEg5 to the Dynactin subunit p150glued. *J Biol. Chem.* 272:19418-19424.

Blomberg, M., and S.J. Doxsey. 1998. Rapid isolation of centrosomes. *Meth. Enzymol.* 298:228-238.

Bobbinec, Y., A. Khodjakov, L.M. Mir, C.L. Rieder, B. Edde, and M. Bornens. 1998. Centriole disassembly *in vivo* and its effect on centrosome structure and function in vertebrate cells. . 143:1575-1589.

Boveri, T. 1914. *The Origin of Malignant Tumours.* Williams and Wilkins, Baltimore.

Brinkley, B.R., and E. Stubblefield. 1970. Microtubule organizing centers. *Ann. Rev. Cell Biol.* 1:119-172.

Brown, R., S.J. Doxsey, L. Hong-Brown, R.L. Martin, and W. Welsh. 1996a. Molecular chaperones and the centrosome: a role for TCP-1 in microtubule nucleation. *J. Biol. Chem.* 271:824-832.

Buendia, B., Draetta, G. and Karsenti, E. 1992. Regulation of protein kinases associated with cyclin A and cyclin B and their effect on microtubule dynamics and nucleation. *J. Cell Biol.* 117: 1055-1066.

Burkhardt, J.K., C.J. Echeverri, T. Nilsson, and R.B. Vallee. 1997. Overexpression of the dynamitin (p50) subunit of the dynactin complex disrupts dynein-dependent maintenance of membrane organelle distribution. *J. Cell Biol.* 139:469-484.

Carrington, W., R.M. Lynch, E.D. Moore, G. Isenberg, K.E. Fogarty, and F.S. Fay. 1995. Superresolution three-dimensional images of fluorescence in cells with minimal light exposure. *Science*. 268:1483-1486.

Casenghi, M., P. Meraldi, U. Weinhart, P.I. Duncan, R. Korner, and E.A. Nigg. 2003. Polo-like kinase 1 regulates Nlp, a centrosome protein involved in microtubule nucleation. *Dev Cell.* 5:113-125.

Centonze, V.E., and G.G. Borisy. 1990. Nucleation of microtubules from mitotic centrosomes is modulated by a phosphorylated epitope. *J. Cell Sci.* 95:405:411.

Chang, P., T.H. Giddings, Jr., M. Winey, and T. Stearns. 2003. Epsilon-tubulin is required for centriole duplication and microtubule organization. *Nat Cell Biol.* 5:71-76.

Chen, D., A. Purohit, E. Halilovic, S. J. Doxsey, and A.C. Newton. 2004. Centrosomal anchoring of protein kinase C betaII by pericentrin controls microtubule organization, spindle function, and cytokinesis. *J. Biol. Chem.* 279:4829-4839.

Chen, X.P., H. Yin, and T. Huffaker. 1998. The yeast spindle pole body component Spc72p interacts with Stu2p and is required for proper microtubule assembly. *J. Cell Biol.* 141:1169-1179.

Clark, I.B., and D.I. Meyer. 1999. Overexpression of normal and mutant Arp1a (centractin) differentially affects microtubule organization during mitosis and interphase. *J. Cell Sci.* 112:3507-3518.

Compton, D.A., Szilak, J. and Cleveland, D.W. 1992. Primary structure of NuMA, an intranuclear protein that defines a novel pathway for segregation of proteins at mitosis. *J. Cell Biol.* 116:1395-1408.

Compton, D.A. 1998. Focusing on spindle poles. *J. Cell Sci.* 111:1377-1481.

Dammermann, A., and A. Merdes. 2002. Assembly of centrosomal proteins and microtubule organization depends on PCM-1. *J Cell Biol.* 159:255-266.

Dasso, M. 2002. The Ran GTPase: theme and variations. *Curr Biol.* 12:R502-508.

DeDuve, C.J., J. Berthet, and H. Beaufay. 1959. Gradient centrifugation of cell particles: theory and applications. *Prog. Biphys. Biophys. Chem.* 236: 1372-1379.

DeHaen, C. 1987. Molecular weight standards for calibration of gel filtration and sodium dodecyl sulfate-polyacrylamide electrophoresis: ferritin and apoferritin. *Anal. Biochem.* 166:235-245.

Dictenberg, J., W. Zimmerman, C. Sparks, A. Young, C. Vidair, Y. Zheng, W. Carrington, F. Fay, and S.J. Doxsey. 1998. Pericentrin and gamma tubulin form a protein complex and are organized into a novel lattice at the centrosome. *J. Cell Biol.* 141:163-174.

Ding, R., R.R. West, M. Morphew, B.R. Oakley, and J.R. McIntosh. 1997. The spindle pole body of *Schizosaccharomyces pombe* enters and leaves the nuclear envelope as the cell cycle proceeds. *Mol. Biol. Cell.* 8:1461-1479.

Dionne, M.A., L. Howard, and D.A. Compton. 1999. NuMA ia a component of an insoluble matrix at mitotic spindle poles. *Cell Motil. Cytoskel.* 42:189-203.

Diviani, D., L.K. Langeberg, S.J. Doxsey, and J.D. Scott. 2000. Pericentrin anchors protein kinase A at the centrosome through a newly identified RII-binding domain. *Curr Biol.* 10:417-420.

do Carmo Avides, M., and D.M. Glover. 1999. Abnormal spindle protein, ASP, and the integrity of mitotic centrosomal microtubule organizing centers. *Science*. 283:1733-1735.

Doxsey, S.J. 1998. The centrosome--a tiny organelle with big potential. *Nature Genetics*. 20:104-106.

Doxsey, S.J. 2001. Re-evaluating centrosome function. *Nature Reviews in Molecular Biology*. 2:688-699.

Doxsey, S.J., P. Stein, L. Evans, P. Calarco, and M. Kirschner. 1994. Pericentrin, a highly conserved protein of centrosomes involoved in microtubule orgainzation. *Cell*. 76: 639-650.

Dransfield, D.T., J.L. Yeh, A.J. Bradford, and J.R. Goldenring. 1997. Identification and characterization of a novel A-kinase-anchoring protein (AKAP120) from rabbit gastric parietal cells. *Biochem. J.* 322:801-807.

Echeverri, C.J., B.M. Paschal, K.T. Vaughan, and R.B. Vallee. 1996. Molecular characterization of the 50-kD subunit of dynactin reveals function for the complex in

chromosome alignment and spindle organization during mitosis. *J. Cell Biology.* 132:617-633.

Elder, R.T., Z. Benko, and Y. Zhao. 2002. HIV-1 VPR Modulates cell cycle G2/M transition through an alternative cellular mechanism other than the classic mitotic checkpoints. *Frontiers in Bioscience.* 7:d349-357.

Englander, S., A.H. Sharp, V. Colmer, M.K. Tokito, A. Lanahan, P. Worley, and e. al. 1997. Huntington-associated protein 1 (HAP1) interacts with the p150*Glued* subunit of dynactin. *Hum. Mol. Genet.* 6:2205-2212.

Erickson, H.P., and D. Stoffler. 1996. Protofilaments and rings, two conformations of the tubulin family conserved from bacterial FtsZ to alpha/beta and gamma tubulin. *J Cell Biol.* 135:5-8.

Felix, M.-A., C. Antony, M. Wright, and B. Maro. 1994. Centrosome assembly in vitro: Role of g-tubulin recriutment in Xenopus sperm aster formation. *J. Cell Biol.* 124:19-31.

Fire, A., S. Xu, M. K. Montgomery, S. A. Kostas, S. E. Driver, and C. C. Mello. 1998. Potent and specific genetic interference by double-stranded RNA in Caenorhabditis elegans. *Nature.* 391:806-811.

Flory, M.R., and T.N. Davis. 2003. The centrosomal proteins pericentrin and kendrin are encoded by alternatively spliced products of one gene. *Genomics*. 82:401-405.

Flory, M.R., M. Morphew, J.D. Joseph, A.R. Means, and T.N. Davis. 2002. Pcp1p, an Spc110p-related Calmodulin Target at the Centrosome of the Fission Yeast Schizosaccharomyces pombe. *Cell Growth Differ.* 13:47-58.

Flory, M.R., M.J. Moser, R.J. Monnat, Jr., and T.N. Davis. 2000. Identification of a human centrosomal calmodulin-binding protein that shares homology with pericentrin. *Proc Natl Acad Sci U S A.* 97:5919-5923.

Freed, E., K.R. Lacey, P. Huie, S.A. Lyapina, R. Deshaies, T. Stearns, and P. Jackson. 1999. Components of an SFC ubiquitin ligase localize to centrosomes and regulate the centrosome duplication cycle. *Genes and Devel.* 13:2242-2257.

Friedmann, D.B., H. A. Sundberg, H. A. Huang, and T. N. Davis. 1996. The 110-kD spindle pole body component of *Saccharomyces cerevisiae* is a phosphoprotein that is modified in a cell cycle dependent manner. *J. Cell Biol.* 132:903-914.

Friedmann, D.B., J. W. Kern,B. J. Huneycutt, D. B. N. Vinh, D.K. Crawford, E. Steiner, D. Scheitz, J. Yates III, K. A. Resing, N. G. Ahn, M. Winey, and T. N. Davis.

2001. Yeast Mps1p phosphorylates the Spindle Pole Component Spc110p in the N-terminal Domain. J. Biol. Chem. 276:17958-17967.

Fry, A.M., T. Mayor, P. Meraldi, Y.D. Stierhof, K. Tanaka, and E.A. Nigg. 1998a. C-Nap1, a novel centrosomal coiled-coil protein and candidate substrate of the cell cycle-regulated protein kinase Nek2. *J Cell Biol.* 141:1563-1574.

Fry, A.M., P. Meraldi, and E.A. Nigg. 1998b. A centrosomal function for the human Nek2 protein kinase, a member of the NIMA family of cell cycle regulators. *Embo J.* 17:470-481.

Gaglio, T., M.A. Dionne, and D. Compton. 1997. Mitotic spindle poles are organized by structural and motor proteins in addition to centrosomes. *J. Cell Biol.*:1055-1066.

Gard, D., Hafezi, S., Zhang, T., and Doxsey, S.J. 1990. Centrosome duplication continues in cycloheximide-treated Xenopus blastulae in the absence of a detectable cell cycle. *J. Cell Biol.* 110:2033-2042.

Garrett, S., K. Auer, D.A. Compton, and T.M. Kapoor. 2002. hTPX2 is required for normal spindle morphology and centrosome integrity during vertebrate cell division. *Curr Biol.* 12:2055-2059.

Giet, R., D. McLean, S. Descamps, M.J. Lee, J.W. Raff, C. Prigent, and D.M. Glover. 2002. Drosophila Aurora A kinase is required to localize D-TACC to centrosomes and to regulate astral microtubules. *J Cell Biol.* 156:437-451.

Gillingham, A.K., and S. Munro. 2000. The PACT domain, a conserved centrosomal targeting motif in the coiled- coil proteins AKAP450 and pericentrin. *EMBO Rep.* 1:524-529.

Glover, D.M., H. Ohkura, and A. Tavares. 1996. Polo kinase: the choreographer of the mitotic stage? *135*:1618-1684.

Gould, R.R., and G.G. Borisy. 1977. The pericentriolar material in Chinese hamster ovary cells nucleates microtubule formation. *J. Cell Biol.* 73:601-615.

Griffiths, G. 1993. Fine Structure Immunocytochemistry. Springer-Verlag, New York.

Gruss, O.J., R.E. Carazo-Salas, C.A. Schatz, G. Guarguaglini, J. Kast, M. Wilm, N. Le Bot, I. Vernos, E. Karsenti, and I.W. Mattaj. 2001. Ran induces spindle assembly by reversing the inhibitory effect of importin alpha on TPX2 activity. *Cell.* 104:83-93.

Gueth-Hallonet, C., J. Wang, J. Harborth, K. Weber, and M. Osborn. 1998. Induction of a regular nuclear lattice by overexpression of NuMA. *Exp. Cell Res.* 243:434-452.

Hamill, D.R., A.F. Severson, J.C. Carter, and B. Bowerman. 2002. Centrosome maturation and mitotic spindle assembly in C. elegans require SPD-5, a protein with multiple coiled-coil domains. *Dev Cell.* 3:673-684.

Hannak, E., M. Kirkham, A.A. Hyman, and K. Oegema. 2001. Aurora-A kinase is required for centrosome maturation in Caenorhabditis elegans. *J Cell Biol.* 155:1109-1116.

Hannak, E., K. Oegema, M. Kirkham, P. Gonczy, B. Habermann, and A.A. Hyman. 2002. The kinetically dominant assembly pathway for centrosomal asters in Caenorhabditis elegans is gamma-tubulin dependent. *J Cell Biol.* 157:591-602.

Hans, F., and S. Dimitrov. 2001. Histone H3 phosphorylation and cell division. *Oncogene*. 20:3021-3027.

Harborth, J., L. Howard, and D.A. Compton. 1999. Self assembly of NuMA: multiarm oligomers as structural units of a nuclear lattice. *EMBO J.* 18:1680-1700.

Harlow, E., and Lane, D. 1988. Antibodies: A Laboratory Manual. Cold Spring Harbor Laboratory Press, Cold Spring Harbor, New York.

Hartman, J., J. Mahr, K. McNally, S. Thomas, S. Cheeseman, J. Heuser, R. Vale, and F. McNally. 1998. Katanin, a microtubule-severing protein, is a novel AA ATPase that targets to the centrosome using a WD40-containing subunit. *Cell.* 93:277-287.

Heald, R., R. Tournebize, T. Blank, R. Sandaltzopoulos, P. Becker, A. Hyman, and E. Karsenti. 1996. Self-organization of microtubules into bipolar spindles around artificial chromosomes in Xenopus egg extracts. *Nature.* 382:420-425.

Heim, R., Cubbit, A.B. and Tsien, R. 1995. Improved green fluorescence. *Nature.* 373:663-664.

Helps, N.R., N.D. Brewis, K. Lineruth, T. Davis, K. Kaiser, and P.T.W. Cohen. 1998. Protein phosphatase 4 is an essential enzyme required for organization of microtubules at centrosomes in Drosophila embryos. *J. Cell Sci.* 111:1331-1340.

Hinchcliffe, E.H., G. Cassels, C. Rieder, and G. Sluder. 1998. The coordination of centrosome reproduction with nuclear events of the cell cycle in the sea urchin zygote. *J. Cell. Biol.* 140:1417-1426.

Hinchcliffe, E.H., C. Li, E.A. Thompson, J.L. Maller, and G. Sluder. 1999. Requirement of Cdk2-cyclin E activity for repeated centrosome reproduction in Xenopus egg extracts. *Science*. 283:851-854.

Howell, B.J., D.B. Hoffman, G. Fang, A.W. Murray, and E.D. Salmon. 2000. Vizualization of Mad2 dynamics at kinetochores, along spindle fibers, and at spindle poles in living cells. *J. Cell Biol.* 150:1233-1249.

Huang, J.-Y., and J.W. Raff. 1999. The disappearance of cyclin B at the end of mitosis is regulated spatially in Drosophila cells. *EMBO Journal*. 18:2184-2195.

Hyman, A., and E. Karsenti. 1998. The role of nucleation in patterning microtubule networks. *J. Cell Sci.* 111:2077-2083.

Jacobson, M.P., P.R. Willis, and D.J. Winsor. 1996. Thermodynamics analysis of effects of small inert cosolutes in ultrasedimentation of noninteracting proteins. *Biochemistry*. 35:13173-13179.

Job, D., O. Valiron, and B. Oakley. 2003. Microtubule nucleation. *Curr Opin Cell Biol.* 15:111-117.

Joshi, H.C., M. J. Palacios, L. McNamara, and D. W. Cleveland. 1992. Gamma-tubulin is a centrosome protein required for cell cycle-dependent microtubule nucleation. *Nature (Lond.).* 356:80-83.

Karki, S., and E.L.F. Holzbaur. 1999. Cytoplasmic dynein and dynactin in cell division and intracellular transport. *Curr. Opin. Cell Biol.* 11:45-53.

Kashina, A.S., G.C. Rogers, and J.M. Scholey. 1997. The bimC family of kinesins: essential bipolar mitotic motors driving centrosome separation. *Biochim. Biophys Acta.* 1357:257-271.

Katayama, H., H. Zhou, Q. Li, M. Tatsuka, and S. Sen. 2001. Interaction and feedback regulation between STK15/BTAK/Aurora-A kinase and protein phosphatase 1 through mitotic cell division cycle. *J Biol Chem.* 276:46219-46224.

Kawaguchi, S.-i., and Y. Zheng. 2003. Characterization of a Drosophila centrosome protein CP309 that shares homology with Kendrin and CG-NAP. *Mol. Biol. Cell* 15:37-45.

Keating, T.J., J.G. Peloquin, V. Rodionove, D. Momcilovic, and G.G. Borisy. 1997. Microtubule release from the centrosome. *Proc. Natl. Acad. Sci.* 94:5078-5983.

Kellogg, D.R., M. Moritz, and B.M. Alberts. 1994. The centrosome and cellular organization. *Annu. Rev. Biochem.* 63:639-674.

Keryer, G., B. Di Fiore, C. Celati, K.F. Lechtreck, M. Mogensen, A. Delouvee, P. Lavia, M. Bornens, and A.-M. Tassin. 2003a. Part of Ran Is Associated with AKAP450 at the Centrosome: Involvement in Microtubule-organizing Activity. *Mol. Biol. Cell.* 14:4260-4271.

Keryer, G., O. Witczak, A. Delouvee, W.A. Kemmner, D. Rouillard, K. Tasken, and M. Bornens. 2003b. Dissociating the Centrosomal Matrix Protein AKAP450 from Centrioles Impairs Centriole Duplication and Cell Cycle Progression. *Mol. Biol. Cell.* 14:2436-2446.

Khodjakov, A., and C.L. Rieder. 1999. The sudden recruitment of gamma tubulin to the centrosome at the onset of mitosis and its dynamic exchange throughout the cell cycle, do not require microtubules. *J. Cell Biol.* 146:585-596.

Khodjakov, A., C.L. Rieder, G. Sluder, G. Cassels, O. Sibon, and C.L. Wang. 2002. De novo formation of centrosomes in vertebrate cells arrested during S phase. *J Cell Biol.* 158:1171-1181.

King, S.J., and T.A. Schroer. 2000. Dynactin increases the processivity of the cytoplasmic dynein motor. *Nat. Cell biol.* 2:20-24.

Kirkham, M., T. Muller-Reichert, K. Oegema, S. Grill, and A.A. Hyman. 2003. SAS-4 is a *C. elegans* centriolar protein that controls centrosome size. *Cell.* 112:575-587.

Knop, M., and E. Schiebel. 1997. Spc98p and Spc97p of the yeast gamma-tubulin complex mediate binding to the spindle pole body via their interaction with Spc110p. *Embo J.* 16:6985-6995.

Knop, M., and E. Schiebel. 1998. Receptors determine the cellular localization of a gamma-tubulin complex and thereby the site of microtubule formation. *Embo J.* 17:3952-3967.

Kotani, S., S. Tugenreich, M. Fujii, P.-M. Jorgensen, N. Watanabe, C. Hoog, P. Hieter, and K. Todokoro. 1998. PKA and MPF-activated polo-like kinase regulate anaphase-promoting complex activity and mitosis progression. *Molecular Cell.* 1:371-380.

Kubo, A., H. Sasaki, A. Yuba-Kubo, S. Tsukita, and N. Shiina. 1999. Centriolar satellites: molecular characterization, ATP-dependent movement toward centrioles and possible involvement in ciliogenesis. *J Cell Biol.* 147:969-980.

Kumar, S., I.H. Lee, and M. Plamann. 2000. Cytoplasmic dynein ATPase activity is regulated by dynactin dependent phosphorylation. *J. Biol Chem.* 275:31798-31804.

Kuriyama, R., and Borisy, G.G. 1981. Microtubule-nucleating activity of centrosomes in chinese hamster ovary cells is independent of the centriole cycle but coupled to the mitotic cycle. *J. Cell Biol.* 91:822-826.

Lacey, K.R., P.K. Jackson, and T. Stearns. 1999. Cyclin-dependent kinase control of centrsome duplication. *Roc. Nat. Acad. Sci.* 96:2817-2822.

Lane, H., and E. Nigg. 1997. Cell cycle control: Polo-like kinases join the outer circle. *Trends Cell Biol.* 7:63-68.

Lane, H.A., and E.A. Nigg. 1996. Antibody microinjection reveals an essential role for human polo-like kinase (Plk1) in the functional maturation of centrosomes. *J. Cell Biol.* 135:1701-1713.

Li, F., A. G., E.Y. Chu, J. Plescia, T. S., P. Marchisio, and A. D.C. 1998. Control of apoptosis and mitotic spindle checkpoint by survivin. *Nature.* 396:580-584.

Li, Q., D. Hansen, A. Killilea, H.C. Joshi, R.E. Palazzo, and R. Balczon. 2001. Kendrin/pericentrin-B, a centrosome protein with homology to pericentrin that complexes with PCM-1. *J Cell Sci.* 114:797-809.

Lifschitz, L., J. Collins, E. Moore, J. Gauch. 1994. Computer vision and graphics in fluorescence microscopy. IEEE Computer Soc. Press.

Lingle, W.L., W.H. Lutz, J.N. Ingle, N.J. Maihle, and J.L. Salisbury. 1998. Centrosome hypertrophy in human breast tumors: implications for genomic stability and cell polarity. *Proc. Natl. Acad. Sci.* 95:2950-2955.

Ludwig, M., N.F. Hensel, and R.J. Hartman. 1992. Calibration of a resonance energy transfer imaging system. *Biophys. J.* 61:845-857.

Marschall, L.G., and T. Stearns. 1997. Cytoskeleton: anatomy of an organizing center. *Curr. Biol.* 7:R754-R756.

Marshall, F., and J. Rosenbaum. 1999. Cell division: The renaissance of the centriole. *Current Biol.* 9:R218-220.

Marshall, W.F., Y. Vucica, and J.L. Rosenbaum. 2001. Kinetics and regulation of de novo centriole assembly. Implications for the mechanism of centriole duplication. *Curr Biol.* 11:308-317.

Martin, O.C., R.N. Gunawardane, A. Iwamatsu, and Y. Zheng. 1998. Xgrip109: a gamma tubulin-associated protein with an essential role in gamma tubulin ring complex (gammaTuRC) assembly and centrosome function. *J Cell Biol.* 141:675-687.

Martin, R.G., and B.N. Ames. 1960. A method for determining the sedimentation behavior of enzymes; application to protein mixtures. *J. Biol. Chem.* 236:1372-1379.

McNally, F.J., Okawa, K., Iwamatsu, A. and Vale, R.D. 1996. Katanin, the microtubule-severing ATPase, is concentrated at centrosomes. *J. Cell Sci.* 109:561-567.

McNally, F.J., and S. Thomas. 1998. Katanin is responsible for the M-phase microtubule-severing activity in Xenopus eggs. *Mol. Biol. Cell.* 9:1847-1861.

Megraw, T.L., K. Li, L.R. Kao, and T.C. Kaufman. 1999. The centrosomin protein is required for centrosome assembly and function during cleavage in Drosophila. *Development.* 126:2829-2839.

Mello, C.C., C. Schubert, B. Draper, W. Zhang, R. Lobel, and J.R. Priess. 1996. The PIE-1 protein and germline specification in *C. elegans* embryos. *Nature*. 382:710-712.

Merdes, A., and D.W. Cleveland. 1997. Pathways of spindle pole formation: different mechanisms; conserved components. *J. Cell Biol.* 138:953-956.

Merdes, A., R. Heald, K. Samejima, W.C. Earnshaw, and D.W. Cleveland. 2000. Formation of spindle poles by dynein/dynactin-dependent transport of NuMA. *J Cell Biol.* 149:851-862.

Merdes, A., K. Ramyar, J.D. Vechio, and D.W. Cleveland. 1996. A complex of NuMA and cytoplasmic dynein is essential for mitotic spindle assembly. *Cell.* 87:447-458.

Mikhailov, A., and C.L. Rieder. 2002. Cell Cycle: Stressed Out of Mitosis. *Current Biology.* 12:R331-R333.

Miyawaki, A., J. Llopis, J.M. McCaffrey, J.A. Adams, M. Ikura, and R.Y. Tsien. 1997. Fluoresence indicators for calcium based on green fluorescent proteins and calmodulin. *Nature*. 388:882-887.

Mogensen, M.M., J.B. Mackie, S.J. Doxsey, T. Stearns, and J.B. Tucker. 1997. Centrosomal deployment of gamma-tubulin and pericentrin: Evidence for a microtubule-nucleating domain and a minus-end docking domain in certain mouse epithelial cells. *Cell Motil. Cytoskel.* 36:276-290.

Moritz, M., M.B. Braunfeld, J.W. Sedat, B. Alberts, and D.A. Agard. 1995a. Microtubule nucleation by gamma-tubulin-containing rings in the centrosome. *Nature.* 378:638-640.

Moritz, M., M. Braunfled, J. Fung, J. Sedat, B. Alberts, and D. Agard. 1995b. Three-dimensional structural characterization of centrosomes from early Drosophila embryos. *J. Cell Biol.* 130:1149-1159.

Moritz, M., Y. Zheng, B.M. Alberts, and K. Oegema. 1998. Recruitment of the g tubulin ring complex to Drosophila salt-stripped centrosome scaffolds. *J. Cell Biol.* 142:775-786.

Murphy, S.M., A.M. Preble, U.K. Patel, K.L. O'Connell, D.P. Dias, M. Moritz, D. Agard, J.T. Stults, and T. Stearns. 2001. GCP5 and GCP6: two new members of the human gamma-tubulin complex. *Mol Biol Cell.* 12:3340-3352.

Murphy, S.M., L. Urbani, and T. Stearns. 1998. The mammalian gamma-tubulin complex contains homologues of the yeast spindle pole body components Spc97p and Spc98p. *J Cell Biol.* 141:663-674.

Murray, A.W., and Kirschner, M.W. 1989. Cyclin synthesis drives the early embryonic cell cycle. *Nature*. 339:275-280.

Murray, A.W. 1991. Cell cycle extracts. *Methods Cell Biol.* 36:581-605.

Nachury, M.V., T.J. Maresca, W.C. Salmon, C.M. Waterman-Storer, R. Heald, and K. Weis. 2001. Importin beta is a mitotic target of the small GTPase Ran in spindle assembly. *Cell.* 104:95-106.

Navara, C.S., L.C. Hewitson, C.R. Simerly, P. Sutovsky, and G. Schatten. 1997. The implications of a paternally derived centrosome during human fertilization: consequences for reproduction and the treatment of male factor infertility. *Amer. J. Repro. Immunol.* 37:39-49.

Nguyen, T., D.B. Vinh, D.K. Crawford, and T.N. Davis. 1998. A genetic analysis of interactions with Spc110p reveals distinct functions of Spc97p and Spc98p, components of the yeast gamma-tubulin complex. *Mol Biol Cell.* 9:2201-2216.

Nicolas, M.-T., and Bassot, J-M. 1993. Freeze substitution after fast-freeze fixation in preparation for immunocytochemistry. *Microscopy Res. and Tech.* 24:474-487.

Novakova, M., Draberova, E., Schurmann, W., Czihak, G., Viklicky, V., and Draber, P. 1996. Gamma-tubulin reditribution in taxol-treated mitotic cells probed by monoclonal antibodies. *Cell Motil. Cytoskel.* 33:38-51.

Oakley, B.R., C.E. Oakley, Y. Yoon, and M.K. Jung. 1990. Gamma-tubulin is a component of the spindle pole body that is essential for microtubule function in Aspergillus nidulans. *Nature.* 338:662-664.

Oakley, C.E., and B.R. Oakley. 1989. Identification of gamma tubulin, a new member of the tubulin superfamily encoded by mipA gene of *Aspergillus nidulans. Nature.* 338:662-664.

Oegema, K., C. Wiese, O.C. Martin, R.A. Milligan, A. Iwamatsu, T.J. Mitchison, and Y. Zheng. 1999. Characterization of two related Drosophila gamma-tubulin complexes that differ in their ability to nucleate microtubules. *J Cell Biol.* 144:721-733.

Pawson, T., and J.D. Scott. 1997. Signaling through scaffold, anchoring, and adapter proteins. *Science.* 278:2075-2080.

Pereira, G., K. Knop, and E. Schiebel. 1998. Spc98p Directs the Yeast γ-Tubulin Complex into the Nucleus and is subject to Cell Cycle-dependent Phosphorylation on the Nuclear Side of the Spindle Pole Body. *Mol. Biol. Cell* 9:775-793.

Piehl, M., U.S. Tulu, P. Wadsworth, and L. Cassimeris. 2004. Centrosome maturation: Measurement of microtubule nucleation throughout the cell cycle by using GFP-tagged EB1. *PNAS.* 101:1584-1588.

Piekorz, R.P., A. Hoffmeyer, C.D. Duntsch, C. McKAy, H. Nakajima, V. Sexl, L. Snyder, J. Rehg, and J.N. Ihle. 2002. The centrosomal protein TACC3 is essential for hematopoietic stem cell function and genetically interfaces with p53 regulated apoptosis. *EMBO Journal.* 21:653-664.

Pihan, G., A. Purohit, H. Knecht, B. Woda, P. Quesenberry, and S.J. Doxsey. 1998. Centrosome defects and genetic instability in malignant tumors. *Cancer Research.* 58:3974-3985.

Pihan, G.A., and S.J. Doxsey. 1999. The mitotic machine as a source of genetic instability in cancer. *Sem. Cancer Res.* 9:289-302.

Pines, J., and C.L. Rieder. 2001. Re-staging mitosis: a contemporary view of mitotic progression. *Nature Cell Biology*. 3:E3-E6.

Prahlad, V., M. Yoon, R.D. Moir, R.D. Vale, and R.D. Golgman. 1998. Rapid movements of vimentin on microtubule tracks: Kinesin-dependent assembly of Intermediate filament networks. *J. Cell Biol.* 143:159-170.

Prasher, D.C., Eckenrode, V.D., Ward, W.W., Prendergast, F.G. and Cormier, M.J. 1992. Primary structure of the Aequorea victoria green-fluorescent protein. *Gene.* 111:229-233.

Preuss, U., H. Bierbaum, P. Buchenau, and K.H. Scheidtmann. 2003. DAP-like kinase, a member of the death-assocaited protein kinase family, associates with centrosomes, centromers, and the contractile ring during mitosis. *European Journal of Cell Biology*. 82:447-459.

Prigozhina, N.L., C.E. Oakley, A.M. Lewis, T. Nayak, S.A. Osmani, and B.R. Oakley. 2004. {gamma}-Tubulin Plays an Essential Role in the Coordination of Mitotic Events. *Mol. Biol. Cell.* 15:1374-1386.

Purohit, A., S.H. Tynan, R. Vallee, and S.J. Doxsey. 1999. Direct interaction of pericentrin with cytoplasmic dynein light intermediate chain contributes to mitotic spindle organization. *J. Cell Biol.* 147:481-491.

Rajagopalan, S., A. Binbo, M.K. Balasubramanian, and S. Oliferenko. 2004. A potential tension-sensing mechanism that ensures timely anaphase onset upon metaphase spindle orientation. *Curr. Biol.* 14:69-74.

Reed, J.C., and S.I. Reed. 1999. Survivin' cell-separation anxiety. *Nature Cell Biology.* 1:E199-E200.

Rieder, C.L., and G.G. Borisy. 1982. The centrosome in PTK2 cells: asymmetric distribution and structural changes in the pericentriolar material. *Biol. cell.* 44:117-132.

Rosenbaum, J.L., D.G. Cole, and D.R. Diener. 1999. Intraflagellar transport: the eyes have it. *J Cell Biol.* 144: 385-388.

Rosenblatt, J., L.P. Cramer, B. Baum, and K. M. McGee. 2004. Myosin II-dependent cortical movement is required for centrosome separation and spindle positioning during mitotic spindle formation. Cell 117: 361-372.

Salisbury, J.L. 1995. Centrin, centrosomes and mitotic spindle poles. *Current Opinion in Cell Biology*. 7:39-45.

Sampaio, P., E. Rebollo, H. Varmark, C.E. Sunkel, and C. Gonzalez. 2001. Organized microtubule arrays in gamma-tubulin-depleted Drosophila spermatocytes. *Curr Biol.* 11:1788-1793.

Sandal, T., L. Aumo, L. Hedin, B.T. Gjertsen, and S.O. Doskeland. 2003. Irod/Ian5: An Inhibitor of γ-Radiation- and Okadaic Acid-induced Apoptosis. *Molecular Biology of the Cell.* 14:3292-3304.

Sawin, K.E., and Mitchison, T.J. 1991. Poleward microtubule flux in mitotic spindles assembled in vitro. *J. Cell Biol.* 112:941-954.

Schiebel, E. 2000. gamma-tubulin complexes: binding to the centrosome, regulation and microtubule nucleation. *Curr Opin Cell Biol.* 12:113-118.

Schnackenberg, B.J., A. Khodjakov, C.L. Rieder, and R.E. Palazzo. 1998. The disassembly and reassembly of functional centrosomes in vitro. *Proc. Natl. Acad. Sci.* 95:9295-9300.

Schnapp, B.J. 1999. RNA localization: A glimpse of the machinery. *Current Biology.* 9:R725-R727.

Schroer, T.A. 1996. Structure and function of dynactin. *Semin. Cell Biol.* 7:321-328.

Scolnick, D.M., and T.D. Halazonetis. 2000. Chfr defines a mitotic stress checkpoint that delays entry into metaphase. *Nature.* 406:430-435.

Shah, J.V., L.A. Flanagan, P.A. Jammey, and J.P. Leterrier. 2000. Bidirectional translocation of neurofilaments along microtubules mediated in part by dynein/dynactin. *Mol. Biol. Cell.* 11:3495-3508.

Sharp, D.J., G.C. Rogers, and J.M. Scholey. 2000. Microtubule motors in mitosis. *Nature.* 407:41-47.

Siegel, L.M., and K.L. Monty. 1966. Determination of molecular weights and frictional ratios of proteins in impure systems by use of gel filtration and density gradient centrifugation: application to crude preparations of sulfite and hydroxylamine reductases. *Biochem. Biophys. Acta.* 112:346-362.

Sobel, S.G. 1997. Mini Review: mitosis and the spindle pole body in *Saccharomyces cerevisiae. J. Experimental Zoology.* 277:120-138.

Sodeik, B. 2000. Mechanisms of viral transport in the cyctoplasm. *Trends Microbiol.* 8:465-472.

Sohrmann, M., S. Schmidt, I. Hagen, and V. Simanis. 1998. Asymmetric segregation on spindle poles of the *Schizosaccharomyces pombe* septum-inducing protein kinase Cdc7p. *Genes Dev.* 12:84-94.

Sparks, C., E. Fey, C. Vidair, and S. Doxsey. 1995. Phosphorylation of NuMA occurs during nuclear breakdown not spindle assembly. *J. Cell Sci.* 108:3389-3396.

Stearns, T., Evans, L. and Kirschner, M. 1991. Gamma tubulin is a highly conserved component of the centrosome. *Cell.* 65:825-836.

Stearns, T., and M. Kirschner. 1994. Reconstitution of centrosome assembly, role of gamma tubulin. *Cell.* 76: 623-637.

Stearns, T., and M. Winey. 1997. The cell center at 100. *Cell.* 91:303-309.

Strome, S., J. Powers, M. Dunn, K. Reese, C.J. Malone, J. White, G. Seydoux, and W. Saxton. 2001. Spindle Dynamics and the Role of gamma-Tubulin in Early Caenorhabditis elegans Embryos. *Mol Biol Cell.* 12:1751-1764.

Stryer, L. 1978. Flourescence energy transfer as a spectroscopic ruler. *Annu. Rev. Biochem.* 47:819-846.

Sumiyoshi, E., A. Sugimoto, and M. Yamamoto. 2002. Protein phosphatase 4 is required for centrosome maturation in mitosis and sperm meiosis in C. elegans. *J Cell Sci.* 115:1403-1410.

Sunkel, C.E., R. Gomes, P. Sampaio, J. Perdigao, and C. Gonzalez. 1995. Gamma-tubulin is required for the structure and function of the microtubule organizing centre in Drosophila neuroblasts. *Embo J.* 14:28-36.

Suomalainen, M., M.Y. Nakano, K. S., K. Bouche, R.P. Stidwill, and U.F. Gerber. 1999. Microtubule-dependent plus- and minus end- directed motilities are competing processes for nuclear targeting of adenovirus. *J. Cell Biol.* 144:657-672.

Swedlow, J.R., and T. Hirano. 2003. The Making of the Mitotic Chromosome: Modern Insights into Classical Questions. *Molecular Cell.* 11:557-569.

Tai, A.W., J. Chuang, C. Bode, U. Wolfrum, and C.-H. Sung. 1999. Rhodopsin's carboxy-terminal cytoplasmic tail acts as a membrane receptor for cytoplasmic dynein by binding to the dynein light chain Tctex-1. *Cell.* 97:877-887.

Takahashi, M., A. Yamagiwa, T. Nishimura, H. Mukai, and Y. Ono. 2002. Centrosomal proteins CG-NAP and kendrin provide microtubule nucleation sites by anchoring gamma-tubulin ring complex. *Mol Biol Cell.* 13:3235-3245.

Tassin, A.M., C. Celati, M. Mougjou, and M. Bornens. 1998. Characterization of the human homologue of the yeast SPC98p and its association with γ tubulin. *J. Cell Biol.* 17:689-701.

Tassin, A.M., C. Celati, M. Paintrand, and M. Bornens. 1997. Identification of an Spc110p-related protein in vertebrates. *J Cell Sci.* 110:2533-2545.

Terada, Y., Y. Uetake, and R. Kuriyama. 2003. Interaction of Aurora-A and centrosomin at the microtubule-nucleating site in Drosophila and mammalian cells. *J. Cell Biol.* 162:757-764.

Thompson-Coffe, C., G. Coffee, H. Schatten, D. Mazia, and G. Schatten. 1996. Cold-treated centrosome: isolation of centrosomes from mitotic sea urchin eggs, production of an anticentrosomal antibody and novel ultrastructural imaging. *Cell Motil. Cytoskel.* 33:197-207.

Tugendreich, S., Tomkiel, J., Earnshaw, W. and Hieter, P. 1995. Cdc27Hs colocalizes with cdc16Hs to the centrosome and mitotic spindle and is essential for the metaphase to anaphase transition. *Cell.* 81:261-268.

Tyler, K.L., P. Clarke, R.L. DeBiasi, D. Kominsky, and G.J. Poggioli. 2001. Reoviruses and the host cell. *TRENDS in MIcrobiology.* 9:560-564.

Tynan, S.H., A. Purohit, S.J. Doxsey, and R.B. Vallee. 2000. Light intermediate chain 1 defines a functional subfraction of cytoplasmic dynein which binds to pericentrin. *J Biol Chem.* 275:32763-32768.

Urata, Y., Parmalee, S.J. Agard, D.A. and Sedat, J.W. 1995. A three-dimensional structural dissection of Drosophila polytene chromosomes. *J. Cell Biology.* 131:279-295.

Urbani, L., and T. Stearns. 1999. The centrosome. *Current Biology.* 9:R315-317.

Vaughn, K., and J. Harper. 1998. Microtubule organizing centers and nucleating sites in land plants. *Int. Rev. Cytol.* 181:75-149.

Vogel, J.M., T. Stearns, C.L. Rieder, and R.E. Palazzo. 1997. Centrosomes isolated from Spistula solidissima oocytes contain rings and an unusual stoichiometric ratio of a/b tubulin. *J. Cell Biol.* 137:193-202.

Vogel, J., B. Drapkin, J. Oomen, D. Beach, K. Bloom, and M. Snyder, 2001. Phosphorylation of gamma tubulin regulates microtubule organization in budding yeast. *Dev. Cell* 5:621-31.

Vorobjev, I.A., and Y.S. Chentsov. 1982. Centrioles in the cell cycle. I. Epithelial cells. *J Cell Biol.* 93:938-949.

Walczak, C.E., Mitchison, T.J., Desai, A. 1996. XKCM1: A Xenopus kinesin-related protein that regulates microtubule dynamics during mitotic spindle assembly. *Cell.* 84:37-48.

Wang, P.J., and T.C. Huffaker. 1997. Stu2p: a microtubule-binding protein that is an essential component of the yeast spindle pole body. *J. Cell Biol.* 139:1271-1280.

Waters, J.C.a.S., E.D. 1997. Pathways of spindle assembly. *Current Opinion of Cell BIology.* 9:37-43.

Wiese, C., A. Wilde, M.S. Moore, S.A. Adam, A. Merdes, and Y. Zheng. 2001. Role of importin-beta in coupling Ran to downstream targets in microtubule assembly. *Science*. 291:653-656.

Wiese, C., and Y. Zheng. 2000. A new function for the gamma-tubulin ring complex as a microtubule minus-end cap. *Nat Cell Biol.* 2:358-364.

Wigge, P., O. Jesen, S. Holmes, Soues, M. Mann, and J. Kilmartin. 1998. Analysis of the Sacharomyces spindle pole by matrix-assisted laser desorbtion/ionization (MALDI) mass spectrometry. *J. Cell Biol.* 141:967-977.

Wilde, A., and Y. Zheng. 1999. Stimulation of microtubule aster formation and spindle assembly by the small GTPase ran. *Science*. 284:1359-1362.

Wilson, E.B. 1925. The Cell in Development and Heredity. Macmillan, Inc., New York.

Wittmann, T., M. Wilm, E. Karsenti, and I. Vernos. 2000. TPX2, A novel xenopus MAP involved in spindle pole organization. *J Cell Biol.* 149:1405-1418.

Wittmann, T., A Hyman, and A. Desais. 2001. The spindle: a dynamic assembly of microtubules and motors. *Nature Cell Biol.* 3:E28-E34.

Wu, P., and L. Brand. 1994. Resonance energy transfer: Methods and applications. *Anal. Biochem.* 218:1-13.

Yang, C.H., Lambie, E.J., and Snyder, M. 1992. NuMa: An unusually long coiled-coil related protein in the mammalian nucleus. *J. Cell Biol.* 116:1303-1317.

Young, A., J. Dictenberg, A. Purohit, R. Tuft, and S. Doxsey. 2000. Dynein-mediated assembly of pericentirn and gamma tubulin onto centrosomes. *Mol. Biol. Cell.* 11:2047-2056.

Young, A., R. Tuft, W. Carrington, and S.J. Doxsey. 1998. Centrosome dynamics in living cells. *Meth. Cell Biol.* 58:223-238.

Zheng, Y., Jung, M.K., Oakley, B.R. 1991. γ-Tubulin is present in Drosophila melanogaster and Homo sapiens and is associated with the centrosome. *Cell.* 65:817-823.

Zheng, Y., M.L. Wong, B. Alberts, and T. Mitchison. 1995. Nucleation of microtubule assembly by a gamma tubulin-containing ring complex. *Nature.* 378:578-583.

Zheng, Y., M.L. Wong, B. Alberts, and T. Mitchison. 1998. Purification and assay of the gamma tubulin ring complex. *Meth. Cell Biol.* 298:218-228.

Zimmerman, W., C.A. Sparks, and S.J. Doxsey. 1999. Amorphous no longer: the centrosome comes into focus. *Curr. Opin. Cell Biol.* 11:122-128.

Zimmerman, W., and S.J. Doxsey. 2000. Construction of centrosomes and spindle poles by molecular motor-driven assembly of protein particles. *Traffic.* 1:927-934.

Zimmerman, W.C., J. Sillibourne, J. Rosa, and S.J. Doxsey. 2004. Mitosis specific anchoring of γ tubulin complexes by pericentrin controls spindle organization and mitotic entry. *Molecular Biology of the Cell.* In Press.